

# Electrical Characterization of Leukocyte Activation for Monitoring Sepsis Progression Using Dielectrophoresis

by

Hao-Wei Su

B. S. Electrical Engineering, National Taiwan University, 2009

S. M. Electrical Engineering and Computer Science  
Massachusetts Institute of Technology, 2012

SUBMITTED TO THE DEPARTMENT OF ELECTRICAL ENGINEERING AND COMPUTER SCIENCE IN PARTIAL FULFILLMENT OF THE REQUIREMENTS FOR THE DEGREE OF DOCTOR OF PHILOSOPHY IN ELECTRICAL ENGINEERING AND COMPUTER SCIENCE

AT THE  
MASSACHUSETTS INSTITUTE OF TECHNOLOGY

FEBRUARY 2016

© 2016 Massachusetts Institute of Technology  
All rights reserved.

**Signature redacted**

Signature of Author \_\_\_\_\_

Hao-Wei Su

Department of Electrical Engineering and Computer Science

October 30, 2015

**Signature redacted**

Certified by \_\_\_\_\_

Joel Voldman

Professor of Electrical Engineering and Computer Science

Thesis Supervisor

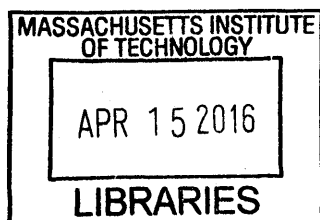
**Signature redacted**

Accepted by \_\_\_\_\_

Leslie A. Kolodziejski

Professor of Electrical Engineering and Computer Sciences  
Chairman, Department Committee on Graduate Committee

ARCHIVES





# **Electrical Characterization of Leukocyte Activation for Monitoring Sepsis Progression Using Dielectrophoresis**

**By**

**Hao-Wei Su**

## **ABSTRACT**

This thesis describes the development of a rapid dielectrophoretic characterization tool for monitoring leukocyte activation, and its application for monitoring sepsis progression. Sepsis is an uncontrolled activation of the immune system that causes an excessive inflammatory response or an impaired immunity. The unpredictable immune status makes the immunotherapy treatment difficult. One crucial aspect of sepsis is leukocyte activation, which plays an important role in the attacking the pathogens, stimulating the tissues, and resulting in organ function failures. Monitoring leukocyte activation in sepsis may provide real-time indicators for diagnosis, prognosis, and guiding therapy.

To measure leukocyte activation, we used Iso-dielectric Separation (IDS) and dielectrophoretic spring (DEP spring) method which can rapid characterize of thousands of cells to provide statistically meaningful results. To adapt to measuring septic blood with clumpy and sticky leukocytes, the double-sided electrodes was developed and characterized for higher throughput and anti-fouling measurement. The human neutrophils were successfully isolated and activated with chemicals and their electrical properties were measured across many conditions and compared to the non-activated ones. We found repeatable and consistent electrical changes using both IDS and DEP spring method: an increase in effective conductivity of activated neutrophils at higher frequencies (above 5MHz). We then developed an electrical model and an experiment pipeline of inhibiting neutrophil functions to hypothesize the underlying mechanism.

Using the blood samples from a cecal-ligation and puncture (CLP) model of sepsis in mice, we estimated the number of activated leukocytes by looking into the difference in electrical properties at 10 MHz. We found that the activated leukocyte percentage correlated with the neutrophil activation percentage obtained from flow cytometry, indicating potential use for monitoring sepsis progression. We designed a multi-parametric time series experiment to understand the prognostic value of leukocyte activation and the role of leukocyte activation in sepsis at a system level. We found that the neutrophil activation percentage of non-survivors were significantly larger than survivors at 24 hours after the CLP procedure. We also found the neutrophil activation percentage positively correlates with inflammatory cytokine interleukin-6 and interleukin-10. Finally, we initiated a pilot study of monitoring neutrophil activation in critically-ill human patients with suspected sepsis. We found, with a limited dataset, the effective conductivity of neutrophils in critically-ill human patients is higher than the healthy control. To show the feasibility of becoming an point-of-care bedside device, the sample preparation of red blood cell removal was integrated in for rapid test that can profile >1,000 leukocytes within 15 minutes from sample to result, providing a simple assay to monitor leukocyte activation in sepsis progression.

Thesis Supervisor: Joel Voldman

Title: Professor of Electrical Engineering and Computer Science

## Acknowledgements

I want to thank everyone I met during my research life at MIT. It has been a tough and fun journey for exploring science, engineering, and my own personal interest. Specifically, I want to thank Joel for helping me, guiding, and encouraging me to experience both research and teaching. He has been a fantastic mentor, a great teacher, and an outstanding leader for us.

When I first came to MIT, I did not know what I want to do exactly but I do know that I want to contribute to healthcare and medicine. Luckily, I have been involved in the DARPA project of dialysis-like therapeutics (DLT) after finishing my Master of Science. Even though doing a quarterly report and being reviewed every 6 months was not an easy task, we survived after several rounds of intervention. I really want to thank Prof. Jongyong Han for his perseverance of leading our DLT team and sacrificing the chance to go to the MicroTAS conferences. Working with Dr. Bruce Levy and Dr. Rebecca Baron fulfilled my dream of delving into translational science. I am satisfied with my PhD experience which matches my initial goal of leveraging the great engineering, great biological science, and great medical resource in Boston.

Thanks to Joel, most of the postdocs in our labs were very good in dielectrophoresis. I have learned a lot from Tao, Marc, Javier, and Thibault just by coming to the office or knocking on the office next door. The work established by Mike and Javier was the foundation of my PhD research. On the other hand, leaning from other folks in the lab broadened my knowledge in neuroscience, synthetic biology, and immunology. Working in the microscope room by Per was super enjoyable because of his curiosity and exuberance in science as well as musical taste that is similar to me.

I want to thank the new and old Voldman babies. Sarvesh has been always there with me listening to my complaints, sharing the good and bad news, and giving me the honest suggestions as a true friend. Burak has been inspiring me in biological science and teasing me with his humorous words. Aalap is my awesome consultant of career planning, job hunting, and trip organizing. Dan shares tons of good memory with me in late nights and on weekends. Nicha, Boying, and Lisa energize the lab with their enthusiasm. Jaemyon is the guru of video games. You all have made me a happy and colorful graduate life.

Doing the blood work was never a simple task. Thanks to Han-Wei, Lidan, and Diana to make my research possible. I remember Lidan spent her birthday helping me with the times series mice experiments until 9 pm without eating lunch and dinner. I wish all your contributions will eventually make the world a healthier place.

Teaching in 6.S03 was a challenging yet fulfilling experience. Prof. Jacob White, Prof. Elfar Adalsteinsson, Prof. Collin Stultz and Joel spent energy and time to make the class one of the best introductory classes at MIT. The queuing system, MITx, and Gradescope are great tools for teaching innovation.

Finally, I want to thank my dad Shio-Lun Su, my mom Tseun-Fang Wong, my sister Hao-Lin Su, my little niece Yen-Ching Chang, and my girlfriend Hoyu Wu for their unconditional support and love.

## Table of Contents

Acknowledgements.....	4
List of Figures.....	8
List of Tables.....	13
Chapter 1 Introduction and background .....	14
1.1 Sepsis.....	14
1.1.1 Sepsis progression.....	14
1.1.2 Diagnostic and prognostic markers of sepsis.....	15
1.1.3 Treatment of sepsis.....	19
1.1.4 Monitoring tools of sepsis .....	21
1.1.5 Recent advances in monitoring leukocyte activation in sepsis .....	21
1.2 Electrical characterization of leukocytes.....	22
1.2.1 Impedance based electrical characterization of cells .....	22
1.2.2 Electro-rotation based electrical characterization of leukocytes.....	22
1.2.3 Patch-clamp based electrical characterization of leukocytes.....	23
1.2.4 Dielectrophoretic based electrical characterization of leukocytes.....	23
1.3 Thesis overview .....	24
Chapter 2 Dielectrophoretic characterization system .....	25
2.1 Dielectrophoresis theory.....	25
2.1.1 Dielectrophoretic force and Clausius-Mossotti (CM) factor .....	25
2.1.2 Re[CM] map and the Iso-dielectric point .....	28
2.2 Methods of operation.....	29
2.2.1 Dielectrophoretic spring.....	29
2.2.2 Iso-Dielectric separation.....	31
2.3 Device fabrication.....	32
2.3.1 Single-sided electrode fabrication .....	33
2.3.2 Double-sided electrode fabrication.....	33
2.4 System overview & Instrumentation .....	35
2.4.1 Fluidics .....	35
2.4.2 Optics .....	36
2.4.3 Electronics .....	36
2.4.4 Software: Image Processing and GUI program.....	37
2.5 Conclusion .....	38

Chapter 3	In vitro characterization of activation of human neutrophils.....	39
3.1	Electrical properties of human neutrophils .....	39
3.1.1	Electrical characterization of neutrophil activation using patch clamp technique.....	40
3.1.2	Electrical characterization of neutrophil activation using electro-rotation.....	40
3.1.3	Challenges in single cell electrical characterization technique .....	41
3.2	Sample preparation for isolating and activating neutrophils.....	41
3.2.1	Isolating neutrophil through density separation .....	42
3.2.2	Activating neutrophils .....	43
3.2.3	Monitoring oxidative burst of neutrophils after PMA treatment .....	43
3.2.4	Monitoring the adhesion marker of neutrophils after PMA treatment.....	43
3.2.5	Observing neutrophil membrane integrity over time after PMA treatment.....	44
3.3	Dielectrophoretic characterization of neutrophil activation using IDS.....	45
3.3.1	IDS with single-sided electrode .....	46
3.3.2	IDS with double-sided electrode .....	48
3.3.3	Mixing activated granulocytes and non-activated granulocytes.....	48
3.4	Dielectrophoretic characterization of neutrophil activation using DEP spring .....	49
3.5	Dielectrophoretic characterization of neutrophil activation under inhibitors using IDS....	51
3.6	Explanation of electrical changes of neutrophil activation using the double-shell models	53
3.7	Conclusion .....	56
Chapter 4	Monitoring sepsis progression in a murine model.....	57
4.1	Motivation .....	57
4.2	Study design and methods.....	59
4.3	Results.....	63
4.3.1	Severe injured CLP mice with neutrophil activation data (CD 18/Ly6G) .....	63
4.3.2	Comparison between survivors vs non-survivors with severely injured mice .....	65
4.3.3	Correlation between parameters and between time points.....	66
4.3.4	Discussion and conclusion .....	67
4.4	IDS electrical profiling of leukocytes and its correlation with flow cytometry .....	68
4.4.1	Comparing electrical profiling of leukocyte in IDS and neutrophil activation in flow cytometry .....	68
4.4.2	Diagnostic and prognostic values of IDS leukocyte activation and neutrophil activation in flow cytometry.....	69
4.4.3	Understanding the IDS leukocyte profile.....	71

4.4.4	Human leukocyte subpopulation profiling compared to activated neutrophils .....	72
4.4.5	New gating strategy for mice data .....	72
4.5	Conclusion .....	74
Chapter 5	Monitoring sepsis in human patients.....	75
5.1	Monitoring neutrophil activation in human patients.....	75
5.1.1	Motivation.....	75
5.1.2	Experimental design.....	76
5.1.3	Results .....	77
5.1.4	Conclusion and future improvement.....	84
5.2	Integrated system with spiral device for leukocyte isolation.....	85
5.2.1	Motivation.....	85
5.2.2	Results .....	85
5.2.3	Conclusion.....	87
Chapter 6	Conclusion and Future Outlook.....	88
6.1	Conclusion and contribution .....	88
6.2	Future direction .....	89
6.2.1	Technological directions.....	89
6.2.2	Biological directions .....	89
6.2.3	Clinical directions .....	90
Appendix:	Detailed Protocols and MATLAB scripts .....	91
DEP	Spring Force calculation.....	91
Multi-Modal	electrical and optical cytometry and multi-class image classification .....	92
Protocol:	White blood cells separation using IDS.....	102
PBMCs	separation protocol (Ficoll) .....	104
Neutrophil	density isolation and activation protocol.....	106
Human	neutrophil activation assay protocol.....	109
Fabrication	Process Flow .....	111
Reference.....		113

## List of Figures

- Figure 1-1** The progression of sepsis. The mortality rate world-wide is high and increases with severity of sepsis (up to 30% for sepsis, 50% for severe sepsis, and 80% for septic shock). The mortality rate is estimated by Jawad et al., 2012[3]. One older study with U.S. data done by Pittet et al. has lower mortality rates (SIRS: 7%, sepsis: 16%, severe sepsis: 20% and septic shock: 46%) [4]. 15
- Figure 1-2** Neutrophil functional responses during recruitment to a site of bacterial infection. The broken lines represent chemoattractants generated at the site of infection that activate the endothelium and capture the intravascular neutrophils. The neutrophils flatten and adhere to the endothelium, migrate out of the vessel towards the infectious site, phagocytose and kill the bacteria, secrete cytokines to recruit other inflammatory cells and eventually undergo programmed cell death (apoptosis). The figure and caption are adapted from [19]. 18
- Figure 1-3** The three type of aims in this thesis: Engineering Aim, Biological Aim, and Clinical Aims. 24
- Figure 2-1** Polarization of a particle in an external non-uniform electric field. For relatively conductive particles (left), the dipole moment and electric field align parallel to each other, leading to lower potential energy at higher electric field strengths, known as p-DEP. For relatively insulating particles (right), the dipole moment and external field are anti-parallel, causing particles to be expelled from regions of higher field intensity, known as n-DEP. If the electrical properties of the particle match those of the medium (center), the polarization vanishes and there is no preferential motion towards higher or lower field strengths. Adapted from [57]. 25
- Figure 2-2** Two electrical models of a cell. (a) Single -Shell model. (b) Double-shell model. The cell is composed of concentric uniform layers of different complex permittivity ( $\underline{\epsilon} = \epsilon + \sigma / j\omega$ ). The subscripts refer to the following phases: m, plasma membrane; i, inner phase of cell; cp, cytoplasm; ne, nuclear envelope; np, nucleoplasm. The morphological parameters are:  $R$ , outer radius of cell;  $R_n$ , outer radius of nucleus;  $d$ , thickness of plasma membrane;  $d_n$  thickness of nuclear envelope. Figure adapted from [59]. 27
- Figure 2-3** The real part of the Clausius-Mossotti factor as a function of the frequency of the external electric field and the media conductivity. The blue area on the right side is the condition where the cell experiences n-DEP force ( $\text{Re} [ CM ] < 0$ ) and the left side shows where the cell experiences p-DEP ( $\text{Re} [ CM ] > 0$ ). The white-line shows the condition where the cell experiences no DEP force ( $\text{Re} [ CM ] = 0$ ). We term any point this line as an Iso-dielectric point (IDP), and the related frequency as the cross-over frequency. The electrical parameters for this figure come from dielectric spectroscopy for human white blood cells [47]. 29
- Figure 2-4** (a) The DEP spring method overview. Cells (or other particles) are introduced into the channel along with buffer flow. As the cells flow down the channel they encounter the electrodes where they experience a DEP force (red, inset) that balances the drag force (blue, inset). The equilibrium balance position between the two forces is denoted by  $\delta$ . (b) The DEP force in the x-direction at different balance positions. The balance position decreases when the applied drag force increases, which represents the length of this nonlinear DEP spring. The DEP spring only holds when the drag force is smaller than the maximum n-DEP force. 30



- Figure 2-5 (a) Image of putting different conductivity of liquid into the microfluidic chip. (b) flows into a channel and creates a transverse conductivity gradient. Electrodes apply a DEP force pushing cells to the right as they flow down the channel. Cells escape the DEP barrier at their Iso-dielectric position (IDP) resulting in a transverse distribution of cells. (c) A camera is used to capture images near the end of the channel, which are processed to extract the IDP distributions.** 32
- Figure 2-6 Cells from activated samples stick to the channel walls of the original IDS.** 33
- Figure 2-7 Difference between single-sided IDS and double-sided IDS device. (a) IDS device from a top-down view. (b) Single-sided IDS device (c) Double-sided IDS device** 33
- Figure 2-8 (a) The double-sided electrode with laser-cutted 25  $\mu\text{m}$  tape in between. (b) The double-sided electrode connected with wires and silver epoxy electrically. The PDMS layer on top of the device is for fluidic connection with 1/16 inches tubing.** 34
- Figure 2-9 The image of electrodes with 20x magnification. (a) Focusing on bottom. (b) Focusing on top. The electrode gap is 15  $\mu\text{m}$ . The electrode width is 45  $\mu\text{m}$ . The focus difference between the two images (channel height) is 30  $\mu\text{m}$ .** 34
- Figure 2-10 The overview of the automated system. The MATLAB controls all the equipment with parameters. The image and other parameters for each frame are recorded for processing. The microscope is control with MATLAB script but requires importing the Micro-Manager Core.** 35
- Figure 2-11 The control panel (left) and the Macro panel (right) of the MATLAB GUI.** 38
- Figure 3-1 Illustration of neutrophil activation. Size increase, membrane ruffling, reactive oxygen species generation, nuclear membrane disintegration, and degranulation process are parts of the activation response of neutrophil.** 39
- Figure 3-2 Monitoring electrical changes of neutrophil activation using patch clamp technique. (a) An illustration of using patch clamp to measure the electrical properties of neutrophils. Thick black line indicates cell membrane, gray lines indicates patch pipette.  $R_A$ ,  $G_m$ ,  $C_m$  are access resistance, membrane conductance, and membrane capacitance, respectively. (b) Trace from cell-attached recording. Cell-attached recording from a human neutrophil stimulated with ionomycin. The upper trace ( $I_m$ ) shows stepwise capacitance increases, indicating exocytosis of individual granules. The lower trace ( $R_e$ ) shows transient conductance changes at the time of capacitance steps (for the three middle steps) reflecting the fusion pore opening. Adapted from [36].** 40
- Figure 3-3 (a) In rotating electric fields, the induced dipole moment of a particle is out of phase with the direction of the electric field. The angle between the two ( $\theta$ ) reflects the time taken for the dipole to form. The phase difference will generate a variable torque ( $\Gamma$ ) acting on the particle, causing it to rotate. (b) Experimental electrorotation spectra of resting ( $\circ$ ) and activated ( $\square$ ) human neutrophils. The spectra were collected using polynomial electrodes (360  $\mu\text{m}$  tip-to-tip separation) in a field of ca. 56 V  $\text{cm}^{-1}$  (2 V p-p) in a sucrose/PBS medium (2.4% PBS, 400  $\mu\text{S cm}^{-1}$ ). The neutrophils were activated using PMA at a final concentration of 25  $\mu\text{M}$ . The solid line is a simulated spectrum of the resting human neutrophils generated with the double-shell cell model using the parameters in [37]. Adapted from [37].** 41
- Figure 3-4 Density based separation of whole blood using Mono-Poly resolving medium. (a) Successful separation. (b) Bad separation due to insufficient centrifugation, old blood sample, or expired medium.** 42
- Figure 3-5 Fluorescent DCF is a result of the oxidation of DCFH-DA by the byproducts of the oxidative burst in neutrophils. The intensity of DCF over time increases for different PMA doses**

indicating granulocyte activation. The error bars are the standard deviation of three experiments.	43
Figure 3-6 The validation of neutrophils activation with surface markers. The isolated neutrophils were labeled with CD18-APC and CD66b-PE. The activation percentage is 0.25% for untreated neutrophils and the activation percentage is 93.9% after PMA treatment.	44
Figure 3-7 Time lapse imaging of PMA treated neutrophils in a 20 $\mu\text{m}$ height device. (Green: Syto 64, Red: Sytox 9, Blue: Phase)	45
Figure 3-8 IDP distributions of PMA-treated and non-treated human granulocytes at 1 MHz and 5 MHz. Dashed lines indicate medians.	46
Figure 3-9 (a) Aggregated IDP distributions of PMA-treated and non-treated granulocytes. (b) Box-and-whisker plots of mean IDP of PMA-treated and non-treated granulocytes. At 10 MHz the mean IDP of both population types is different (* $p < 0.05$ ). (c) ROC curves of the aggregated samples using the IDP position as classification criteria for different frequencies. Inset shows box-and-whisker plots of the AUC for each frequency across all samples ( $n=3$ ). The unit here has been transferred from pixel into mm and in a reverse order.	47
Figure 3-10 (a) The illustration of changing conductivity gradient by changing flow rates of three buffer with different conductivities. (b) The result of IDPs distributions of activated and non-activated cells with the two different conductivity gradients. (Red: Activated granulocytes, Blue: non-activated granulocytes)	48
Figure 3-11 (a) A screenshot of the video of the mixing of PMA-treated granulocytes stained with Syto 9 (Green) versus non-treated granulocytes (Red) (b) The processed image shows the IDP distribution of PMA-treated granulocytes (Green) versus non-treated granulocytes (Red).	49
Figure 3-12 The balance position histograms of activated and unactivated neutrophils in different frequencies and conductivities. The x-axis is the balance position ( $\mu\text{m}$ ). The y-axis is the number of particle images recorded (events per 100 nm). The red population is the activated neutrophils and the blue population is the unactivated neutrophils. Both of them have two peaks in low frequencies because the existence of the erythrocytes. In high conductivity, the two populations are similar. In middle conductivity, the two populations become different when the frequency goes higher. In low conductivity, the number of cells decreases when the frequency goes higher.	50
Figure 3-13 Mechanism of electrical changes of granulocytes. Granulocytes were treated with drugs to inhibit certain functions, then stimulated by stimulants. fMLP is a bacterial stimuli that initiates calcium transients to activate intracellular signaling. Cytochalasin B (CytB) is an inhibitor of actin polymerization and thus inhibits membrane ruffling. Diphenyleneiodonium chloride (DPI) is an inhibitor of NAPDH oxidase thus blocks the reactive oxygen species (ROS) generation. Comparing the electrical profiles suggests that membrane ruffling dominates the electrical changes at 10 MHz observed in IDS.	52
Figure 3-14 (a) Double shell electrical model of cells. (b) The simulated $\text{Re}[CM]$ of human neutrophil as a function of different frequency and surrounding medium conductivity. Neutrophils parameters are from Table 3-1.	53
Figure 4-1 Timeline of the blood collection in CLP murine model with 8 independent parameters measured.	59
Figure 4-2 Collecting peripheral blood from pre-installed catheter. The mouse was put into plastic cylindrical restrictor to fix its movement. The preinstalled catheter was lengthened by tweezers. Stainless steel plug was removed before the needle put inside the catheter.	60

- Figure 4-3** The sample sparing assay work-flow for obtaining multiple biomarkers from 20  $\mu$ L of whole blood. 62
- Figure 4-4** Data of 16 mice with multi-parametric time series profiling. Mice blood was drawn at -1, 6, 24, 48, 72, 144 hours after the CLP procedure. The last time point plotted at 154 hours indicate data from the heart at 144 hours. (a) The platelet counts. (b) The white blood cell counts. (c) The neutrophil-to-lymphocyte ratio. (d) The neutrophil counts deduced by b and c. (e) The activated (Ly6G<sup>+</sup>CD18<sup>+</sup>) neutrophil counts deduced by d and f (f) The activated (Ly6G<sup>+</sup>CD18<sup>+</sup>) neutrophil percentage (g) The lymphocyte counts deduced by b and c (h) The level of IL-6 in plasma (in logarithmic scale) (i) The level of IL-10 in plasma (in logarithmic scale) 64
- Figure 4-5** Comparison of survivors and non-survivors with multi-parametric time series profiling (N = 24, for all 75% ligation, 2 holes mice). At 24 hours, 5 parameters have significant difference ( $P < 0.05$  under both Mann-Whitney U test and Student's t-test with Welch's correction). However there is no statistical significance at other time points. 65
- Figure 4-6** Correlation plot between parameters at 24 hours after CLP procedure. The number on each box indicates the correlation coefficient of the column parameter and the row parameter. Given the 24 mice,  $R > 0.405$  or  $R < -0.405$  will correspond to p-value  $< 0.05$  (two-tailed probability),  $R > 0.47$  or  $R < -0.47$  will correspond to p-value  $< 0.01$  (two-tailed probability). 66
- Figure 4-7** Correlation plots between 6 hour data and 24 hour data. The number on each box indicates the correlation coefficient of the column parameter and the row parameter. Given the 24 mice,  $R > 0.405$  or  $R < -0.405$  will correspond to p-value  $< 0.05$  (two-tailed probability),  $R > 0.47$  or  $R < -0.47$  will correspond to p-value  $< 0.01$  (two-tailed probability). 67
- Figure 4-8** (a) Monitoring sepsis progression in a CLP mouse model with IDS leukocyte profiling and flow cytometry granulocyte profiling. (b) The percentage of activated cells increases over time in both IDS and flow cytometry (\*  $p < 0.05$  under MW U-test). (c) The correlation between IDS activation percentage and flow cytometry activation percentage ( $R = 0.84$ ,  $R^2 = 0.71$ ,  $p < 0.001$ ,  $N = 19$ ). 69
- Figure 4-9** (a) The neutrophil activation percentage in flow cytometry across time after CLP. (b) The leukocyte activation percentage in IDS across time after CLP. (c) The correlation between the flow cytometry activated neutrophil percentage and IDS activated leukocyte percentage. ( $R^2 = 0.0567$ ) 70
- Figure 4-10** Comparison of the activation level of (a) IDS leukocytes activation percentage and (b) Flow Cytometry neutrophil activation percentage between survivors (Blue) and non-survivors (Red). 70
- Figure 4-11** IDS scatter plot of Syto 64 mean intensity and iso-dielectric point (IDP). Putative neutrophils have higher Syto 64 mean intensity and larger IDP while putative lymphocytes have smaller Syto 64 mean intensity and lower IDP. The green gate indicates the threshold for leukocyte activation. 71
- Figure 4-12** (a) IDP distribution of PMA activation of neutrophils with different durations. (b) Overlay the PBMCs population with the neutrophil profiles. 72
- Figure 4-13** The gating for IDS includes three parts. The left most part are cells with highest conductivity (likely activated leukocytes). The middle part contains cells with medium conductivity (likely lymphocytes with slightly activated neutrophils). The rightmost part contains cells with lower conductivity (likely the non-activated neutrophils). 73
- Figure 4-14** Comparison between IDS 3parts electrical profiling with the hypothetical flow cytometry parameters. (Red: Survivors, Blue: Non-survivors) 73
- Figure 5-1** The summary of critically-ill patients' outcomes. 77

<b>Figure 5-2</b>	<b>The neutrophil activation levels of IDS, CD66b, CD11b, and CD18 for two patients with sepsis who were treated with antibiotics from Day 0.</b>	<b>79</b>
<b>Figure 5-3</b>	<b>The correlation matrix between average IDPs, CD66b, CD11b, and CD18 on neutrophils. Numbers in the corners are correlation coefficients (Red indicates p-value &lt; 0.05).</b>	<b>81</b>
<b>Figure 5-4</b>	<b>(a) Comparison of surface expression of neutrophils from the healthy donors versus critically-ill patients (the value is the average and the error bar is the standard deviation) (b) Comparison of expression ratio of surface expression under treatment with plasma, plasma +fMLP, and plasma + PMA.</b>	<b>82</b>
<b>Figure 5-5</b>	<b>CD66b expression on neutrophils from patients.</b>	<b>83</b>
<b>Figure 5-6</b>	<b>CD11b expression on neutrophils from patients.</b>	<b>83</b>
<b>Figure 5-7</b>	<b>CD18 expression on neutrophils from patients.</b>	<b>84</b>
<b>Figure 5-8</b>	<b>Integrated IDS system with inertial sorter. (a) A spiral inertial microfluidic sorter isolates leukocytes, and stores them in an injection loop (Load mode).The injection loop then pushes cells into the IDS device for enumeration and electrical characterization (Inject mode). (b) Comparison of leukocyte activation level between input, after spiral sorter, after RBC lysis buffer, and after PMA treatment (positive control). Spiral sorter has smaller effect on activation than RBC lysis buffer. (c)The spiral sorter removes 90 % RBCs while recovering 90 % of WBCs.</b>	<b>86</b>
<b>Figure 5-9</b>	<b>Continuous monitoring of electrical profile of human leukocytes by IDS. The human leukocytes were separated from spiral sorter and measured IDS every 30 minutes.</b>	<b>86</b>
<b>Figure 5-10</b>	<b>Image of an integrated system. The injection loop connects spiral device and IDS.</b>	<b>87</b>

## List of Tables

<b>Table 1-1 The definition of systemic inflammatory response syndrome (SIRS) (Bones et al. 1992[2])</b>	<b>14</b>
<b>Table 1-2 Biomarkers for diagnosing sepsis</b>	<b>16</b>
<b>Table 3-1 The parameter values and literature source of double shell electrical model of human neutrophil. This table is modified from Griffith et al. [37].</b>	<b>53</b>
<b>Table 3-2 The change in IDPs at different frequencies under (1) volume increase (2) cytoplasmic conductivity increase (3) nuclear membrane disintegration (4) membrane capacitance increase (5) membrane conductivity increase (blue: non-activated, red: activated). The five black lines indicate 1 MHz, 2 MHz, 5 MHz, 10 MHz, and 15 MHz.</b>	<b>55</b>
<b>Table 5-1 Different treatments for neutrophils before the measurement in flow cytometry.</b>	<b>76</b>
<b>Table 5-2 The three surface markers for quantifying neutrophil activation with flow cytometry.</b>	<b>77</b>
<b>Table 5-3 Summary of blood test of 10 suspected septic samples (with 1 healthy control).</b>	<b>78</b>
<b>Table 5-4 Suspected human septic patients with IDS raw data.</b>	<b>80</b>

## Chapter 1 Introduction and background

This thesis describes the development of a rapid electrical characterization tool for monitoring leukocyte activation, and then its application for monitoring sepsis progression. This chapter first gives an introduction of sepsis and the motivation for monitoring immune status. Secondly, we point out evidence that supports that leukocyte activation can be important in sepsis, different ways of measuring leukocyte activation, and why we chose electrical methods. Lastly, we review different electrical characterization methods and how they were used in experiments of leukocyte activation.

### 1.1 Sepsis

Sepsis is an uncontrolled systemic immune response to invading pathogens. It is a potentially lethal condition that has a 30~50% mortality rate with 18 million patients suffering worldwide yearly [1]. Traditional sepsis diagnosis is based on systemic inflammatory response syndrome (Table 1-1) in addition to clinical signs of infection with a pathogen. However, the diagnosis of sepsis is not always straightforward, especially in the intense care unit (ICU). Patients in the ICU usually have other clinical issues that might have overlapping symptoms with sepsis. Currently, most suspected patients with sepsis are treated with antibiotics due to the high risk of increased mortality if infection is not treated early, resulting in the growing drug resistance of bacteria and the declining antibiotic treatment efficacy. Despite killing the pathogens, some patients still die as a result of multi organ failure or immune suppression due to an imbalanced immune response. In this section we discuss two current problems in sepsis: (1) growing antibiotic resistance and (2) lack of correct immune therapy, and we describe how measuring leukocyte activation may help in solving them.

Table 1-1 The definition of systemic inflammatory response syndrome (SIRS) (Bones et al. 1992[2])

<b>Systemic Inflammatory Response Syndrome (SIRS) = Two or more of the following four conditions</b>	
<b>Conditions</b>	<b>Details</b>
<b>Abnormal temperature</b>	Hyperthermia (> 38°C) or hypothermia (< 36°C)
<b>Abnormal heart rate</b>	Tachycardia (> 90 beats/min)
<b>Abnormal respiration rate</b>	Tachypnea (> 20 breath/min) or PaCO <sub>2</sub> < 32mmHg
<b>Abnormal white blood cells</b>	Leukocytosis (> 12,000 cells/mm <sup>3</sup> ) or leukopenia (< 4,000 cells/mm <sup>3</sup> ) or presence of immature neutrophils "bands cells" (>10%)

#### 1.1.1 Sepsis progression

Sepsis occurs when the normal host response to an infection becomes exaggerated and then dysregulated. The infection can be due pathogens such as bacteria, viruses or fungi. The infection may result in vasodilation that may disrupt blood flow to the brain or kidneys and lead to organ failure. In certain cases, serious hypotension (low blood pressure) may cause tissue lack of perfusion and irreversible injury to end-organs. Figure 1-1 illustrates the progression of sepsis. The mortality rate increases rapidly with severity of sepsis. Typically, sepsis is identified through SIRS and signs of infection such as local symptoms of documented or suspected pneumonia, suspected meningitis, suspected urine tract infection, etc. Sepsis develops into severe sepsis if the patient has

failure of one or more organs. The patient is identified as having septic shock if the patient has refractory hypotension as well.

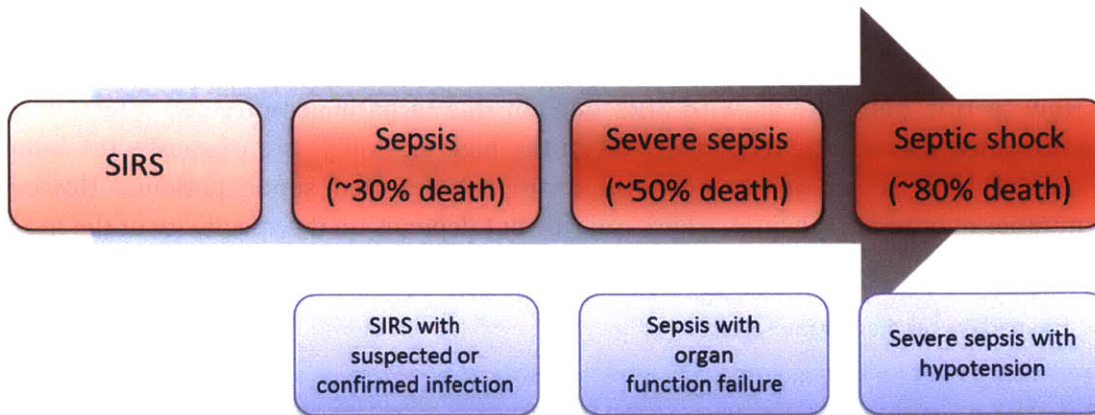


Figure 1-1 The progression of sepsis. The mortality rate world-wide is high and increases with severity of sepsis (up to 30% for sepsis, 50% for severe sepsis, and 80% for septic shock). The mortality rate is estimated by Jawad et al., 2012[3]. One older study with U.S. data done by Pittet et al. has lower mortality rates (SIRS: 7%, sepsis: 16%, severe sepsis: 20% and septic shock: 46%) [4].

Hypotension results from increased vascular permeability when macrophages and neutrophils begin to massively produce pro-inflammatory cytokines and reactive oxygen species (ROS). On the other hand, the anti-inflammatory process may happen at the same time, which involves altered monocyte antigen presentation, decreased lymphocyte proliferation and function and increased apoptosis. The systemic deactivation of the immune system is called compensatory anti-inflammatory response syndrome (CARS). This resulting immuno-depression may increase the risk of nosocomial (hospital-acquired) infections. The immune status of sepsis is a dynamic process and thus makes the decisions behind immunomodulation therapy difficult. There is still an essential need for developing tools for monitoring sepsis progression to help evaluate when and what kind of immunomodulation should be applied. Leukocyte activation plays a key role in immunopathogenesis of sepsis. It is responsible for eliminating pathogens, stimulating tissue, and organ function failures. In addition, it is temporally regulated and cell type specific. Even though the peripheral venous leukocyte counts and differential white blood cell counts are commonly ordered for suspected septic patients, the state of leukocyte activation is still not constantly probed. Being able to monitor progression of leukocyte activation may be valuable to understand the immune status of septic patients.

### 1.1.2 Diagnostic and prognostic markers of sepsis

Currently, blood culture is the gold standard for finding pathogens in the blood of suspected septic patients. However, blood cultures may take up to 48 hours to show positive results. Negative results do not exclude the possibility of having sepsis. Delayed antimicrobial therapy correlates with increasing mortality rate. Timely effective antimicrobial treatment is directly linked to the survival rate of hypotensive shock [5]. The risk of delayed therapy is too high such that antimicrobial therapy is usually applied to a suspected patient regardless of the blood culture result. The widespread and extensive use of antimicrobial drugs has resulted in a serious and growing

drug resistance problem. An earlier and specific diagnostic marker of sepsis has been sought after but does not currently exist. The clinical challenges of sepsis diagnosis are

- (1) How to identify sepsis early enough to decrease the mortality rate with early treatment? The biomarker needs to show the signal early in the sepsis progression.
- (2) How to rule out patients with SIRS but not due to pathogen-directed infection to avoid unnecessary antibiotic treatment? Given the high mortality rate of sepsis, the biomarkers require high sensitivity in order to avoid non-detected septic patients. However, the number of patients the biomarkers can rule out depends on the specificity of the marker.
- (3) How to identify pathogens earlier for targeted antimicrobial drugs?

Table 1-2 Biomarkers for diagnosing sepsis

Markers	Equipment	Time (clinical)	Diagnostic value	Clinical usage
<b>Complete Blood Count(CBC) with differential [6]</b>	Hematology Analyzer	~1 hour	WBC may be elevated or suppressed in severe infection/sepsis and >10% band forms may be seen in the systemic inflammatory response and/or sepsis	Common
<b>CRP (C-Reactive Protein) [7]</b>	ELISA	~1 hour	Elevated in inflammatory states.	Uncommon
<b>Procalcitonin(PCT) [8]</b>	ELISA	~1 hour	Can be useful in distinguishing bacterial from other infections. Has been used for ruling out patients who do not have sepsis	Uncommon
<b>Erythrocyte Sedimentation Rate (ESR) [9]</b>	Automated ESR machine in lab	~1 hour	Increases with inflammation; also can increase in pregnancy.	Uncommon
<b>Cytokines(TNF-<math>\alpha</math>, IL family, HMGB1) [10-12]</b>	ELISA	~1 hour	Mediators of the sepsis response	~Never
<b>Surface markers: CD14, CD40 CD64 [13], mHLA-DR</b>	Clinical Flow cytometry	~1 hour	CD64 upregulated in response to inflammatory cytokines. Has variable sensitivity and specificity in sepsis diagnosis and prognosis. Potential reason for the variation could be natural activation of leukocytes.	~Never
<b>PCR of bacterial DNA [14]</b>	SepsiTest (Roche)	4 hours	SepsiTest (Roche) has 25-41 common bacterial and fungal pathogens; has specificity in sepsis diagnosis but unclear sensitivity	Rare

Table 1-2 lists a few diagnostic tests related to sepsis. The complete blood count (CBC) test is a very common blood test in intensive care units and includes information about white blood cell counts



(WBC), immature white blood cell counts (band cells), absolute neutrophil count (ANC), etc. [6]. C-reactive protein (CRP) is known to increase with inflammation but it is not very specific to sepsis [7]. Procalcitonin (PCT) has been found to be more specific to bacterial infections causing sepsis and therefore has been used to guide therapy (i.e., shorten the antibiotic treatment [8]) but is not universally used. Cytokines are part of the host acute inflammatory response to microbial invasion or tissue injury. For example, the levels of IL-6, TNF- $\alpha$  and IL-8 in serum have been shown to correlate with sepsis mortality [10-12]. The multiplex-based cytokine measurements have also been used to evaluate the inflammatory response [15]. Cell activation plays an important role during the inflammatory response. For example, the CD64 marker on neutrophils has been found to be promising in diagnosing sepsis with high sensitivity and specificity for bacterial and viral infection, but is not widely available [13]. Other existing tests for detecting inflammation includes erythrocyte sedimentation rate (ESR) and plasma viscosity (PV) which are easy to measure but non-specific [9]. Accurate pathogen identification by bacterial PCR can in theory narrow down the source of infection and precision treatment can be applied to avoid development of drug resistance; Roche developed the SepsiT<sub>est</sub> to identify 25-41 different bacterial or fungal pathogens [14] but also has not been widely applied.

### **In search of better sepsis biomarkers**

Pierrakos et al. reviewed research into sepsis biomarkers studied as of 2009 Feb [16]. There are more than 170 potential biomarkers that have been studied clinically and experimentally for septic patients. There are 64 studies with data from more than 50 people, 83 studies with 20 to 50 patients and 40 studies with fewer than 20 patients. Most of the biomarkers examined are prognostic markers or correlated with APACHE (Acute Physiology and Chronic Health Evaluation) score or Sequential Organ Failure Assessment (SOFA) clinical scoring systems. Only a few of them can diagnose sepsis. Out of the 178 potential markers, only 5 of them have shown both sensitivity and specificity greater than 90% for diagnosing sepsis: CD11b, CD64, IL-12, IP-10, and PLA2-II. It is interesting that two of them come from neutrophil surface markers.

Other than sensitivity and specificity, the cost of the test, the turnaround time of a test, and the possibility of doing multiple test across different time points are all important factors for use in clinics or at the bedside. According to the ASSURED criteria from World Health Organization [17], an ideal diagnostic test should be Affordable, Sensitive, Specific, User-friendly, Rapid and robust, Equipment-free or minimal equipment necessary and Deliverable to end-users. Considering all the criteria, there is no single marker good enough to be routinely used in the clinical settings. Therefore, an opportunity exists for developing a rapid diagnostic test.

### **Leukocyte activation in sepsis**

Leukocytes (immune cells) defend our body against pathogens. Leukocytes integrate many signals from the immune system, thus making cell-based diagnosis or staging of sepsis promising. The physical properties of leukocytes such as size, electrical properties, granularity, can be measured with hematology analyzers using so-called VCS technology (volume, conductivity and scatter) such as Coulter LH Series. Research found that the VCS properties of leukocytes can change due to activation. For example, average volume of neutrophil increases and average light scatter of

neutrophil decreases in acute bacterial infection[18]. In addition, some hematology analyzers such as System XE-2100 are capable of quantifying immature granulocytes which can also be used as a measure of infection [6].

In sepsis, the total leukocyte concentration and the band cells concentration have already been used as part of the current SIRS criteria. However, the activation state of leukocyte is missing from the current criteria which may be similarly important and provide complementary information. As we mentioned earlier, 2 out of 5 sepsis biomarkers with potential markers are related to neutrophil activation. To be more specific, there are different aspects of neutrophil activation. Figure 1-2 summarizes the functional response of neutrophils to invading bacteria [19]. Neutrophils, the majority of circulating leukocytes in healthy humans, are reduced in number in the circulation in the early stages of bacterial or fungal infections. Neutrophils are recruited to the infection site by rolling on the surface of activated endothelial cells with the assistance of the selectin family of ligands, followed by deformation and firm adhesion. They deform further and infiltrate through vessel walls and phagocytose the bacteria. During the activation process, neutrophils perform several antimicrobial functions including degranulation, reactive oxygen species generation and neutrophil extracellular trap formation to kill the invading pathogens. Degranulation is a process of neutrophil (or other granulocytes) releasing the granules which are vesicles encapsulating antimicrobial contents. Reactive oxygen species such as superoxide come from oxidative burst of neutrophils via NADPH oxidase. The reactive oxygen species eventually result in hypochlorite generation which is import in destroying bacteria. The neutrophil extracellular trap (NET) is a relative new concept of how neutrophil to kill bacteria. NETs form when neutrophils are stimulated and release the DNA with chromatin and granules to form extracellular fiber networks which can bind to, and kill bacteria [20].

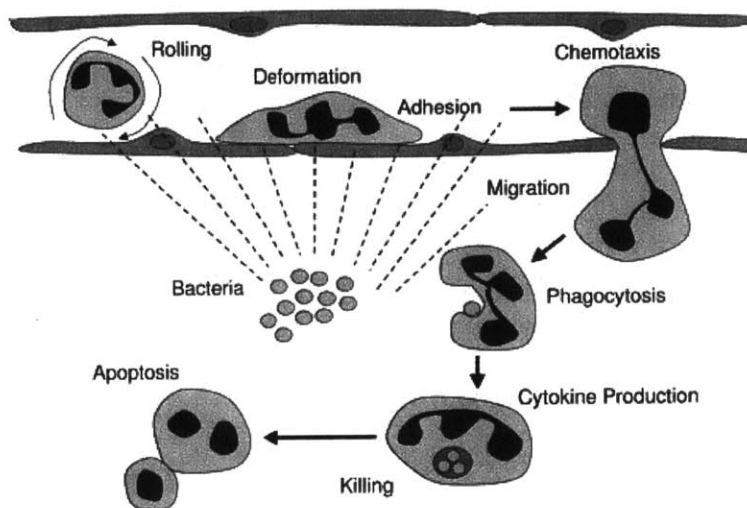


Figure 1-2 Neutrophil functional responses during recruitment to a site of bacterial infection. The broken lines represent chemoattractants generated at the site of infection that activate the endothelium and capture the intravascular neutrophils. The neutrophils flatten and adhere to the endothelium, migrate out of the vessel towards the infectious site, phagocytose and kill the bacteria, secrete cytokines to recruit other inflammatory cells and eventually undergo programmed cell death (apoptosis). The figure and caption are adapted from [19].

There are many neutrophil activation assays to qualitatively or quantitatively measure the activation levels of neutrophils, or more generally, the neutrophil's functions. Neutrophil Methods and Protocols [21] listed experimental details of these assays, including calcium activity, cytoskeletal actin (F-actin), adhesion and aggregation, chemotaxis, phagocytosis, reactive oxygen species generation, degranulation, and gene expression and transcription factors.

Conversely, neutrophil activation has been pointed out as one of the major causes of organ function failure. There is a balance in all hosts of antimicrobial activity that is beneficial to clearing the infection, versus anti-host effects of activated neutrophils that might be detrimental to the host. Identifying that balance for each host at each point in time during infection represents a major challenge in sepsis therapeutics. While the current standard of care for sepsis represents antimicrobial therapy, source control to eliminate the infectious pathogens, and hemodynamic support with fluids and vasopressors, there clearly exists a void in targeted therapeutics for sepsis. Recently, Weber et al. [22] utilized immunosuppressive therapy using IL-3 inhibitors, showing that a reduction in activated neutrophils was related to less organ function failure and better survival outcome. Measuring neutrophil activation in sepsis thus has potential as a novel approach for diagnosis, prognosis, and monitoring sepsis progression.

Part of the goal of this thesis is to evaluate the feasibility of using electrical properties of neutrophils as sepsis biomarkers. Measuring electrical properties of the neutrophils can be affordable, requires minimal equipment, and is rapid and robust. It may be sensitive for sepsis diagnosis but it is less likely to be specific for sepsis. The reason is that neutrophil is the key player for innate immune response which does not have high selectivity as adaptive immune response. It may become activate in chronic inflammation or cancer [23, 24]. To be specific to sepsis, the marker needs to distinguish infection versus inflammation. However, we will present data supporting the concept that neutrophil activation is feasible as part of a panel of parameters for diagnosis, prognosis, or staging of sepsis.

### **1.1.3 Treatment of sepsis**

Current standards of care for sepsis management are antimicrobial therapy, elimination of the infectious source, and adjunctive therapy [25]. If the pathogens are not known at the time of patient presentation, broad spectrum antibiotics are recommended, as each hour that inappropriate antibiotics are administered results in increasing mortality from sepsis. The results of blood cultures help narrow the antibiotic treatment after 24-48 hours. Other sepsis treatment focuses on adjunctive treatment such as resuscitation with fluids and vasopressors to maintain blood pressure due to vasodilation, and organ support for critically-ill patients with organ failure.

Despite the eradication of pathogens, the mortality can still be high. Research into improving sepsis treatment outcomes has pointed to several immunosuppressive therapies. The claims for applying the immunosuppressive therapy were:

- (1) Patients with elevated target markers are more likely to die.
- (2) Blocking target markers in animals improved survival.
- (3) Injection of target markers into animals to induce death and organ injury.

Despite strong rationale, several immunosuppressive therapies which targeted inflammation markers such as tumor necrosis factor alpha (TNF- $\alpha$ ) and interleukin 1 beta (IL-1 $\beta$ ) failed in human clinical trials [26], even though they had proved beneficial in murine studies. Recently, the only FDA approved drug for sepsis, Xigris (activated protein C), was pulled from the market in 2011 after 10 years of clinical trials [27] because it did not show consistent survival benefits and increased the risk for significant bleeding as a side effect.

The approach of modulating inflammatory cytokines may ultimately be helpful; however, the disappointing clinical trials might be due to imprecise timing, imprecise dosages, or incorrect individual cytokines [28]. Understanding the immune status of the patients at a given point in time may be the key to a successful immunomodulation therapy. Being able to monitor the immune status across time may help sepsis treatment in

- (1) Understanding whether immunosuppressive or immune-stimulatory therapy is suitable for the patients.
- (2) Determining the right dose and right time for therapy.
- (3) Examining the effectiveness of the treatment.

An ideal monitoring system should not only measure the target markers but also capture information of global immune status like the cells, cytokines, inflammation sites and other organ functions. Such monitoring system may provide detailed evaluation of treatment effectiveness and detect any potential side effect of the treatment. For example, inhibiting single proinflammatory cytokine may reduce that particular cytokine but measuring the level of that cytokine does not reflect the inflammation status because the level of that cytokine has been modulated. Monitoring multiple parameters is important to retrieve more accurate immune status.

Recently, DARPA initiated a program for novel research on dialysis-like therapeutics (DLT), which is a novel therapeutic strategy to remove pathogens and mitigate overreact immune response with extracorporeal circuits similar to a dialysis machine. Several new research results came out of the project, including extracorporeal circuits for pathogen and toxins removal [29] (spun out as Opsonix), cytokines removal [30], and broad spectrum removal of pathogens and cytokines/toxins [31]. While the effects on mitigating the immune response through DLT and other filtering approaches have proven successful in pre-clinical models of bacteremia and sepsis, the survival benefits still need to be optimized in experimental models. Integrating a leukocyte functional monitoring system with the extracorporeal circuits would bring benefits in understanding the therapy status in real-time, and help to optimize the duration of the therapy and has the potential to change the direction of immunomodulation therapy.

In this thesis, we are developing a tool for monitoring leukocyte activation that can be used alone or easily integrated into a DLT system. Even without integration with the DLT system, a timely bedside assessment of leukocyte activation may increase the success rate of immunomodulation treatment by careful patient selection or at least help understand the treatment effect on individual patients.

#### **1.1.4 Monitoring tools of sepsis**

Currently, most monitoring tools of sepsis focus on clinical parameters in severe sepsis and septic shock patients who are critically-ill. The monitoring tools include the central venous catheter (CVC) for monitoring central venous pressure (CVP) and central venous oxygen saturation (ScvO<sub>2</sub>), mean arterial pressure (MAP), and blood tests for lactate level (4~6 hours) and CRP. The monitored data may alter the medical practice for under certain protocol called bundles. A bundle is numerous medical practices that when implemented as a group are better than individual therapies. For example, Surviving Sepsis Campaign provides 3-hour and 6-hour bundles, and Loma Linda University provides a 24 hour bundles and a sepsis bundle flowchart which provides treatment algorithms used by clinicians as a reference. The goal of the bundles is to provide consistent patients management to create evidence-based guidelines. The Surviving Sepsis Campaign was developed to provide a platform of guidelines and bundles for managing septic patients during critical illness in critical care [32] and improved mortality rate of severe sepsis and septic shock [33]. However, in the clinical setting, the immune-monitoring of sepsis remains an untapped area.

If one successfully develops a tool of immune monitoring, it can be combined with the sepsis bundle to collect time series data to provide the better insight of immunopathogenesis of sepsis and eventually improve the survival outcome by utilizing evidence-based medicine.

#### **1.1.5 Recent advances in monitoring leukocyte activation in sepsis**

Recently in the microfluidic community, researchers have been trying to develop miniaturized neutrophil activation assays in Lab-on-a-Chip platform, including the following.

##### **CD64 markers on neutrophils**

LeukoDx is designing a point-of-care flow cytometry method. One of the first applications is to quantify CD64 on neutrophils for sepsis diagnosis. They utilize a microfluidic cartridge to enable rapid quantification of CD64 markers on neutrophils. As mentioned in 1.1.2, CD64 on neutrophils has been studied in sepsis and found both sensitive (86%) and specific (87%) as estimated from 17 different studies [13].

##### **Characterizing chemotaxis of neutrophil**

A group at the Massachusetts General Hospital developed a microfluidic device to study chemotaxis of neutrophils [34]. They found that neutrophils from patients after major burns have confused chemotaxis behavior, termed spontaneous neutrophil migration. They quantify this behavior and calculate a score that correlates with the timing of sepsis in burn patients.

##### **Deformability cytometer for measuring neutrophil activation**

Neutrophil activation may change nuclear and cytoskeletal structures thus result in quantifiable changes in deformability. Recently, the startup CytoVale aimed to tackle the sepsis problem by measuring such changes for early detection of sepsis. CytoVale spun out from the UCLA Di Carlo Laboratory, leveraging the inertial focusing and hydrodynamic stretching to quantify mechanical properties of cells [35]. Cytovale claimed to measure >10 biophysical cell markers in 2000 cells per second, enabling new mechanomic characterization of cells.

In this thesis, we aim to use a different approach to measure neutrophil activation. Supported by early literature on neutrophil electrophysiology [36] and electro-rotation experiments [37], we believe there are quantifiable changes in electrical properties during neutrophil activation. Electrical properties are one of the intrinsic properties that can be easily measured without any labels and additional chemicals. Therefore, quantifying electrical properties of activated neutrophils may be promising as a potential marker for rapid diagnosis, prognosis, and continuous monitoring of sepsis.

## **1.2 Electrical characterization of leukocytes**

Electrical properties of the cells, especially dielectric properties of membrane and cytoplasm have been used in medical application and scientific studies [38]. We describe some important methods of characterizing dielectric properties of cells below

### **1.2.1 Impedance based electrical characterization of cells**

The Coulter Counter principle was the most successful method to measure the electrical properties of single cells. It measures the impedance of two reservoirs with a connected aperture. The impedance of a cell is usually smaller than the media at DC or low frequencies. When the small particles go through the aperture, the impedance changes are proportional to the size of the particles. In commercialized machines, cells are usually only scanned in DC or low frequency to make a size measurement. Only a few machines provide radio frequency measurements for quantifying cytoplasm conductivity [18]. However, the exact frequency used in high end machines is not public information to our knowledge. Morgan et al. developed a microfluidic impedance cytometer based on this principle and can distinguish monocytes, granulocyte, and lymphocytes with impedance measurement of two frequencies [39]. The impedance cytometer used two lock-in amplifiers to measure the real-parts and imaginary parts of both high frequency (1707 kHz) and low frequency (501 kHz). The impedances of lymphocytes at 501 kHz are smaller than the ones of granulocytes and monocytes. The impedance ratio between 1707 kHz and 501 kHz can slightly distinguish monocytes and granulocytes but not too much (granulocytes with higher size-normalized impedance than monocytes). Without leveraging the light scatter difference or density difference, electrically differentiating monocytes and granulocytes can be difficult. In addition, detecting activation of eosinophil [40] using impedance measurement has also been reported. However, the main drawback of an impedance based method for AC is the complicated electronics. Even though Analog device offers IC AD5933 with single chip programmable impedance analysis using direct digital synthesizer (DDS) and fast Fourier transform (FFT), the sampling rate of the impedance is only 500 Hz even after integrated system with a field-programmable gate array system.[41]. To build a Coulter Counter with high speed counting and sizing, the mixers for modulation and demodulation, the circuit of peak detection, and peak quantization should also be included.

### **1.2.2 Electro-rotation based electrical characterization of leukocytes**

Electro-rotation is a technique to study the electrical properties of particle by measuring the rotation rate of the particle under a rotating electric field. Normally, the rotation rates of the particle with respect to different frequencies are recorded, forming a spectrum that can represent the electrical fingerprint of a single cell.

The electro-rotation can probe the dielectric response at different frequencies for a single cell, but only very slowly. Hu et al. applied electro-rotation to study the electrical properties of lymphocytes from mice spleen after lipopolysaccharide (LPS) with 72 hours of LPS or concanabalin A [42]. They found an increase in membrane capacitance and a size increase. Griffith et al. studied neutrophil activation and found potential cytoplasm conductivity decrease (more details in 3.1.2) [37].

### **1.2.3 Patch-clamp based electrical characterization of leukocytes**

Patch clamping has also been used to study membrane potentials, and ion channels [43]. It provides high temporal resolution of electrical activity for a single cell. Interestingly, it has also been used for studying the neutrophil calcium flux and respiratory burst (more details in 3.1.1). However, like electro-rotation, it is also limited by the throughput. In addition, since the cells like neutrophils migrate on surfaces, the cells might move around the micropipette tips [36].

### **1.2.4 Dielectrophoretic based electrical characterization of leukocytes**

Dielectrophoresis (DEP) is forced-based method for not only electrical cell characterization but also electrical cell separation [44, 45]. It has been used to resolve different cellular identities in heterogeneous populations and to monitor cell state without extrinsic biomarkers [46].

In the application of blood cells, Peter Gascoyne's group has separated T- and B- lymphocytes, monocytes, and granulocytes using DEP field-flow-fractionation (DEP-FFF) [47]. The DEP-FFF method separates cells by levitating cells with negative DEP force. Cells with different electrical properties and density ratio levitate at different heights and thus become separable with a transverse flow. They used DEP-FFF to separate of cancer cells from blood [48], and to enrich CD34+ cells from peripheral blood stem cell harvests [49]. Recently, the DEP-FFF method has been used for characterizing different NCI-60 cancer cell lines [50] and isolating circulating tumor cells [51] by the same group. ApoCell has developed a product ApoStream using a similar platform to commercialize this technology. The goal is to fill the niche of anti-body independent circulating tumor cell isolation. However, the DEP-FFF method depends on not only the electrical properties but also the density of the cells, which makes the electrical characterization results hard to interpret for other platforms.

Ronald Pethig's group has studied the electrical properties of human embryonic stem cells and their differentiating derivatives [52] using cross-over frequency methods. The cross-over frequency is the frequency that between positive DEP and negative DEP. At the cross-over frequency, there is no net DEP force acting on the cells. The method requires cells to soak in low conductive media such as sucrose and dextrose for the entire characterization time, which may alter the electrical properties of cells. The method is not continuous. It operates in batches with mediocre throughput (hundreds of cells per experiment).

Han et al. used lateral electrodes to deflect white blood cell subpopulations with DEP [53]. However, their operation conditions separate cells based on size instead of electrical properties of cells. Our group has previously introduced isodielectric separation (IDS) as a continuous method to measure the electrical properties of single cells independently of their size [54]. The IDS method offers continuous electrical characterization of cells in a size insensitive manner. Therefore, it is one of the promising DEP technologies for quantifying the electrical changes instead of size changes. In

addition, we also developed another method, DEP spring [55], to rapidly screen the electrical properties of cells at different frequencies and conductivities. In this method, we can observe the effects from both size-based and electrical changes of cells. In this thesis, we adapted IDS and DEP spring to assay the electrical properties of neutrophil activation for monitoring sepsis.

### 1.3 Thesis overview

In this thesis, there are engineering goals, biological goals, and clinical goals. We are building a system to enable rapid electrical profiling of leukocytes. The system also results in an improved experimental platform for studying the biophysical changes that underlie leukocyte activation (with proper inhibition). Finally we present data measuring neutrophil activation in a preclinical murine sepsis model and human patients with suspect sepsis to start to assess clinical applicability of our technology.

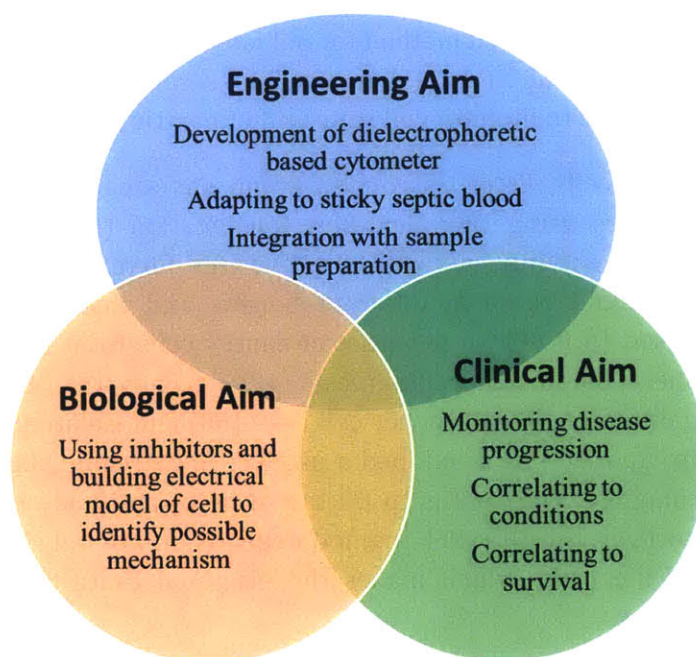


Figure 1-3 The three type of aims in this thesis: Engineering Aim, Biological Aim, and Clinical Aims.

In Chapter 2, we introduce the methods and systems we use in this thesis, addressing the challenges of throughput and fouling septic blood and our solutions to them. In Chapter 3, we use the system to develop a study on human neutrophil activation *in vitro*. We build a mathematical model to explain the potential changes and we design a set of experiments to understand the mechanism of the electrical changes. In Chapter 4, we apply the system to monitor sepsis progression in a murine model. We correlate leukocyte activation with multiple parameters at different time points and correlate leukocyte activation to survival outcome. In Chapter 5, we start a pilot study using blood *ex vivo* from patients with suspected sepsis and describe the integration with an inertial spiral sorter for sample preparation. In Chapter 6, we summarize the thesis contribution and provide on-going or possible future directions.



## Chapter 2 Dielectrophoretic characterization system

Measuring subtle changes in electrical properties of cells is difficult because an ideal system needs to provide enough sensitivity as well as enough speed to provide statistically meaningful measurements. This chapter describes the theory of dielectrophoresis and its application of characterizing the electrical properties of cells. More importantly, we describe the two complimentary high throughput methods we developed to characterize the electrical properties of cells, namely Iso-Dielectric separation (2.2.2) and Dielectrophoretic spring (2.2.1). In Chapter 3, we use the two methods to characterize the electrical changes of neutrophil activation. During the process of characterizing neutrophil activation, we discovered the drawback of the older system, which is that the activated neutrophils are very sticky and clog the channel easily. In 2.3, we describe the fabrication of the microfluidic devices and the technical improvements used to create a new device, which increase throughput and ameliorate fouling. In 2.4, we describe how we build the automated system that surrounds the microfluidic device to perform consistent and robust measurements.

Portions of this chapter are adapted from Su, H.-W., J. L. Prieto and J. Voldman (2013). "Rapid Dielectrophoretic Characterization of Single Cells Using the Dielectrophoretic Spring." *Lab on a Chip* 2013(20): 4109-4117 and my Master's thesis. The design and implementation of the device and system is in collaboration with Javier Prieto.

### 2.1 Dielectrophoresis theory

#### 2.1.1 Dielectrophoretic force and Clausius-Mossotti (CM) factor

Inside a static electric field ( $\mathbf{E}$ ), the particle and the surrounding media are both polarized to form a dipole moment. The effective induced dipole moment ( $\mathbf{p}$ ) is either parallel or anti-parallel to the applied field (Figure 2-1) [56]. If the electric field is uniform, there is no net force acting on the particle. However, in a spatially non-uniform electric field, the dielectrophoretic (DEP) force will either move the particle toward stronger electric field (positive DEP) or toward the weaker electric field (negative DEP). The direction of the force depends upon the electrical properties of the particle and medium.

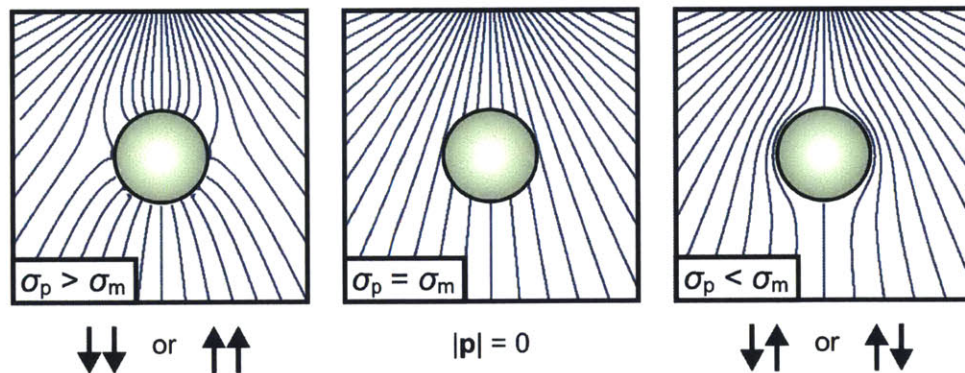


Figure 2-1 Polarization of a particle in an external non-uniform electric field. For relatively conductive particles (left), the dipole moment and electric field align parallel to each other, leading to lower potential energy at higher electric field strengths, known as p-DEP. For relatively insulating particles (right), the dipole moment and external field are anti-parallel, causing particles to be expelled from regions of higher field intensity, known as n-DEP. If the electrical properties of the particle match those of the medium (center), the polarization vanishes and there is no preferential motion towards higher or lower field strengths. Adapted from [57].

In an AC electric field, the first order time-average DEP force is approximated as:

$$\overline{F_{DEP}} = (\overline{p \cdot \nabla}) \overline{E} = 2\pi R^3 \varepsilon_m \operatorname{Re}[CM(\omega)] \nabla E^2 \quad (2-1)$$

where  $R$  is the particle radius,  $\varepsilon_m$  is the permittivity of the media,  $E$  is the amplitude of the electric field,  $\omega$  is the frequency, and  $CM(\omega)$  is the Clausius-Mossotti(CM) factor which is given by

$$CM(\omega) = \frac{\underline{\varepsilon}_p - \underline{\varepsilon}_m}{\underline{\varepsilon}_p + 2\underline{\varepsilon}_m} \quad (2-2)$$

where  $\underline{\varepsilon}_p$  and  $\underline{\varepsilon}_m$  are the complex permittivity of the particle and media, respectively. The sign of the  $\operatorname{Re}[CM(\omega)]$  determines the force direction. Due to the mathematical formulation of CM factor, the real part of the CM factor is always between -0.5 and 1.

The media can be considered as a loss-free capacitor in parallel with a resistor. Therefore, the complex permittivity of the media  $\underline{\varepsilon}_m$  is a combination of permittivity and conductivity of the media solution.

$$\underline{\varepsilon}_m = \varepsilon_m + \frac{\sigma_m}{j\omega} \quad (2-3)$$

For example, in phosphate buffered saline (PBS), the media permittivity  $\varepsilon_m$  is  $78.5 \varepsilon_0$  and the media conductivity  $\sigma_m$  is 1.6 S/m. For typical DI (de-ionized) water, the media conductivity  $\sigma_m$  is around 0.01 mS/m. For ideal pure water at room temperature, the media conductivity  $\sigma_m$  is 5.5  $\mu\text{S/m}$ .

The complex permittivity of the particle is determined by the materials comprising the particle. If the particle is composed of a uniform material, the particle can be modeled similarly to the media.

$$\underline{\varepsilon}_p = \varepsilon_p + \frac{\sigma_p}{j\omega} \quad (2-4)$$

For example, for polystyrene (PS) latex beads, the permittivity  $\varepsilon_p$  is  $2\sim 3 \varepsilon_0$  and the conductivity  $\sigma_p$  is composed of two parts: the surface conductivity  $\sigma_s$  and the bulk conductivity  $\sigma_b$ . In theory, the bulk conductivity of micron-to-submicron latex beads is negligible compared to the surface conductivity  $\sigma_s$ , which is inversely proportional to the particle radius  $R$  and proportional to the general surface conductance  $K_s$  ( $\sim 1$  nS for PS beads).

$$\sigma_p = \sigma_b + \sigma_s = \sigma_b + \frac{K_s}{R} \quad (2-5)$$

In the low frequency range, the CM factor mainly depends on the conductivity of the particle and media.

$$CM(\omega) = \frac{(\epsilon_p + \frac{\sigma_p}{j\omega}) - (\epsilon_m + \frac{\sigma_m}{j\omega})}{(\epsilon_p + \frac{\sigma_p}{j\omega}) + 2(\epsilon_m + \frac{\sigma_m}{j\omega})} = \frac{(j\omega\epsilon_p + \sigma_p) - (j\omega\epsilon_m + \sigma_m)}{(j\omega\epsilon_p + \sigma_p) + 2(j\omega\epsilon_m + \sigma_m)} \approx \frac{\sigma_p - \sigma_m}{\sigma_p + 2\sigma_m} \quad (2-6)$$

As a result, for micron size PS beads, the CM factor is positive in low-conductivity media (DI water) and negative in high-conductivity media (ionic solution).

Unlike uniform latex beads, cells have a more complex composition and a different behavior than beads. Dielectrically, the cells are composed of several layers of materials. For example, a typical mammalian cell consists of the cell membrane, the cell cytoplasm, the nuclear membrane, and the nucleoplasm from the outermost layer of the cell to the innermost. Each layer of the cell has distinct dielectric properties.

In order to match the true composition of the cell, the shell model has been developed to simulate the dielectric properties of the cell [58]. The single shell model (a) and double shell model (b) consider the cell to be composed of two and four concentric spherical shell layers of uniform conductivity and permittivity, respectively.

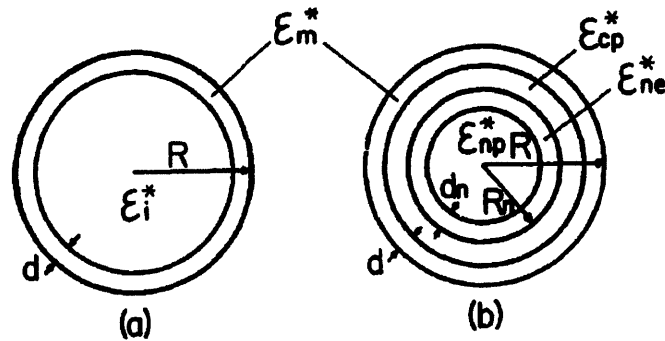


Figure 2-2 Two electrical models of a cell. (a) Single –Shell model. (b) Double-shell model. The cell is composed of concentric uniform layers of different complex permittivity( $\underline{\epsilon} = \epsilon + \sigma/j\omega$ ). The subscripts refer to the following phases: m, plasma membrane; i, inner phase of cell; cp, cytoplasm; ne, nuclear envelope; np, nucleoplasm. The morphological parameters are:  $R$ , outer radius of cell;  $R_n$ , outer radius of nucleus;  $d$ , thickness of plasma membrane;  $d_n$ , thickness of nuclear envelope. Figure adapted from [59].

For the single shell model (a), there are six parameters, including  $R, d, \epsilon_{mem}, \sigma_{mem}, \epsilon_i, \sigma_i$ . The effective complex permittivity of the cell  $\underline{\epsilon}_p$  is given by

$$\underline{\epsilon}_p = \underline{\epsilon}_{mem} \frac{\left(\frac{R}{R-d}\right)^3 + 2\left(\frac{\epsilon_i - \epsilon_{mem}}{\epsilon_i + 2\epsilon_{mem}}\right)}{\left(\frac{R}{R-d}\right)^3 - \left(\frac{\epsilon_i - \epsilon_{mem}}{\epsilon_i + 2\epsilon_{mem}}\right)} \quad (2-7)$$

where the membrane complex capacitance  $\underline{C}_{mem} = C_{mem} + G_{mem} / j\omega$ .  $C_{mem}$  and  $G_{mem}$  are the membrane capacitance and conductance which is derived from  $\epsilon_{mem}/d$  and  $\sigma_{mem}/d$ .

Similarly, the mathematical formulation of equation (2-7) can be recursively done with multiple layers of different material.

Asami *et al.* measured the dielectric properties of mouse lymphocytes and erythrocytes in suspension using dielectric spectroscopy [59]. They fitted the measured complex permittivity  $\underline{\epsilon}_p$  of erythrocytes and lymphocytes with the simulation of single-shell and double-shell model. They extracted out the parameters of the shell model which have been referenced from various publications since then.

### 2.1.2 Re[CM] map and the Iso-dielectric point

From the single shell and double shell model, one can deduce the frequency dependency of the DEP behavior by their mathematical formulations. At lower frequencies, DEP force mainly depends on membrane properties. At higher frequencies, the force mainly depends on the cytoplasm conductivity (and/or the nuclear and cytoplasm ratio for double layer model). DEP force is not only a function of frequency but also a function of electrical properties of the media. The common approach to disturb the DEP response of cell is to change the media conductivity and the frequency. Therefore, we often use 2-D (media conductivity and frequency) Re[CM] maps to explain the dielectric response or the DEP separation of cells. The 2-D Re[CM] map as a function of frequency and media conductivity in Figure 2-3 can help us estimate the magnitude and the sign of the DEP force. In general, for cells, the Re[CM] is usually negative at high conductivity media because the media is more polarizable than the cell.

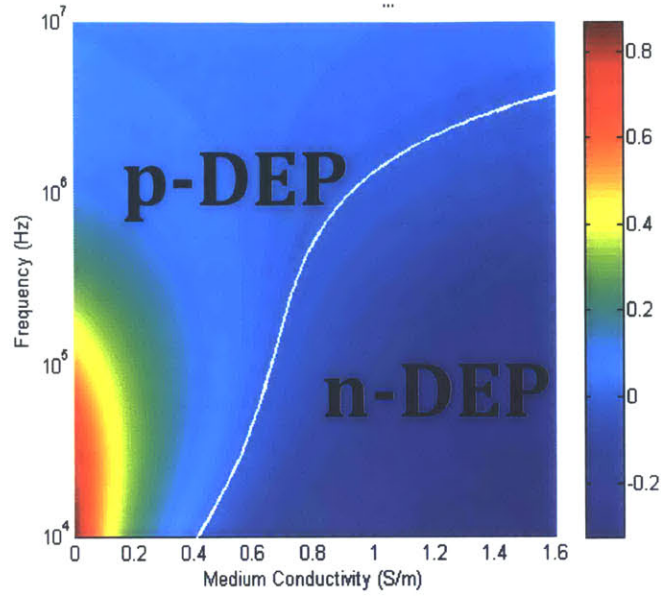


Figure 2-3 The real part of the Clausius-Mossotti factor as a function of the frequency of the external electric field and the media conductivity. The blue area on the right side is the condition where the cell experiences n-DEP force ( $\text{Re} [ CM ] < 0$ ) and the left side shows where the cell experiences p-DEP ( $\text{Re} [ CM ] > 0$ ). The white-line shows the condition where the cell experiences no DEP force ( $\text{Re} [ CM ] = 0$ ). We term any point this line as an Iso-dielectric point (IDP), and the related frequency as the cross-over frequency. The electrical parameters for this figure come from dielectric spectroscopy for human white blood cells [47].

## 2.2 Methods of operation

In 2.1.2, we have introduced the definition of the  $\text{Re}[CM]$  map and the iso-dielectric point (IDP). In this subsection, we will introduce how to use the two methods we developed to measure them. The dielectrophoretic spring is designed to measure the n-DEP region in the  $\text{Re}[CM]$  map [55]. On the other hand, Iso-dielectric separation is designed to characterize or separate cells by their Iso-dielectric point [54]. Both methods can be operated using the same device, which will be described in 2.3 .

### 2.2.1 Dielectrophoretic spring

The DEP spring method consists of using a force-balance model to measure the DEP forces acting on cells and inferring the electrical properties of individual cells in a continuous manner. Cells enter the microfluidic channel and encounter a negative DEP force ( $F_{DEP}$ ) that forms a barrier, deflecting the cells (Fig. 1a). A deflected cell reaches a force balance between the hydrodynamic drag ( $F_{Drag}$ ) force and DEP force and moves along the electrodes. We use  $\delta$ , the *balance position* between the hydrodynamic force and the DEP force in the direction perpendicular to the electrodes, to extract the electrical properties of the particles.

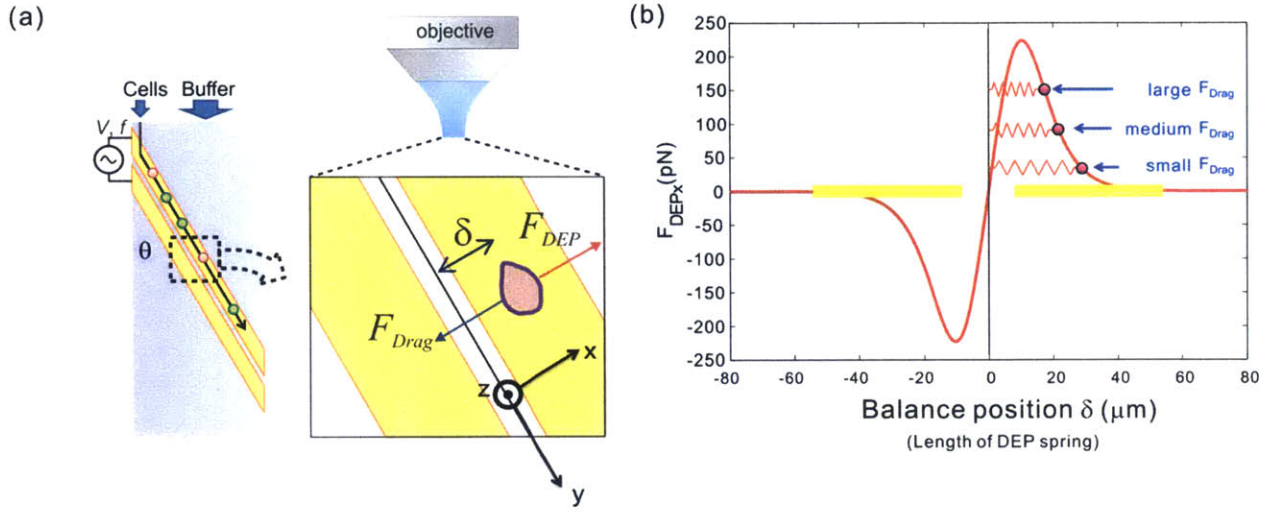


Figure 2-4 (a) The DEP spring method overview. Cells (or other particles) are introduced into the channel along with buffer flow. As the cells flow down the channel they encounter the electrodes where they experience a DEP force (red, inset) that balances the drag force (blue, inset). The equilibrium balance position between the two forces is denoted by  $\delta$ . (b) The DEP force in the  $x$ -direction at different balance positions. The balance position decreases when the applied drag force increases, which represents the length of this nonlinear DEP spring. The DEP spring only holds when the drag force is smaller than the maximum n-DEP force.

The relevant forces acting on the deflected cell are predominantly the DEP force and the hydrodynamic (HD) drag force.

**HD drag force:** For a spherical cell moving in a uniform Stokes' flow (Reynolds number  $\ll 1$ ), the hydrodynamic drag force in the  $x$ -direction ( $F_{Drag}$ ) is given by

$$F_{Drag} = -6\pi R\eta v_x \quad (2-8)$$

where  $R$  is the radius of the cell,  $\eta$  is the viscosity of the fluid, and  $v_x$  is the average  $x$ -velocity of the flow at the center of the cell, given by

$$v_x = \frac{6Q \sin \theta}{wh^3} R(h-R) \quad (2-9)$$

where  $Q$  refers to the volumetric flow rate,  $w$  is the channel width, and  $h$  is the channel height. This flow rate is evaluated at  $z=h-R$  to reflect the fact that the  $z$ -directed DEP force is larger than the lift and gravitational forces, pushing the cell to the ceiling of the channel.

**DEP force:** The analytical representation of the  $x$ -directed DEP force ( $F_{DEP_x}$ ) is derived similar to the approach used in DEP-FFF [60], which is

$$\begin{aligned} F_{DEP_x} &= 2\pi R^3 \varepsilon_m \operatorname{Re}[CM] \frac{\partial E^2(x, h-R)}{\partial x} \\ &= 2\pi R^3 \varepsilon_m \operatorname{Re}[CM] q_R(x) V_{RMS}^2 p(f, \sigma_m) \end{aligned} \quad (2-10)$$

$E^2(x, h-R)$  is the RMS value of the electric field strength modeled from conformal mapping [61] for an applied RMS voltage  $V_{RMS}$  at location  $x$  and height  $h-R$ .  $p(f, \sigma_m)$  is a normalization factor that corrects for any voltage drop at the electrode/solution interface, and varies with frequency ( $f$ ) and media conductivity ( $\sigma_m$ ).  $q_R(x)$  is a function that reflects the positional dependency of the DEP force, which depends on the following parameters of electrode geometry: the electrode gap ( $g$ ), the electrode width/spacing ( $W$ ), and the channel height ( $h$ ). The detailed analytical expression for  $q_R(x)$  is in Appendix.

**Balance position:** Balancing the two forces gives

$$\begin{aligned} \overrightarrow{F_{DEP_x}} + \overrightarrow{F_{Drag_x}} \\ = 2\pi R^3 \varepsilon_m \operatorname{Re}[CM] q_R(\delta) V_{RMS}^2 p(f, \sigma_m) - 6\pi\eta R \sin\theta \left[ \frac{6Q}{wh^3} (h-R)R \right] = 0 \end{aligned} \quad (2-11)$$

We define this *balance position* as  $\delta$ , which is the length of the nonlinear DEP spring.

$$\delta = q_R^{-1} \left( \frac{3\eta \sin\theta \left[ \frac{6Q}{wh^3} (h-R) \right]}{R \varepsilon_m \operatorname{Re}[CM] V_{RMS}^2 p(f, \sigma_m)} \right) \quad (2-12)$$

The balance position decreases with the applied HD drag force, and increases with the voltage or  $\operatorname{Re}[CM]$  (Figure 2-4b). By carefully calibrating the system, we can deduce the  $\operatorname{Re}[CM]$  from balance position and size of the particles. When we measure multiple balance positions at different the media conductivities and frequencies, we can build a  $\operatorname{Re}[CM]$  map mentioned in Figure 2-3. However, the DEP spring method only covers the nDEP part. If the HD drag force surpasses the maximum nDEP force, the spring will break down and the cell will pass through the barrier. When the cell pass through the barrier, the conductivity at this spot is the iso-dielectric point, which is going to be described next.

### 2.2.2 Iso-Dielectric separation

The Iso-dielectric separation method has been developed since 2008 in our lab. This method has been acknowledged as a size-insensitive and continuous method for DEP characterization. The method generates a conductivity gradient across a microfluidic channel (Figure 2-5a). The cells are usually suspended in a high conductivity media and travel from high conductivity to low conductivity media. They are deflected by the electrode because of the negative DEP barrier which becomes smaller and smaller when the cells get to lower conductivity (closer to zero  $\operatorname{Re}[CM]$ ). Once the drag force overcomes the remaining negative DEP force, the cell passes through the electrode and keeps its lateral position as the Iso-dielectric point (IDP) (Figure 2-5b). Different from DEP spring, instead of using a microscope to look at the electrode, the microscope is focused at the end of the device for identifying the IDPs for all cells (Figure 2-5c).

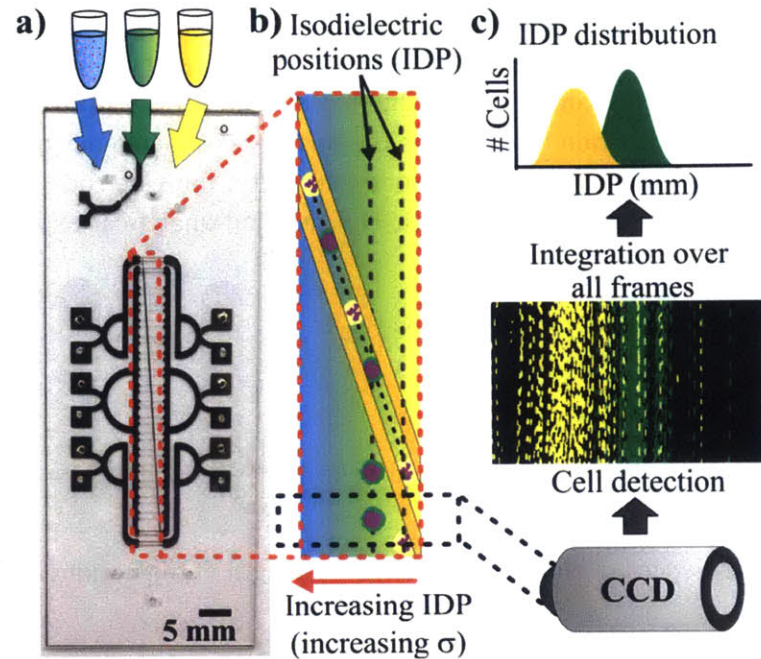


Figure 2-5 (a) Image of putting different conductivity of liquid into the microfluidic chip. (b) flows into a channel and creates a transverse conductivity gradient. Electrodes apply a DEP force pushing cells to the right as they flow down the channel. Cells escape the DEP barrier at their Iso-dielectric position (IDP) resulting in a transverse distribution of cells. (c) A camera is used to capture images near the end of the channel, which are processed to extract the IDP distributions.

Normally, we use phosphate buffered saline (PBS) or cell culture media (DMEM or RPMI) as the high conductivity medium. Low conductivity media is formed by 8.5 % sucrose and 0.3 % dextrose solution, which matches the osmolarity and density of cells while having much lower conductivity than PBS. The middle conductivity media is usually a 50% / 50% mix of high and low conductivity media.

IDS and DEP spring are complimentary methods where IDS measures the IDP (to the first order) and DEP spring quantifies all the DEP forces within the negative DEP region.

### 2.3 Device fabrication

During the experiment of characterizing activated neutrophils, we found that they were extremely sticky and adhered to the surface. Figure 2-6 shows an image of activated neutrophils adhered to the channel walls using the original IDS design. The reasons behind the serious fouling include (1) low flow rate which let the cells sediment to make contact with surface (2) single-sided electrodes generating a net upward force pushing cells to the top of the channel where the cells contact the channel ceiling (Figure 2-7b). With the single-sided IDS device, we found that characterizing the activated neutrophils was difficult due to the clogging and sticky nature of activated neutrophils. Flow rates would be further decreased when analyzing smaller cells like mouse leukocytes, which has smaller diameters and thus experience even smaller DEP forces. Therefore, we developed the double-sided electrodes to prevent clogging and ameliorate fouling (Figure 2-7c). The double-sided electrodes focus the cells in the middle of the electrode and prevent the cells from contacting the



surface. The electric field coming from both sides also allows for an increase in the operating flow rate ( $\sim 2\times$ ).

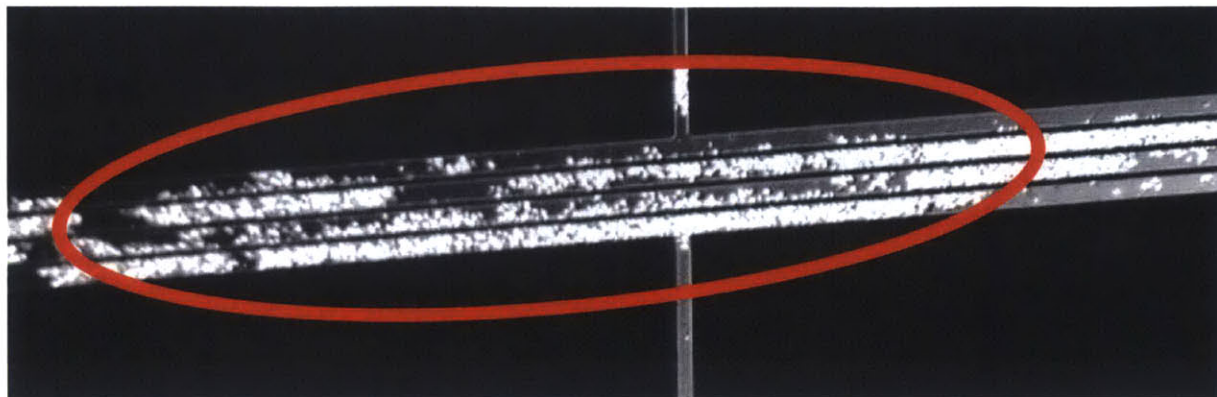


Figure 2-6 Cells from activated samples stick to the channel walls of the original IDS.

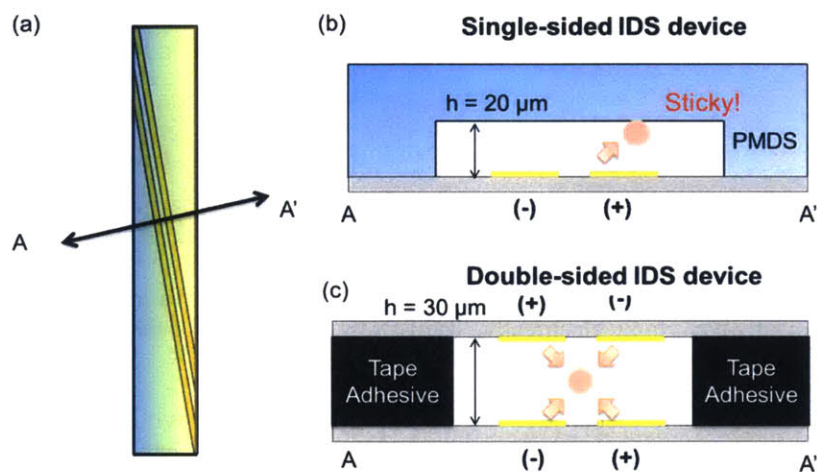


Figure 2-7 Difference between single-sided IDS and double-sided IDS device. (a) IDS device from a top-down view. (b) Single-sided IDS device (c) Double-sided IDS device

The fabrication methods of the two different devices are the following:

### 2.3.1 Single-sided electrode fabrication

We use soft lithography and replica molding to generate a 2 mm wide and  $20\ \mu\text{m}$  tall PDMS microchannel that we bond to a glass substrate with patterned electrodes. To pattern the electrodes on the glass, we e-beam evaporate  $100\ \text{\AA}$  of Ti and  $2000\ \text{\AA}$  of Au and perform lift-off, which generates coplanar electrodes with gap and width of  $15\ \mu\text{m}$  and  $50\ \mu\text{m}$  respectively.

### 2.3.2 Double-sided electrode fabrication

As in Figure 2-8a, the double-sided electrode consists of a microchannel cut in double-sided tape sandwiched by two electrode-patterned glass slides, fabricated in a fashion similar to previous reports[62]. We cut a 2 mm wide microchannel using a laser cutter on a  $25\ \mu\text{m}$  thick double-sided

tape (ARseal 8026 Silicone Transfer Adhesive Tape, Adhesive Research). We align the tape to the substrate under a stereoscope and press with a rubber roller to bond the channel to one of the substrates (bottom glass slide). We drill 2 mm wide holes using diamond bits on the other substrate (top glass slide) to allow fluidic access to the microchannel. The top substrate is then aligned under a stereoscope and pressed onto the topside of the tape. The whole device is then set in a hotplate (90° C) for 1h with 1 kg weight on top to ensure a proper seal. The device is then connected with wires and silver epoxy for electrical connection (Figure 2-8b). For fluidic connection, a PDMS layer with holes is aligned and bonded to the the glass electrodes.

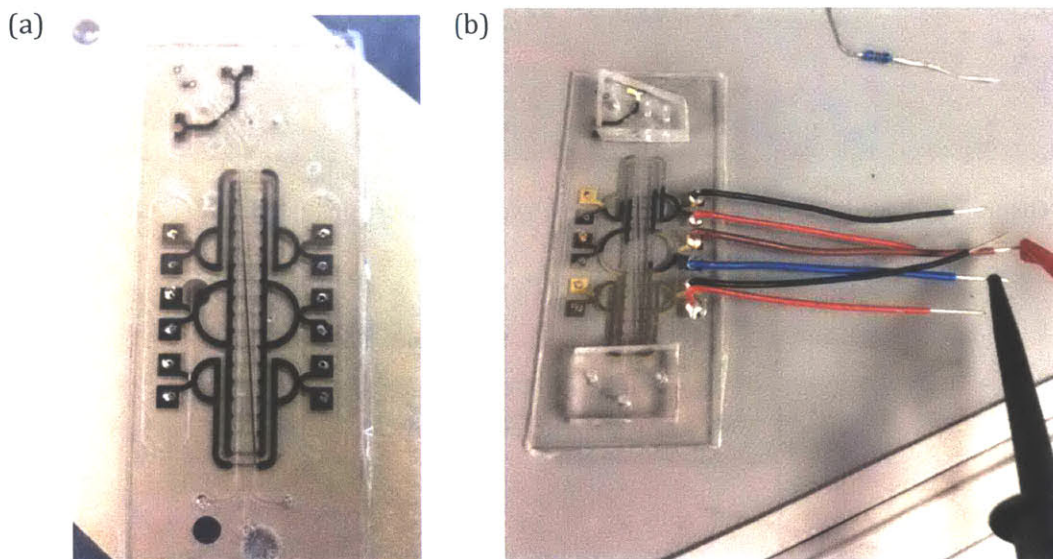


Figure 2-8 (a) The double-sided electrode with laser-cutted 25  $\mu\text{m}$  tape in between. (b) The double-sided electrode connected with wires and silver epoxy electrically. The PDMS layer on top of the device is for fluidic connection with 1/16 inches tubing.

Figure 2-9a is the image of the electrodes under 20x magnification while the focus is on the bottom electrode. Figure 2-9b is the same image while focus is on the top. The electrodes are well aligned with unobservable misaligned in this image.

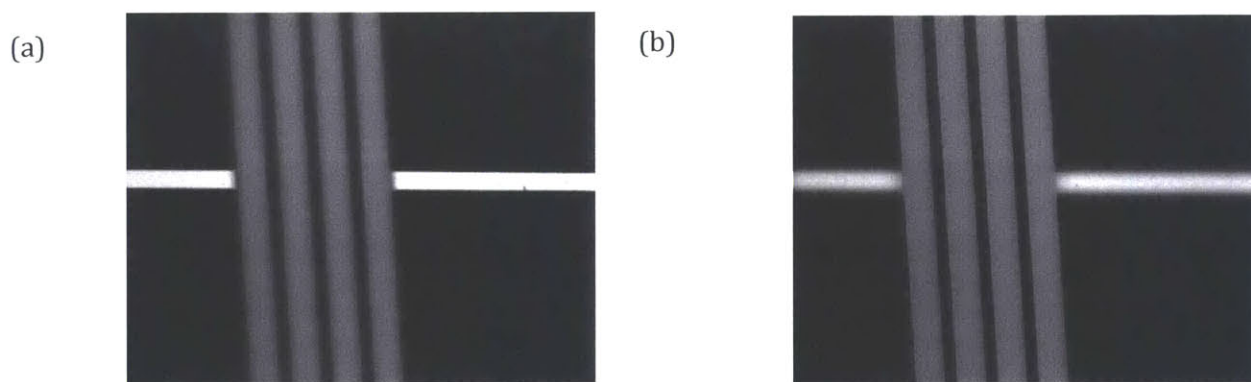


Figure 2-9 The image of electrodes with 20x magnification. (a) Focusing on bottom. (b) Focusing on top. The electrode gap is 15  $\mu\text{m}$ . The electrode width is 45  $\mu\text{m}$ . The focus difference between the two images (channel height) is 30  $\mu\text{m}$ .

## 2.4 System overview & Instrumentation

The dielectrophoretic characterization system contains the computer-controlled fluidic, electrical, and optical system (Figure 2-10). We will describe each element individually in this section.

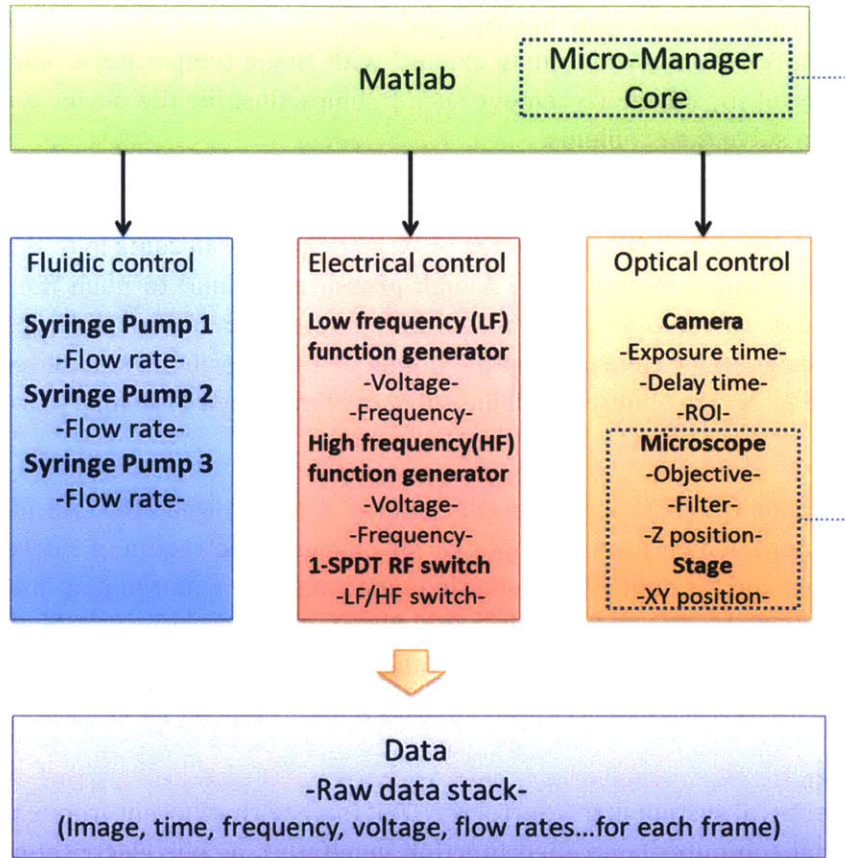


Figure 2-10 The overview of the automated system. The MATLAB controls all the equipment with parameters. The image and other parameters for each frame are recorded for processing. The microscope is control with MATLAB script but requires importing the Micro-Manager Core.

### 2.4.1 Fluidics

Both DEP spring and IDS require steady and accurate flow rate to make the characterization accurate. Therefore, we use a computer-controlled syringe pump (Chemyx Fusion 200) with Hamilton glass syringe (1 mL) to change the flow rate rapidly. To load the syringe with liquid, the bubble needs to be removed first. Bubble removal may reduce the usable volume of sample. Therefore, for loading a previous sample, it is better to have a bubble-free syringe with needle. Namely, the syringe should be connected to a blunt needle, and loaded with buffer first. Then the bubble should be removed from the syringe. Lastly, the sample can be loaded after there is no bubble in the entire fluidic path. To test if the system has any bubble, one can estimate the compliance of the system by looking at the response time of a small jolt of liquid. If the liquid did not respond immediately ( $< 1$  seconds), there are likely bubbles with significant size that need to be removed.

IDS device, like many other microfluidic devices, is very sensitive to any bubbles in the channel. To remove bubbles in the channel, de-gas DI water can help to dissolve any bubbles. We sometimes use ethanol to change the surface tension in order to get rid of larger bubbles. Sometimes, the temperature rise of the system will release the dissolved air inside the liquid. Having a cooled or de-gas liquid will help preventing such a scenario from happening. In addition, with double-sided device, the tape structure is 25  $\mu\text{m}$  but the real height is 30  $\mu\text{m}$  due to the burnt edges. The remaining space stores the air which may expand with rising temperature. The air comes in the channel from niches of the edges. To remove such bubbles, flushing the device with DI water using higher pressure can solve the problems.

One important challenge of running leukocytes in microfluidic devices is cell sticking. Even with a double-sided device, there are still cell clumps or large cells that can come in to the  $<30 \mu\text{m}$  channel. To remove the cell clumps, we can apply a high pressure by hand to push the cleaning solution liquid at high shear rates. One cleaning solution we found useful is TrypLE. TrypLE (Life Technologies) is designed for cleaving peptide bonds on the C-terminal side of lysine and arginine, which is often used to detach adherent cell lines like the function of Trypsin.

#### **2.4.2 Optics**

The camera is LaVision QE (PCO Sensicam QE camera). A customized MATLAB function is used for controlling the camera, which provides options for changing the region of interest (ROI), binning level, exposure time, and bit depth. The recorded video stack is in stored in a MATLAB matrix so it can directly be processed with temporal or spatial filters. The microscope (Zeiss Axio Imager.m1m) and the stage control (MAC 5000) are also controlled by MATLAB via Micro-Manager 1.4 core. They can also be controlled by Zeiss MTB2012 server with proper application interface.

#### **2.4.3 Electronics**

The goal of the electrical system is to control the DEP force with different frequencies and voltages. We use commercial computer-controlled function generators as our electrical source. We have a low-frequency function generator and a high-frequency function generator that are linked to a computer-controlled single-pole double-throw RF switch as the output signal. We control the low-frequency function generator and the RF switch via a USB connection and the high-frequency function generator through the USB-RS232-adpater. The electrical signal is conducted in a 50 ohm co-axial cable with BNC or SMA type connectors to minimize interference and transmission line loss.

The low-frequency function generator (Agilent 33250 A) can supply from DC to 20 MHz output. The maximum output signal is 20 Volt peak-to-peak with output resistance 50 ohm. The high frequency function generator (TTi TGR1014) can supply 10 MHz to 1000 MHz but the output voltage is  $\sim 500$  mV, which is not enough for DEP separation, so we use a high-power amplifier (Mini-Circuits ZHL-20W-13+) to boost the output voltage by 50 dB. Since the amplifier output has a DC offset component that occasionally appears when changing frequencies transition, we use a DC block (block under 300kHz) to avoid passing DC that could cause the electrodes to corrode. The RF switch (Mini-Circuits USB-1SPDT-A18) enables us to switch between the high-frequency and low-frequency function generators as the signal source.

#### 2.4.4 Software: Image Processing and GUI program

After linking all the components to the computer, we wrote a MATLAB GUI that not only controls each of the components but also provides some protection of the device (avoiding illegal inputs and conditions that could cause electrode electrolysis). The GUI consists of two menus (File and Setting) and three blocks (Video display, Control panel and Macro panel).

The File menu has the "Save as" and "Save" items. "Save as" provides the path, file name, and the videos options. "Save" is simply put the video stack and parameters into the assigned path. "Setting" has the camera setting that can change the region of interest, binning, gain, expose time, delay time and bit depth (8 bits or 12 bits).

The Video display shows the real time image acquired from the camera. The frame rate, frame number and the elapsed time is shown below the video box. The control panel includes the individual fluidic, electrical, and optical units. The frequency of the low frequency function generator is set above 100 kHz to prevent electrolysis. The Macro panel provides the following function:

- (1) Voltage Sweep: Change the voltage of the function generator and record the video for each voltage. The length of the video is assigned in the "File-> Save as" menu. The raw data will be automatically saved with incremental names.
- (2) Frequency Sweep: Change the frequency of the function generator and record the video of each frequency. If the frequency is between 100 kHz to 15 MHz, we choose to use the low frequency function generator. If the frequency if between 15 MHz to 1GHz. We choose to use the high frequency function generator.
- (3) Single Cell Frequency Sweep: Apply a continuous frequency sweep to the electrodes (chirp signal). A single cell will experience different frequency while traveling in the region of interest.
- (4) Frequency and conductivity sweep: Provide a two dimensional scan for frequency and conductivity. The conductivity is controlled by the flow rates of the pumps.
- (5) Auto Scan: A user-defined scan.
- (6) Customized Frequency Sequence: To apply frequency sequence with assigned duration and record a video stack with parameters. The "Current Status" will display the current voltage and frequency of the signal.
- (7) Execute Customized Frequency Sequence Stack: To apply a few frequency sequences with assigned duration and record a few video stacks.

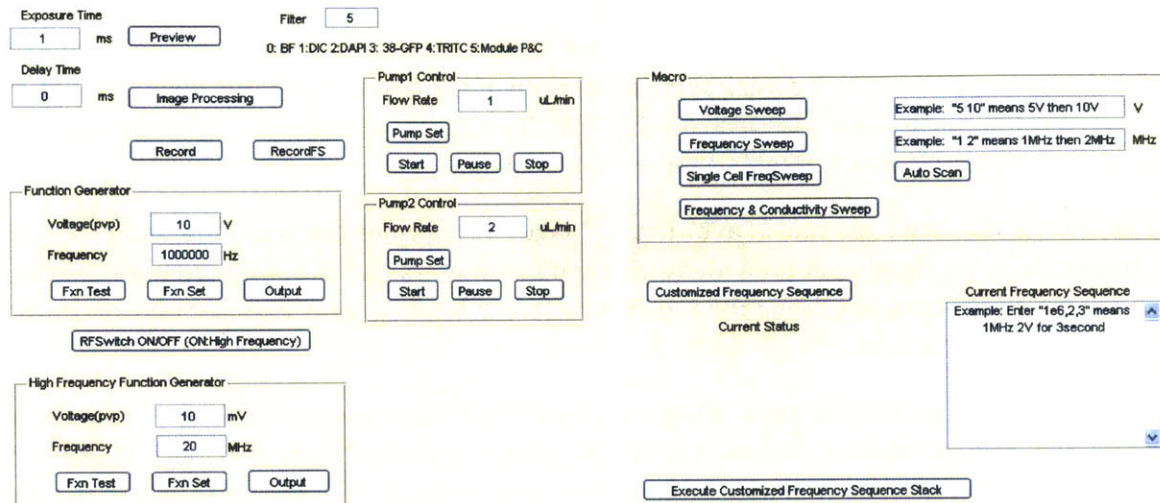


Figure 2-11 The control panel (left) and the Macro panel (right) of the MATLAB GUI.

## 2.5 Conclusion

Based on the dielectrophoresis theory, we developed the dielectrophoretic spring method that can thoroughly characterize the electrical properties of cells as a complimentary to method to iso-dielectric separation. To measure the electrical properties of activated leukocytes, we fabricated the double-sided electrode device that can increase the throughput and reduce the chance of fouling. We built a user-friendly system around the device to rapidly acquire data from different samples. In Chapter 3, we will use this system to characterize electrical changes of human neutrophils after chemical stimulation. The technology improvement enables us to, for the first time, characterize thousands of cells under multiple conditions: different frequencies, different conductivities, and different drug treatments using dielectrophoresis.

One of the potential pitfalls of the IDS is that there is no calibration particle and thus the device to device variation is large. Desai et al. [63] has tried to create giant vesicles as metrology tool of DEP but the giant vesicles are not easy to preserve for a long time. For DEP spring, 10  $\mu\text{m}$  beads and 6  $\mu\text{m}$  beads have shown to be able to calibrate the systems thus easier to compensate for the device to device errors. However, the DEP spring can only measure nDEP and require more accurate sizing. Measuring balance positions at multiple frequencies and using the low frequencies information as DEP sizing may be useful to come up with metrics that is not size dependent and compensated for device to device variation.

## Chapter 3 In vitro characterization of activation of human neutrophils

In this chapter, we will describe the prior work on characterizing the electrical property changes arising from neutrophil activation, namely via the patch clamping and electro-rotation methods. Secondly, we will describe methods for isolating and activating neutrophils followed by results from characterizing neutrophil activation with our high-throughput technologies: IDS and DEP spring. Thirdly, we will describe a set of experiments designed to inhibit certain functions of neutrophils to show that we can rapidly test different conditions with thousands of cells. Finally, we build an electrical model of neutrophil to qualitatively and quantitatively explain the possible underlying electrical changes. Though these results do not conclusively determine the mechanism by which neutrophil activation leads to electrical changes, these platforms act as useful tools to interrogate neutrophil functions in search of the true mechanism underlying the electrical changes.

### 3.1 Electrical properties of human neutrophils

Mature neutrophils contain membrane-enclosed granules and segments of nucleus, which differ from other mononuclear white blood cells. Under stimulation, neutrophils initiate a few processes that could result in electrical changes (Figure 3-1). First of all, during the degranulation process the granules release and fuse to the membrane to release their contents, which could result in electrical changes in both membrane capacitance and cytoplasm conductivity. Secondly, there is a substantial increase in reactive oxygen species generation, which along with the calcium ion dynamics may change the cytoplasmic conductivity. Finally, the cell membrane ruffling and disintegration of the nuclear membrane could alter cell volumes and nuclear volumes, both of which would change the electrical properties of the cells. Some of the events have been studied since the 1980s with the patch-clamp technique under the field of neutrophils electrophysiology, though many reports focus on the calcium flux, which may contribute little to dielectrophoretic behavior.

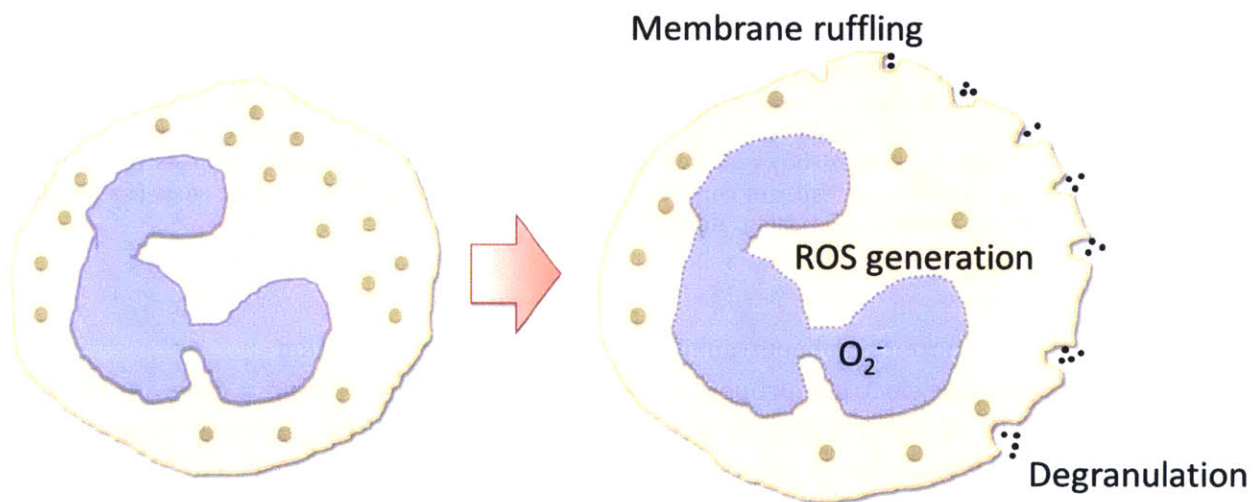


Figure 3-1 Illustration of neutrophil activation. Size increase, membrane ruffling, reactive oxygen species generation, nuclear membrane disintegration, and degranulation process are parts of the activation response of neutrophil.

### 3.1.1 Electrical characterization of neutrophil activation using patch clamp technique

In one of the experiments in neutrophil electrophysiology, Karsten et al. studied the electrical changes accompanying the releases of individual granules using high-resolution patch-clamping [36]. They measured the membrane capacitance and membrane conductance of a single neutrophil continuously during ionomycin stimulation. They were able to observe stepwise increases of membrane capacitance caused by individual granules fused to the surface of the neutrophil (Figure 3-2b). At the same instant of granule fusion, the conductance of the cell membrane increased for a short time, which may reflect the opening of fusion pores. This study supports the notion that there are quantifiable electrical changes upon neutrophil activation, especially during granule exocytosis.

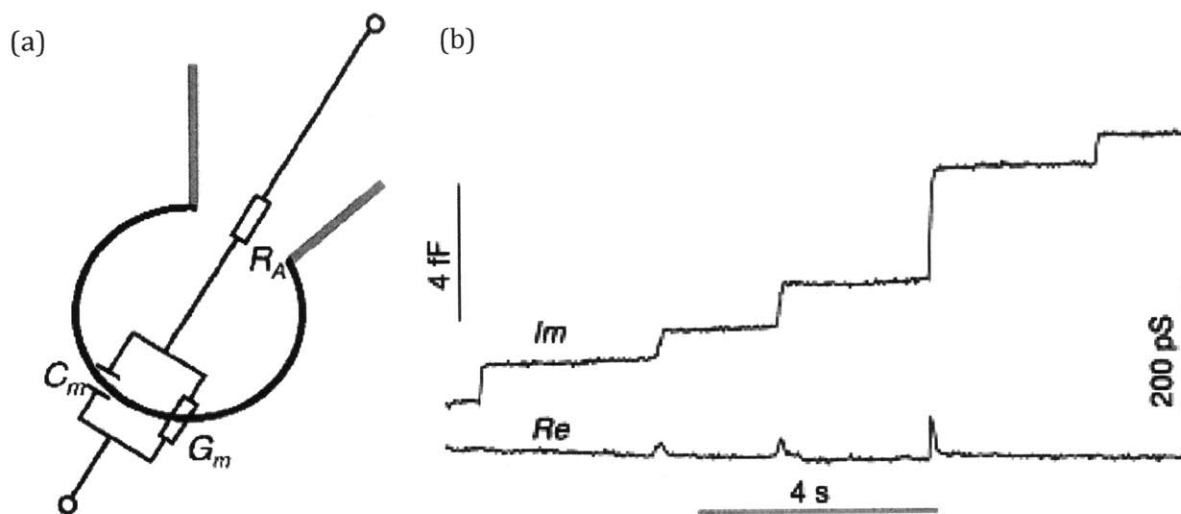


Figure 3-2 Monitoring electrical changes of neutrophil activation using patch clamp technique. (a) An illustration of using patch clamp to measure the electrical properties of neutrophils. Thick black line indicates cell membrane, gray lines indicates patch pipette.  $R_A$ ,  $G_m$ ,  $C_m$  are access resistance, membrane conductance, and membrane capacitance, respectively. (b) Trace from cell-attached recording. Cell-attached recording from a human neutrophil stimulated with ionomycin. The upper trace ( $I_m$ ) shows stepwise capacitance increases, indicating exocytosis of individual granules. The lower trace ( $Re$ ) shows transient conductance changes at the time of capacitance steps (for the three middle steps) reflecting the fusion pore opening. Adapted from [36].

### 3.1.2 Electrical characterization of neutrophil activation using electro-rotation

Griffith et al. studied the electrical properties of neutrophil activation using a different method: electro-rotation [37]. Electro-rotation is a technique for studying the electrical properties of particles by measuring the rotation rate of the particle under a rotating electric field (Figure 3-3a). Normally, the rotation rates of the particle with respect to different frequencies are recorded, forming a spectrum that can represent the electrical fingerprint of a single cell. The rotating field is typically generated by four electrodes with 0, 90, 180, 270 degree phase differences. A cell is put in the middle, and the rotation is observed by a microscope. Griffith et al. monitored the electrical properties of individual neutrophils before and after PMA treatment (Figure 3-3b). They found the rotation rate changed after the PMA treatment in the frequency range of 100 kHz to 10 MHz. They



fitted the experimental result with a double shell model and concluded that a change in cytoplasmic conductivity from 0.3 S/m to 0.05 S/m could possibly explain the electrical changes. It is possible if there is media exchange between inside and outside of the cells because the surrounding medium is 0.04 S/m.

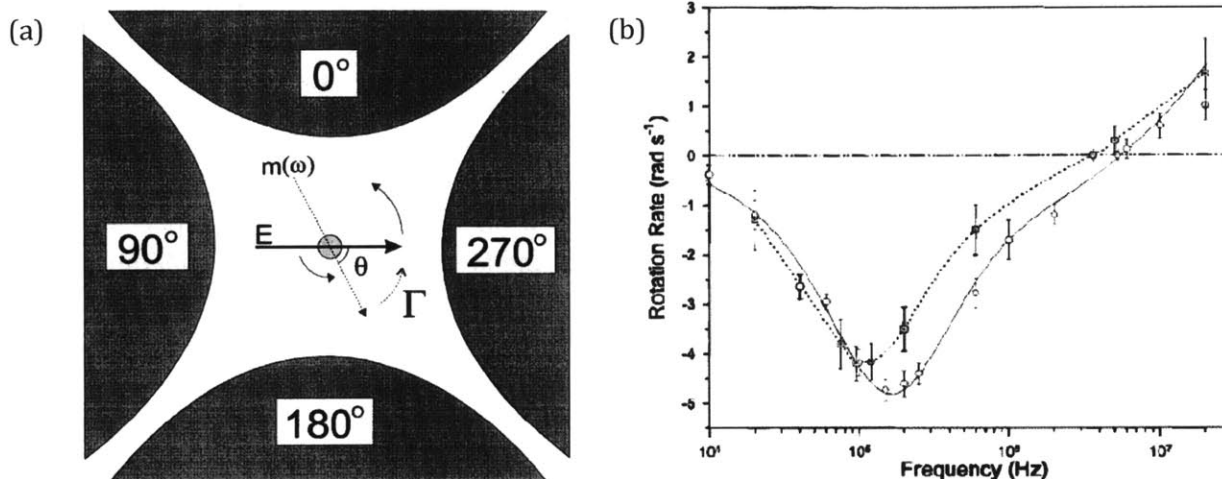


Figure 3-3 (a) In rotating electric fields, the induced dipole moment of a particle is out of phase with the direction of the electric field. The angle between the two ( $\theta$ ) reflects the time taken for the dipole to form. The phase difference will generate a variable torque ( $\Gamma$ ) acting on the particle, causing it to rotate. (b) Experimental electrorotation spectra of resting ( $\circ$ ) and activated ( $\square$ ) human neutrophils. The spectra were collected using polynomial electrodes (360  $\mu\text{m}$  tip-to-tip separation) in a field of ca. 56 V  $\text{cm}^{-1}$  (2 V p-p) in a sucrose/PBS medium (2.4% PBS, 400  $\mu\text{S cm}^{-1}$ ). The neutrophils were activated using PMA at a final concentration of 25  $\mu\text{M}$ . The solid line is a simulated spectrum of the resting human neutrophils generated with the double-shell cell model using the parameters in [37]. Adapted from [37].

### 3.1.3 Challenges in single cell electrical characterization technique

Based on the two studies above, we believe there are quantifiable electrical changes both in membrane capacitance and cytoplasm conductivity during neutrophil activation. However, both patch clamp technique and electro-rotation are single-cell characterization techniques that aim for resolution but not for throughput. In the electro-rotation work, data from only 6 cells was reported. While there have been attempts to develop high-throughput patch clamping [64] and high-throughput electro-rotation [65], there are challenges in properly positioning cells which makes it hard to apply to larger cell numbers. Therefore, we believe our high throughput dielectrophoresis based system is a better solution to continuously characterize thousands of cells to provide statistically meaningful results.

## 3.2 Sample preparation for isolating and activating neutrophils

Before using dielectrophoresis to characterize the neutrophils, we need to make sure that they are properly isolated and activated. Neutrophils are short-lived so they should be used within 6 hours of collection. We needed to establish a rapid isolation protocol as well as a robust activation protocol to show that we are really measuring activated neutrophils versus non-activated ones. The detailed protocol used is in the appendix (Neutrophil density isolation and activation protocol). Here we describe a few important details for isolating and activating the cells followed by the verification of activation.

### 3.2.1 Isolating neutrophil through density separation

Granulocytes are a subpopulation of leukocytes that consist of mainly neutrophils and a smaller number of basophils, eosinophils and mast cells. They contain secretory granules in their cytoplasm and are the majority of leukocytes in healthy blood. They are generally denser than mononuclear cells (mainly lymphocytes and monocytes) but less dense than red blood cells. Since neutrophils are the main constituent of granulocytes in healthy blood, in the following experiments, we use the response of granulocytes as an approximation of the true neutrophil population.

To separate out granulocytes from whole blood by density, one can use Ficoll-1077 media, density of 1.077 g/mL to isolate mononuclear cells from granulocytes and red blood cells, combined with media of 1.119 g/mL to further separate granulocytes from red blood cells. To speed up the isolation protocol, we choose to use a one-step solution, the Mono-Poly® Resolving Medium (MP Biomedicals), which is designed to isolate both mononuclear cells and granulocytes in one single centrifugation. The principle of this product is that the separation media will make the red blood cells shrink and sediment, creating a density gradient along the tube. The granulocytes and the mononuclear cells can be sorted according to their density difference. The successful separation should look like Figure 3-4a, which is clearly layered from top to bottom : (1) plasma with platelets (2) mononuclear cells (3) some resolving medium (4) granulocytes (5) more resolving medium(6) red blood cells.

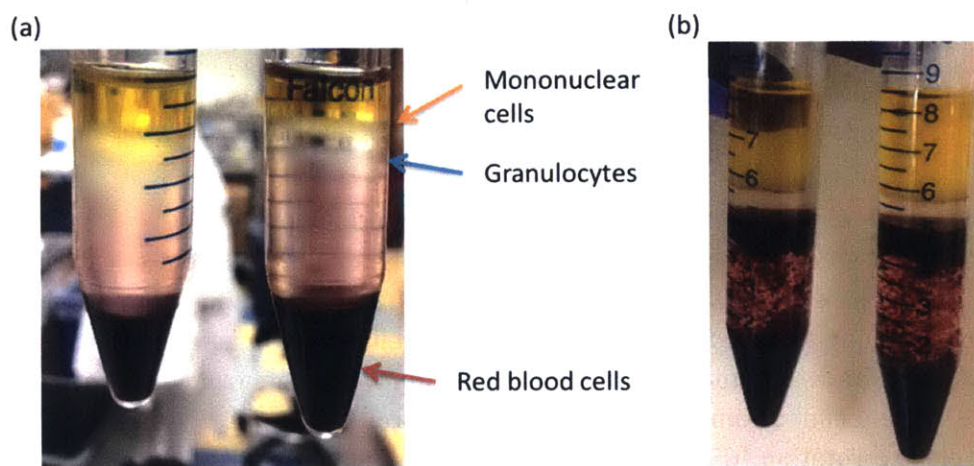


Figure 3-4 Density based separation of whole blood using Mono-Poly resolving medium. (a) Successful separation. (b) Bad separation due to insufficient centrifugation, old blood sample, or expired medium.

The Mono-Poly® Resolving Medium needs to be kept in the dark and properly sealed with parafilm. The medium may change density easily if it resides within an unsealed container. We have found that older products do not give good separations even months before expiration date. Additionally, the separation relies on the RBCs and therefore the separation results may depend on sample hematocrit and age of the blood (time after donation). Sometimes, the sample requires longer duration of centrifugation to make the RBCs sediment. We have found a few cases where the RBCs are not able to sediment to the bottom even after additional centrifugation time (without a brake)

(Figure 3-4b). To resolve this issue, we need to assure the quality of blood, media, and enough centrifuge time.

### 3.2.2 Activating neutrophils

There are many ways of activating neutrophils that will trigger different functions of neutrophils. Common exogenous stimuli are phorbol esters (PMA), formylated peptide (fMLP), and ionomycin. Among these, we chose to use PMA because it does not depend on receptor binding and globally activates neutrophils. PMA was also used in the electro-rotation study [37] and thus should be a promising agent to induce changes in dielectrophoretic behavior. To activate the neutrophils properly, buffer containing  $\text{Ca}^{2+}$  is required (HBSS with  $\text{Ca}^{2+}$  or PBS with  $\text{Ca}^{2+}$ ) because both intracellular and extracellular  $\text{Ca}^{2+}$  are important in neutrophil activation.

### 3.2.3 Monitoring oxidative burst of neutrophils after PMA treatment

To verify if the granulocyte activation was successful, we monitored the oxidative burst by pre-incubating cells for 10 min at room temperature with 100 nM dichloro-fluorescein diacetate (DCFH-DA, Sigma Aldrich). Activation was then quantified by DCF fluorescence. Figure 3-5 shows the dynamic response of how the DCF intensity increases with PMA treatment time. The DCF assay does not give zero base line of negative control cells but higher doses of PMA results in faster increase and higher level of DCF intensity.

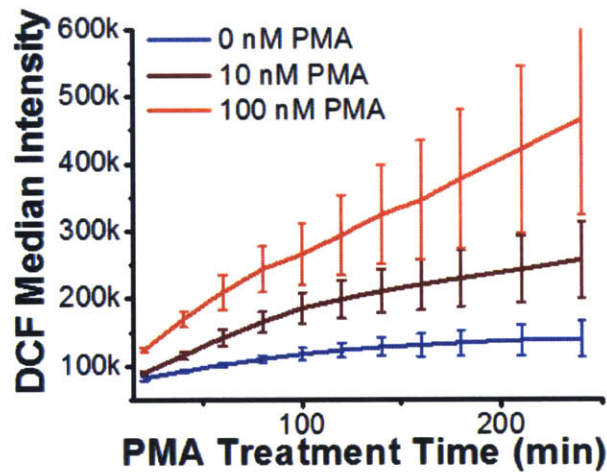


Figure 3-5 Fluorescent DCF is a result of the oxidation of DCFH-DA by the byproducts of the oxidative burst in neutrophils. The intensity of DCF over time increases for different PMA doses indicating granulocyte activation. The error bars are the standard deviation of three experiments.

### 3.2.4 Monitoring the adhesion marker of neutrophils after PMA treatment

To again verify that we have successfully activated the neutrophils, we measured the expression of neutrophil surface markers. In particular, we measured the expression level of CD 18, a leukocyte adhesion marker. In the circulating blood stream, activated neutrophils bind to the endothelial cells via selectins followed by CD18/CD11a to ICAM and CD18/CD11b to an unknown ligand [19]. The increase of CD18 indicates increased adhesion function and successful activation. CD66b is a marker for granulocytes and has also been found at higher expression level after activation [66, 67].

We took a portion of both activated and unactivated granulocytes and stained with PE-conjugated mouse anti-human CD66b monoclonal antibody (BD Biosciences, Accuri) and APC-conjugated mouse anti-human CD18 monoclonal antibody for 30 minutes in the dark at 4°C. After staining, we washed the sample with buffer and analyzed them with flow cytometry (BD Biosciences, Accuri C6).

As expected, we observed clear increases in CD18 and CD66b after activation (Figure 3-6). The activation percentage (CD18+) was 93.9% for PMA-treated neutrophils (CD66b+) versus 0.25% for untreated cells.

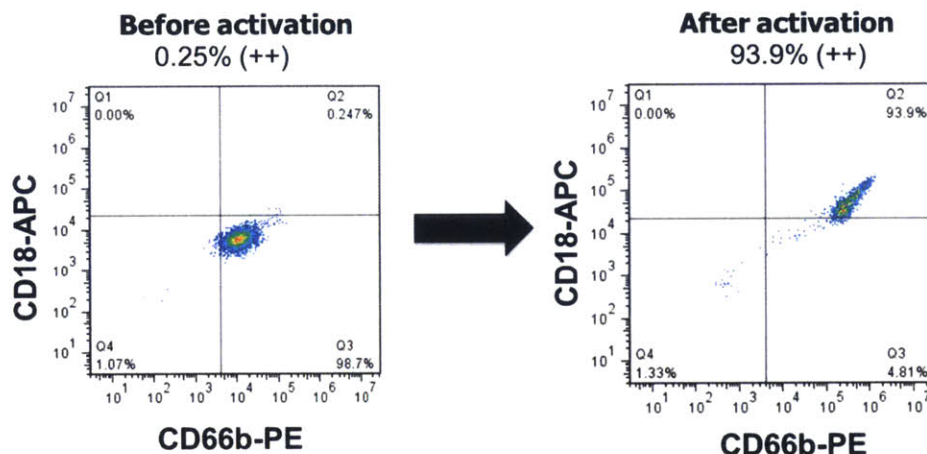


Figure 3-6 The validation of neutrophils activation with surface markers. The isolated neutrophils were labeled with CD18-APC and CD66b-PE. The activation percentage is 0.25% for untreated neutrophils and the activation percentage is 93.9% after PMA treatment.

### 3.2.5 Observing neutrophil membrane integrity over time after PMA treatment

Finally, we examined neutrophil activation with time-lapse fluorescence microscopy to verify successful activation and to assess the degree of activation. We mixed the isolated granulocytes with the same volume of 2  $\mu$ M PMA in PBS. At the same time, we added in membrane permeable nucleic acid dye Syto 64 (1:1000, Life Technologies) and membrane impermeable nucleic acid dye Sytox Green (1:1000, Life Technologies). We then loaded them into a shallow microfluidic device made from 20  $\mu$ m PDMS channel bonded on glass. We took time-lapse videos for 3 hours as in Figure 3-7. Once the neutrophils were no longer in the flow condition, after 5-30 minutes, some of them started to adhere to the surface and flatten out. After 10 minutes, the nuclear membrane started to disintegrate. However, 30 minutes of PMA treatment, the majority of cells maintained membrane integrity. After 50 minutes of PMA treatment, the membrane impermeable Sytox started to leak in the cells. After 70 minutes of PMA treatment, the content inside of cells starts to come out of the cells. The effect of exposing intracellular content is described as neutrophil extracellular net formation (NETosis) [20].

This experiment gives us an estimate of how long it takes to reach NETosis and how long the membrane integrity lasts after activation. Once the cells have a compromised membrane, the cell should change color quickly. It seems that under 30 minutes of treatment the majority of cells still

have complete membrane, indicating that 30 minutes should be a reasonable treatment time for 1  $\mu$ M PMA treatment to activate cells without killing them.

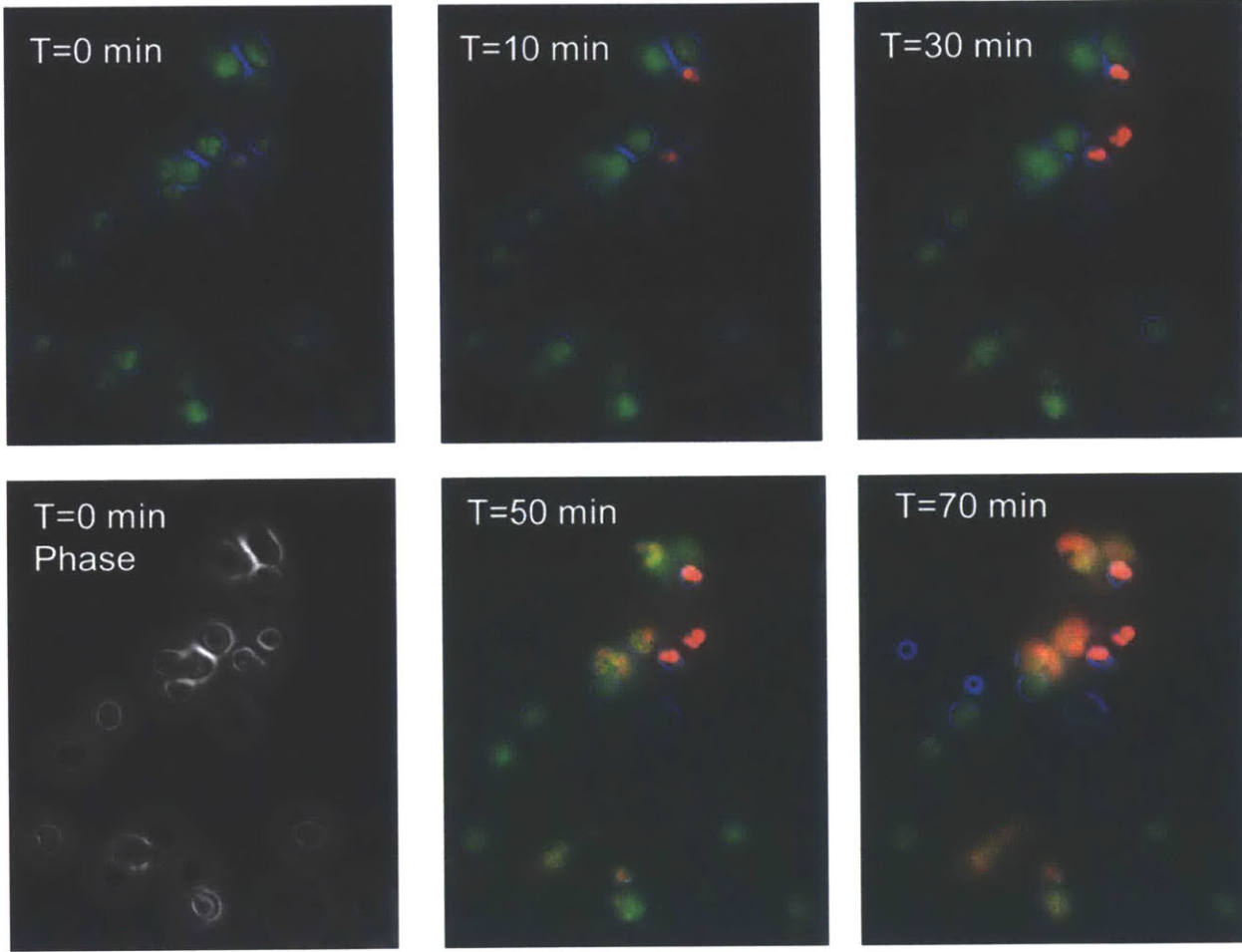


Figure 3-7 Time lapse imaging of PMA treated neutrophils in a 20  $\mu$ m height device. (Green: Syto 64, Red: Sytox 9, Blue: Phase)

### 3.3 Dielectrophoretic characterization of neutrophil activation using IDS

After establishing a robust protocol for isolating neutrophils and activating them, we describe the experimental results of dielectrophoretic characterization of neutrophil activation using the system in Chapter 2. In this set of experiments, we use the single-sided IDS and double-sided IDS to measure the iso-dielectric points (IDPs) before and after the PMA treatment. We then compared the difference in IDPs across the frequencies. To verify that the changes in IDPs are due to changes in effective conductivity of the cells, we show that we can control the IDPs of both populations by changing the conductivity gradient. Finally, we show a true separation of activated neutrophils versus non-activated neutrophils by staining them individually and mixing them.

### 3.3.1 IDS with single-sided electrode

Using a single-sided IDS platform, we characterized the IDP distributions of granulocytes treated with 1  $\mu\text{M}$  PMA and a control population of non-treated granulocytes across different frequencies. Figures and experiments in 3.3.1 are done and created by Javier Prieto.

We loaded cells at 0.4  $\mu\text{l}/\text{min}$  and the intermediate and low conductivity buffer at 0.55  $\mu\text{l}/\text{min}$  (1.5  $\mu\text{l}/\text{min}$  total). We applied a 10 Vpp voltage to the electrodes with frequencies ranging from 0.5 MHz to 15 MHz. To determine the IDP distributions for each frequency and sample we recorded the IDP for  $\sim 45$  seconds. This acquisition provided the characterization of different populations with a median of 330 cells per sample.

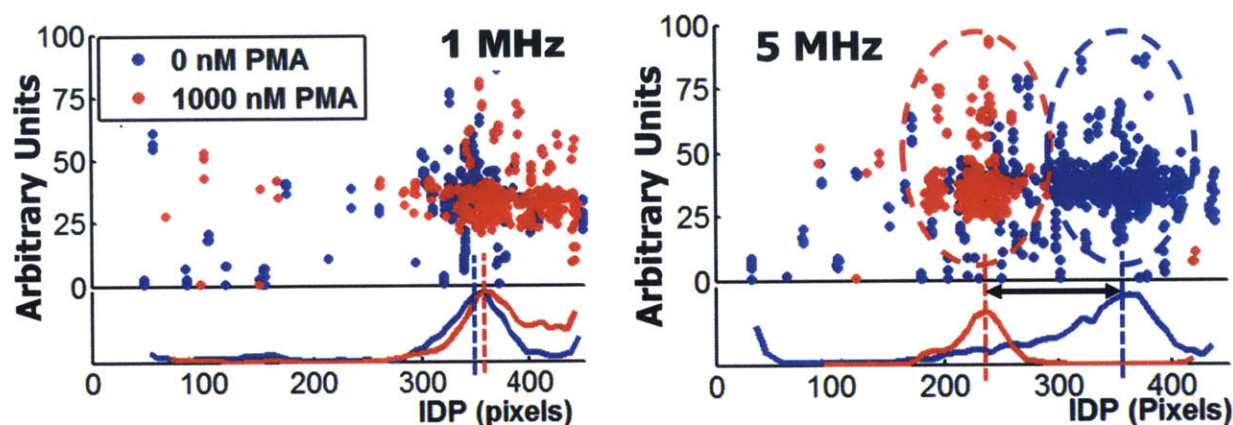


Figure 3-8 IDP distributions of PMA-treated and non-treated human granulocytes at 1 MHz and 5 MHz. Dashed lines indicate medians.

Figure 3-8 is the obtained result. Here, we observed that at 1 MHz, the two populations overlap, whereas at 5 MHz, the two population start to separate. Surprisingly, the decreases of IDP in PMA-treated granulocytes imply that the effective conductivity of the granulocytes increase after activation, which is opposite to the result of Griffith et al. [37]. We will discuss the potential reason in section 3.4.

If we plot the aggregated distributions of all samples for each frequency we can qualitatively see that at low frequencies ( $\leq 2$  MHz) both PMA treated and non-treated populations have similar IDP distributions (Figure 3-9a). As the frequency increases above 2 MHz, however, the IDP distribution of PMA treated granulocytes is displaced towards higher conductivity with respect to the non-treated cells. For convenience of visualization, we flipped the IDP axis and changed it to millimeter.

Results are also consistent with this trend when looking at samples individually across three different days. As a more quantitative measure of the difference, we first look at the average IDP. Figure 3-9b shows the average IDP of three independent samples from three healthy donors. There is a difference in the mean IDP that is statistically significant at 10 MHz ( $p=0.03$ ).

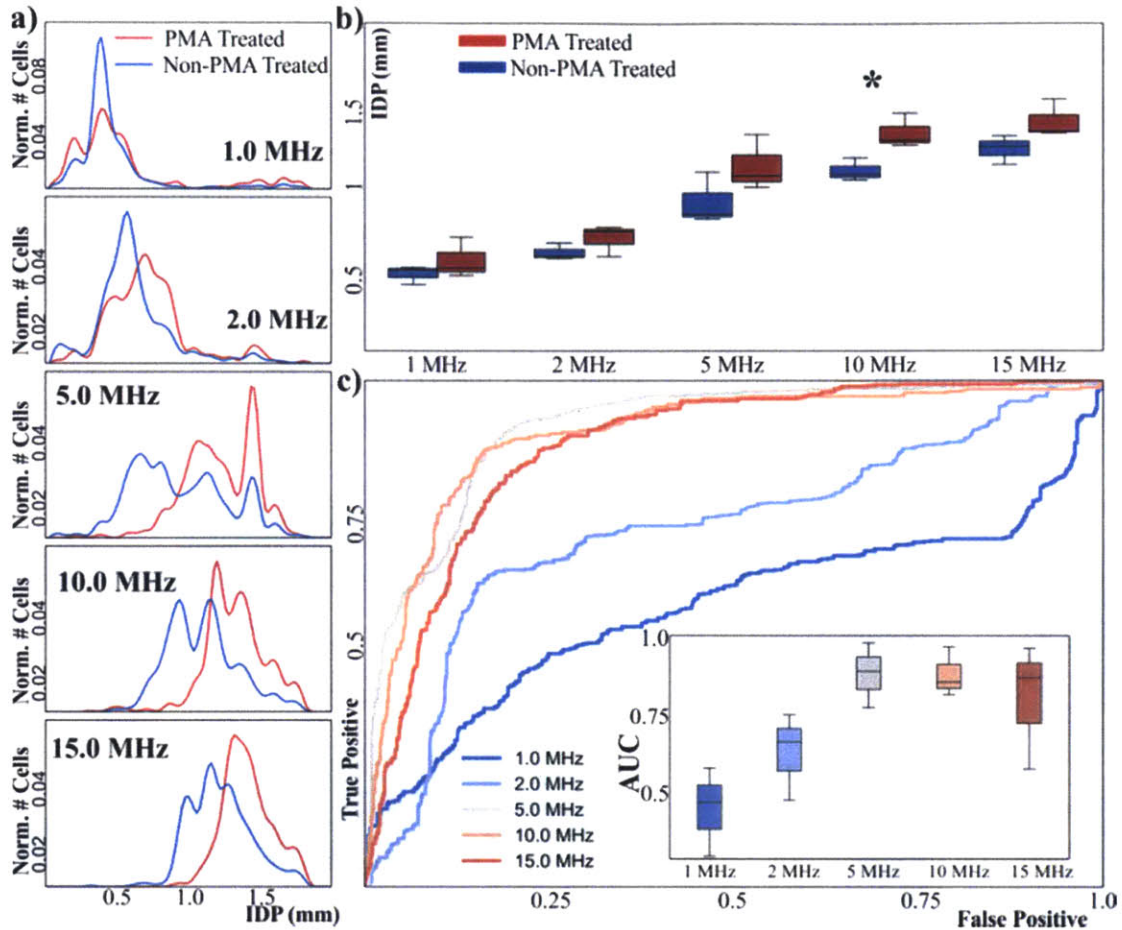


Figure 3-9 (a) Aggregated IDP distributions of PMA-treated and non-treated granulocytes. (b) Box-and-whisker plots of mean IDP of PMA-treated and non-treated granulocytes. At 10 MHz the mean IDP of both population types is different ( $*p < 0.05$ ). (c) ROC curves of the aggregated samples using the IDP position as classification criteria for different frequencies. Inset shows box-and-whisker plots of the AUC for each frequency across all samples ( $n=3$ ). The unit here has been transferred from pixel into mm and in a reverse order.

Given that the IDP distributions of PMA treated and non-treated populations appear to be different on average, we decided to evaluate the use of the IDP as a threshold to classify cells into activated and non-activated at a single-cell level. Receiver-operator characteristics (ROC) are a standard method for assessing if a given test is able to discern two different populations. We used IDP as a classification threshold and we used the original population to determine true positives (i.e. PMA treated cells = activated cells, non-PMA treated cells = non-activated cells). The resulting ROC curves have an area-under-the-curve (AUC) that increases with higher frequencies (see Figure 3-9c).

The peak AUC occurs at frequencies ranging from 5-10 MHz with a value of  $\sim 0.88$ , suggesting that at these frequencies IDP is able to distinguish PMA-treated vs. non-treated human granulocytes. This classification is performed at a single-cell level rather than as a population metric and across 3 samples.

### 3.3.2 IDS with double-sided electrode

In this set of experiments, we are trying to change the media conductivity profile in the gradient, in order to verify the shift in IDS does depend on the gradient profile. Using a double-sided IDS platform, we measured the IDP distributions of granulocytes treated with 1  $\mu$ M PMA and a control population of non-treated granulocytes. The double-sided electrode allows using a higher flow rate (1.5  $\rightarrow$  6  $\mu$ L/min) but also requires a higher voltage (10 Vpp  $\rightarrow$  18 Vpp). We loaded cells at a higher flow rate 2  $\mu$ l/min and the intermediate and low conductivity buffer at 2  $\mu$ l/min (6  $\mu$ l/min in total). We used 10 MHz and 18 Vpp with the amplifier.

We tried two different conductivity gradient profile (Figure 3-10a). As expected, the IDP distribution shifted with the conductivity gradient (Figure 3-10b).

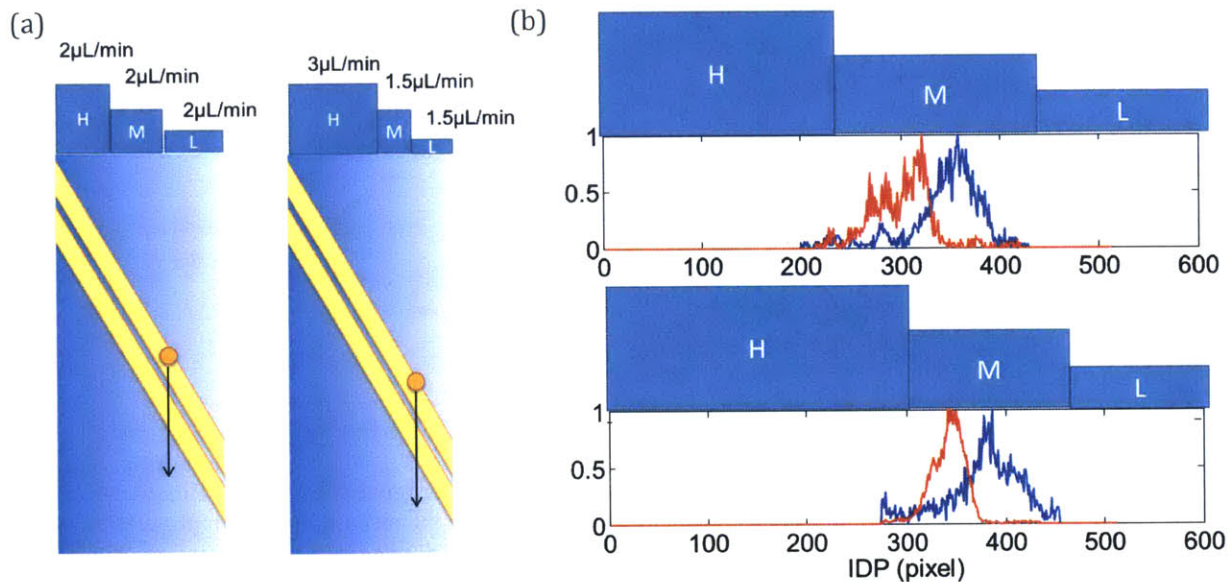


Figure 3-10 (a) The illustration of changing conductivity gradient by changing flow rates of three buffer with different conductivities. (b) The result of IDPs distributions of activated and non-activated cells with the two different conductivity gradients. (Red: Activated granulocytes, Blue: non-activated granulocytes)

### 3.3.3 Mixing activated granulocytes and non-activated granulocytes

The data we have shown so far is expressed by overlaying two population distributions. However, the two populations were not in the device simultaneously; they were introduced the device one after the other. Thus, it is possible that differences between the two populations are due to system drift. To exclude temporal dependence or media-dependent systematic errors, we performed a simultaneous separation by staining the two populations with different fluorescent dyes, mixing them, and characterizing activated and non-activated granulocytes together.

Figure 3-11 shows PMA-treated (stained green) and non-treated (stained red) cells flowing in the IDS device when DEP is active at 10 MHz. By visual inspection, one can see that PMA-treated cells pass through the electrodes at higher conductivity (to the left) and non-treated cells pass through the electrodes in lower conductivity.



There were some challenges we ran into during this experiment. The Syto 9 (1:1000, Life Technolgies) and Syto 64 (1:1000, Life Technolgies) dyes were bright and fast-acting nucleic acid stains. The characterization therefore must be done quickly after the mixing of the two populations since any dyes in the media will start to stain the other populations, which will make them both red and green. The problem is resolved by washing with buffer 3 times. However, the extensive washing steps require additional centrifugation and pipetting which results in cell loss and might activate the non-activated granulocytes. Additionally, the PMA-treated cells sometimes form aggregates, which we are not able to characterize in current IDS system, which is tailored to analyzing single cells.

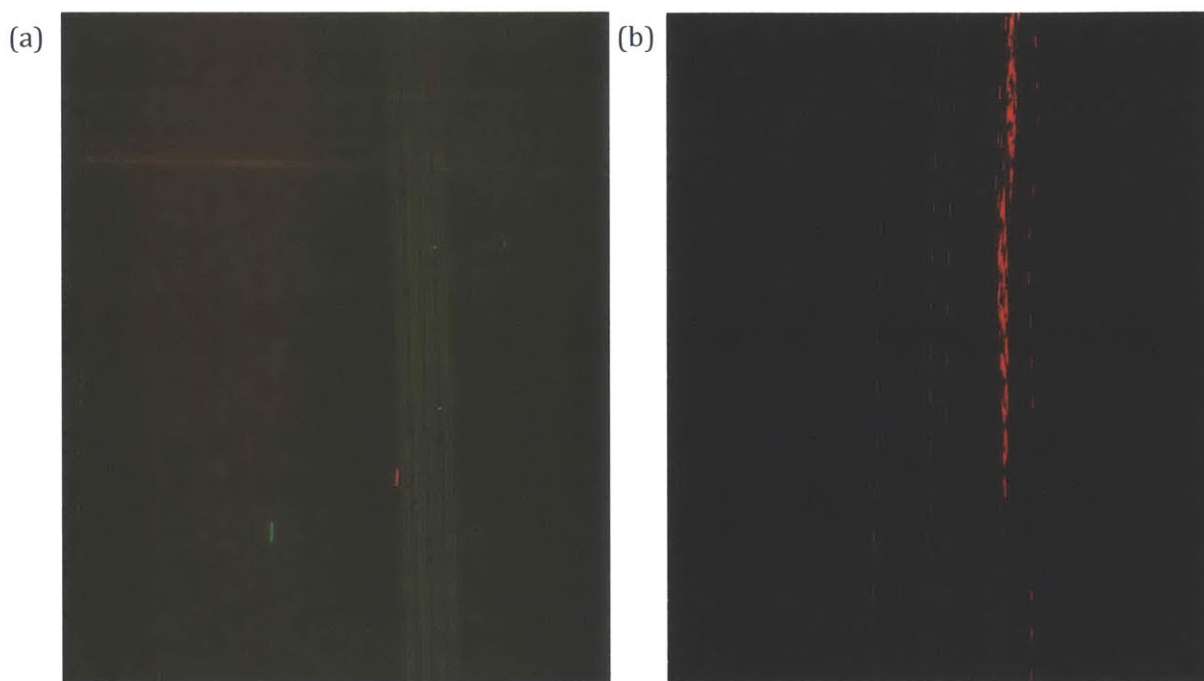


Figure 3-11 (a) A screenshot of the video of the mixing of PMA-treated granulocytes stained with Syto 9 (Green) versus non-treated granulocytes (Red) (b) The processed image shows the IDP distribution of PMA-treated granulocytes (Green) versus non-treated granulocytes (Red).

### 3.4 Dielectrophoretic characterization of neutrophil activation using DEP spring

To understand the dielectrophoretic response not only across frequencies but also conductivities, we used the DEP spring method to screen through the balance positions of DEP force and drag force across 21 conditions. After gathering the balance positions of unactivated neutrophils and activated neutrophils (1  $\mu$ M PMA) at 7 different frequencies (0.2, 0.4, 0.8, 1.6, 3.2, 6.4, 12.8 MHz) and three conductivities (0.34 S/m, 0.89 S/m, 1.36 S/m), we plotted the balance positions of the cells in Figure 3-12 and observed the following.

- (1) In high conductivity solutions (1.36 S/m), both cell populations have similar balance positions at all frequencies.
- (2) In middle conductivity solutions (0.89 S/m), when the frequency goes up, the balance positions of the activated neutrophils decrease faster than the unactivated ones. This is similar to what we observed in IDS.

(3) In low conductivity solutions, the cell number decreases when the frequency increases because the cells pass through the electrodes in higher conductivity region. This is one of the drawbacks of the DEP spring, which is that it only quantifies cells with nDEP conditions.

From this scanning of 7 frequencies and three conductivities, we found the changes in DEP behavior upon PMA treatment are most dramatic at higher frequencies and middle conductivities. Namely, the magnitude of the  $\text{Re}[CM]$  appears to be smaller at 12.8 MHz and 6.4 MHz in the 0.89 S/m solution after activation.

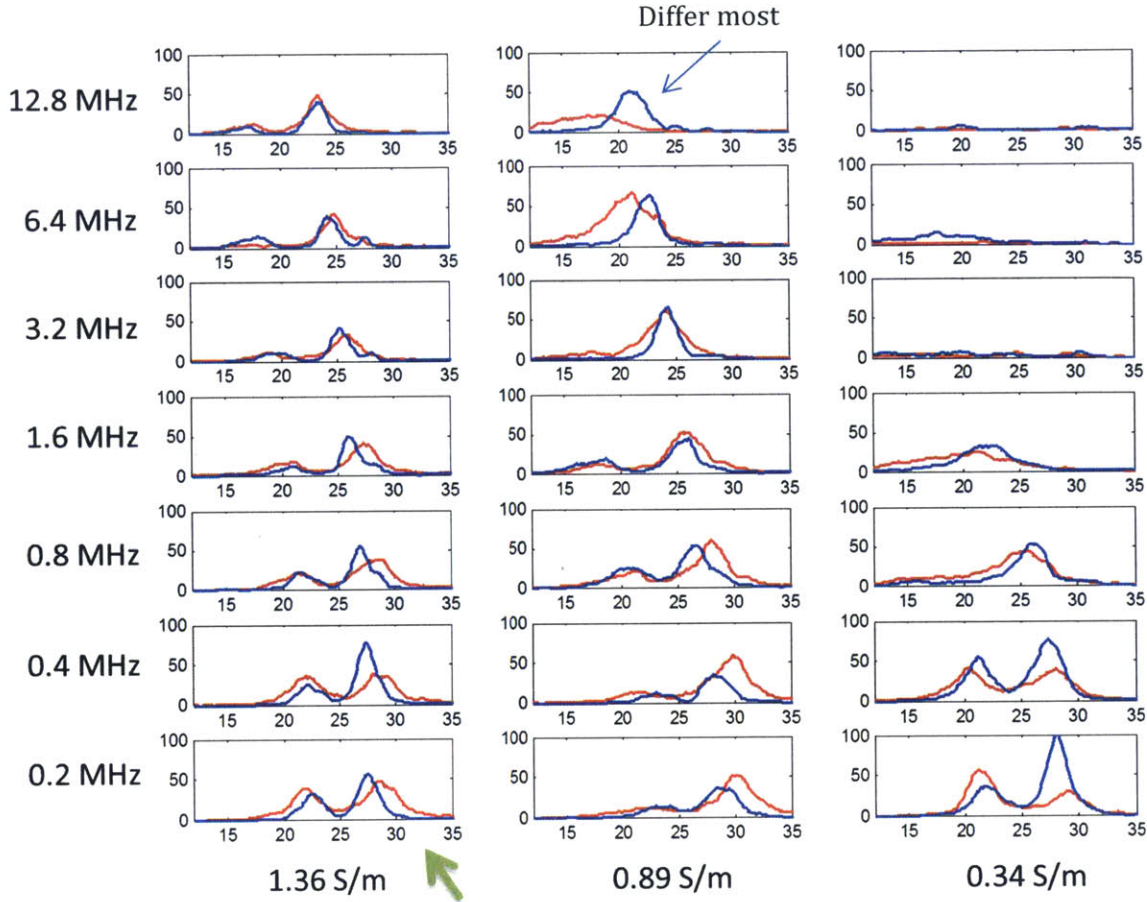


Figure 3-12 The balance position histograms of activated and unactivated neutrophils in different frequencies and conductivities. The x-axis is the balance position ( $\mu\text{m}$ ). The y-axis is the number of particle images recorded (events per 100 nm). The red population is the activated neutrophils and the blue population is the unactivated neutrophils. Both of them have two peaks in low frequencies because of the existence of the erythrocytes. In high conductivity, the two populations are similar. In middle conductivity, the two populations become different when the frequency goes higher. In low conductivity, the number of cells decreases when the frequency goes higher.

Recall that, the balance position of a cell is a function of size and electrical properties. Both changes in size and  $\text{Re}[CM]$  will affect the balance position. To understand the figure, we highlight two observations.

- (1) For low frequencies and high conductivity (Green arrow), the  $\text{Re}[CM]$  should be very close to -0.5, based on the model in Figure 2-3. Thus, the reason that the balance positions of the activated neutrophil increased should due to increase in cell size.
- (2) At the middle conductivity, if we move from lower frequencies to higher frequencies, we see the population of the activated neutrophil shift to the left relative to the non-activated neutrophils. This trend can possibly be explained by an increase of cytoplasmic conductivity which will be discussed in 3.6.

Unlike the decreasing in cytoplasmic conductivity postulated by Griffith et al., we observed the opposite. We scrutinized the experimental condition, and found that one major difference is the medium conductivity surrounding the cells during activation. The electro-rotation experiment is done by soaking the cells in low conductivity media (0.056 S/m) while in our experiments the cells are activated in high conductivity media (1.6 S/m). In our experiments, the neutrophils only encounter low conductivity media when they travel along the electrodes (10~ 20 seconds), and thus in our experiments the cells are primarily exposed to high-conductivity media. In addition, we measured the cell size change after the PMA treatment using the Coulter Counter Z2 (Beckman Coulter) and found that the mean cell volumes of the neutrophils increased by around 40% after activation (350 fL to 491 fL). Therefore, we have the following speculation.

***Speculation: Can the dielectrophoretic behavior change come from rapid endocytic and exocytic activity? If the cell size increased 40% after PMA activation, what is the additional cytoplasm made of? Could it be the media exchange during the rapid endocytosis and exocytosis that changes the effective conductivity of cells?***

### **3.5 Dielectrophoretic characterization of neutrophil activation under inhibitors using IDS**

We stated at beginning of the chapter that it is plausible that the electrical changes will correlate with cellular functional responses, such as degranulation, oxidative burst, and membrane ruffling. To start to identify which aspects of the activation signal sequence are linked to the electrical changes observed by IDS, we designed a set of experiments to selectively inhibit cellular functions. We choose formylated peptide N-Formylmethionyl-leucyl-phenylalanine (fMLP) over PMA because the global activation of PMA is too strong that we might not get a good inhibition of cell functions.

The fMLP is a potent neutrophil chemoattractant that interacts with a family of G-protein coupled formyl peptide receptors (FPR) on neutrophils. fMLP-FPR interactions change cellular pH and initiate calcium transients to activate intracellular signaling cascades. At higher concentrations, fMLP can also assemble the NADPH oxidase and serve as a neutrophil secretagogue.

For inhibition, we selectively use cytochalasin B (CytB), which is an inhibitor of actin polymerization that increases degranulation and inhibits membrane ruffling. We selectively incorporate jasplakinolide (Jasp) into the experimental strategy because this compound is an inducer of actin polymerization, so adding CytB and Jasp will block both degranulation and membrane ruffling. MAPTAM is an intracellular  $\text{Ca}^{2+}$  chelator that can block degranulation and reactive oxygen species (ROS) generation by chelating  $\text{Ca}^{2+}$ . Diphenyleneiodonium chloride (DPI) is

an inhibitor of NAPDH oxidase, which blocks the major source for neutrophil reactive oxygen species (ROS) generation.

The summary of the experiment is in Figure 3-13. We added in CytB (5µg/mL), CytB (5µg/mL) + Jasp (1 µM), and CytB (5µg/mL)+DPI (100 nM) to inhibit membrane ruffling, membrane ruffling and degranulation, and membrane ruffling and ROS generation, respectively for 10 min. The inhibition treatment lasted for ten minutes. For activation, we stimulated them with fMLP in HBSS buffer with Ca<sup>2+</sup> for 20 minutes in room temperature and then loaded into IDS. We used PMA-treated cells as positive control of full activation and non-stimulated cells as a negative control. All the aliquots are treated/stimulated sequentially with around 30 minutes interval.

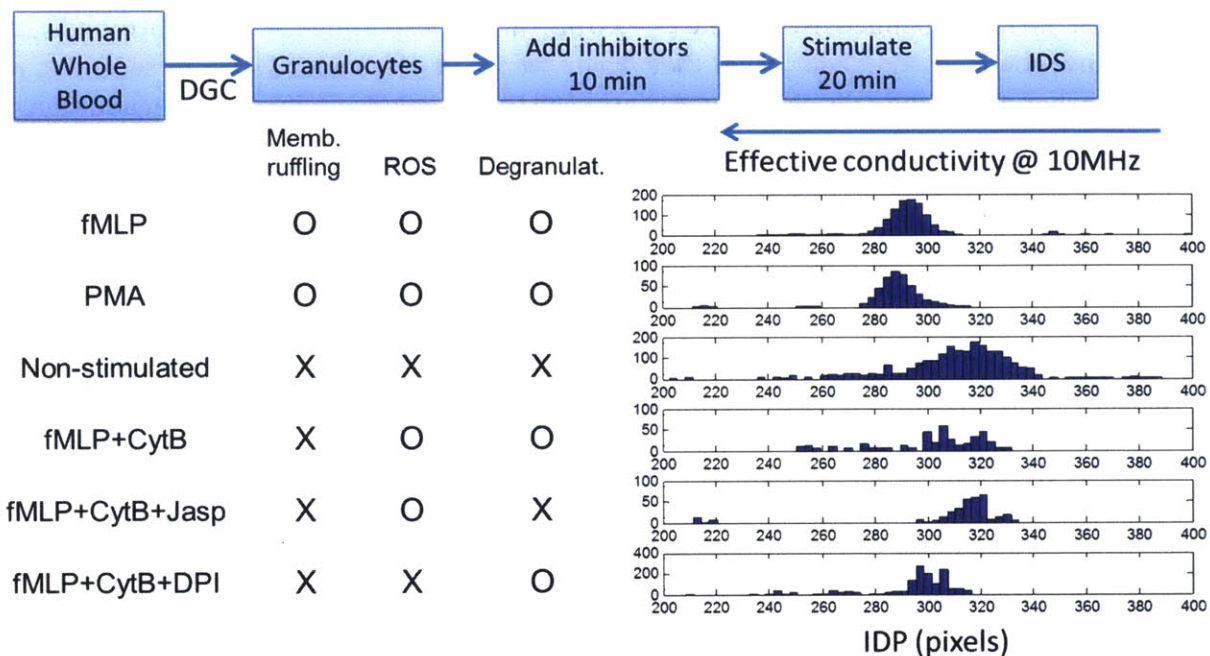


Figure 3-13 Mechanism of electrical changes of granulocytes. Granulocytes were treated with drugs to inhibit certain functions, then stimulated by stimulants. fMLP is a bacterial stimuli that initiates calcium transients to activate intracellular signaling. Cytochalasin B (CytB) is an inhibitor of actin polymerization and thus inhibits membrane ruffling. Diphenyleneiodonium chloride (DPI) is an inhibitor of NAPDH oxidase thus blocks the reactive oxygen species (ROS) generation. Comparing the electrical profiles suggests that membrane ruffling dominates the electrical changes at 10 MHz observed in IDS.

The results are shown on the right hand side of the figure. As we expected, the PMA and fMLP stimulated granulocytes shifted to the left, indicating activation. The doses were 0.5 µM for fMLP and 2 µM for PMA, respectively. All the drug-inhibited cases were less left-shifted than the activated control. Among those, CytB+Jasp seemed to have the most complete inhibition. CytB+DPI was the last sample that we measured, and thus the left-shifting could result from natural activation even before the drug was introduced.

**Speculation: Actin-based activity can be the main reason for electrical phenotype changes at 10MHz. CytB inhibits actin-polymerization thus reduces the media exchange during the**

*endocytic activity. As a result we observe less effective conductivity changes of neutrophils after inhibition.*

### 3.6 Explanation of electrical changes of neutrophil activation using the double-shell models

To qualitative explain the electrical changes we observe in 3.3 and 3.4. We create a double-shell model of neutrophil in Figure 3-14. According to the double shell model and theory explained in 2.1, we simulate the dielectrophoresis response ( $\text{Re}[CM]$ ) of the neutrophil as Figure 3-14b. The white line shows the iso-dielectric points from low frequencies to high frequencies (100 kHz to 100 MHz).

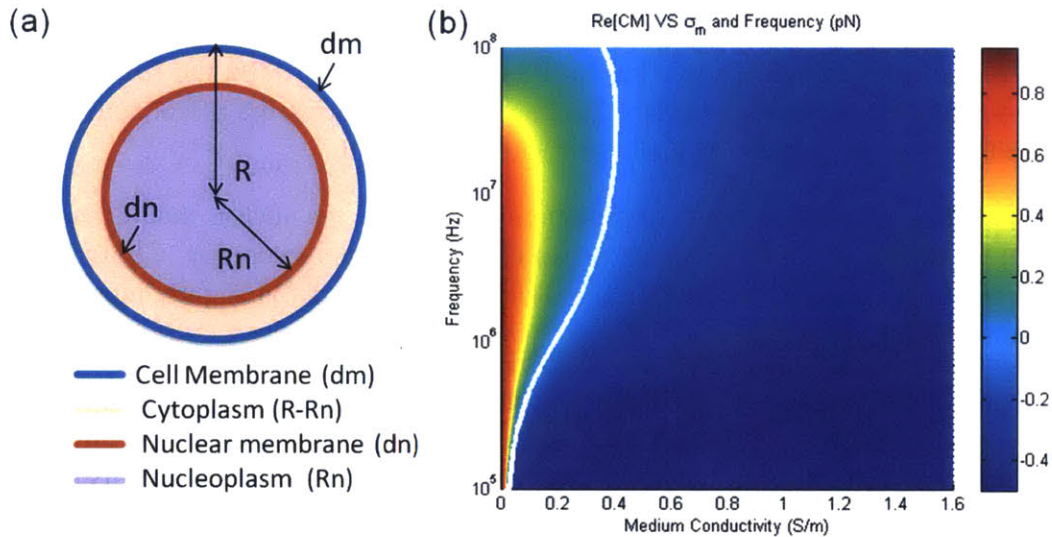


Figure 3-14 (a) Double shell electrical model of cells. (b) The simulated  $\text{Re}[CM]$  of human neutrophil as a function of different frequency and surrounding medium conductivity. Neutrophils parameters are from Table 3-1.

Table 3-1 The parameter values and literature source of double shell electrical model of human neutrophil. This table is modified from Griffith et al. [37].

Parameter list	Value	Source
cell radius ( $R$ )	6 $\mu\text{m}$	Griffith et al. [37]
cell membrane thickness ( $d_m$ )	8 nm	Asami et al. [59]
nucleus radius ( $R_n$ )	3.5 $\mu\text{m}$	Davis et al. [68]
nuclear membrane thickness ( $d_n$ )	20 nm	Asami et al. [59]
cell membrane conductivity ( $\sigma_{\text{mem}}$ )	$1 \times 10^{-12}$ S/m	Ziervogel et al. [69]
cell membrane permittivity ( $\epsilon_{\text{mem}}$ )	$6.2 \epsilon_0$	Ziervogel et al. [69]
cytoplasm conductivity ( $\sigma_{\text{cp}}$ )	0.3 S/m	Ziervogel et al. [69]
cytoplasm permittivity ( $\epsilon_{\text{cp}}$ )	$60 \epsilon_0$	Asami et al. [59]
nuclear membrane conductivity ( $\sigma_n$ )	$6 \times 10^{-3}$ S/m	Asami et al. [59]
nuclear membrane permittivity ( $\epsilon_n$ )	$28 \epsilon_0$	Asami et al. [59]
nucleoplasm conductivity ( $\sigma_{\text{np}}$ )	1.35 S/m	Asami et al. [59]
nucleoplasm permittivity ( $\epsilon_{\text{np}}$ )	$52 \epsilon_0$	Asami et al. [59]
permittivity of free space ( $\epsilon_0$ )	$8.854 \times 10^{-12}$ F m $^{-1}$	CRC Handbook
medium permittivity ( $\epsilon_{\text{med}}$ )	$79 \epsilon_0$	Arnold et al. [70]
medium conductivity ( $\sigma_{\text{med}}$ )	0 ~ 1.6 S/m	Varying

In the experiment of IDS characterization with single-sided electrode, we observe the PMA-treated cells increase the IDPs in higher frequencies compared to the non-activated control (Section 3.3,

Figure 3-9). We are looking for reasonable changes in parameters of this double shell model to match the observation. We listed five possible changes with their simulated IDPs in Table 3-2 and the discussion below:

(1) volume increase: in our experiment, we found the neutrophil size measured in the Coulter Counter increases after activation. The volume increase rate is around 40%. In the simulation, the IDP at 10 MHz decreases a little upon activation which is inconsistent with our observation.

(2) cytoplasmic conductivity increase: as a phagocyte, the cytoplasmic conductivity of neutrophil may increase due to reactive oxygen species generation,  $\text{Ca}^{2+}$  activity, and the exocytosis and endocytosis process. In the simulation, the trend of cytoplasmic conductivity increase matches our observation in IDS experiment. At 1 MHz the IDPs of activated and non-activated neutrophil overlaps. As frequencies increases, the IDP of activated neutrophil gradually becomes larger than non-activated neutrophil.

(3) nuclear membrane disintegration: upon activation, the nuclear membrane disintegrates and the shape of nuclear changes as we can observe in microscopy in both PMA and fMLP stimulations. The nuclear membrane disintegration results in slightly increases of the IDP from 1 MHz to 10 MHz.

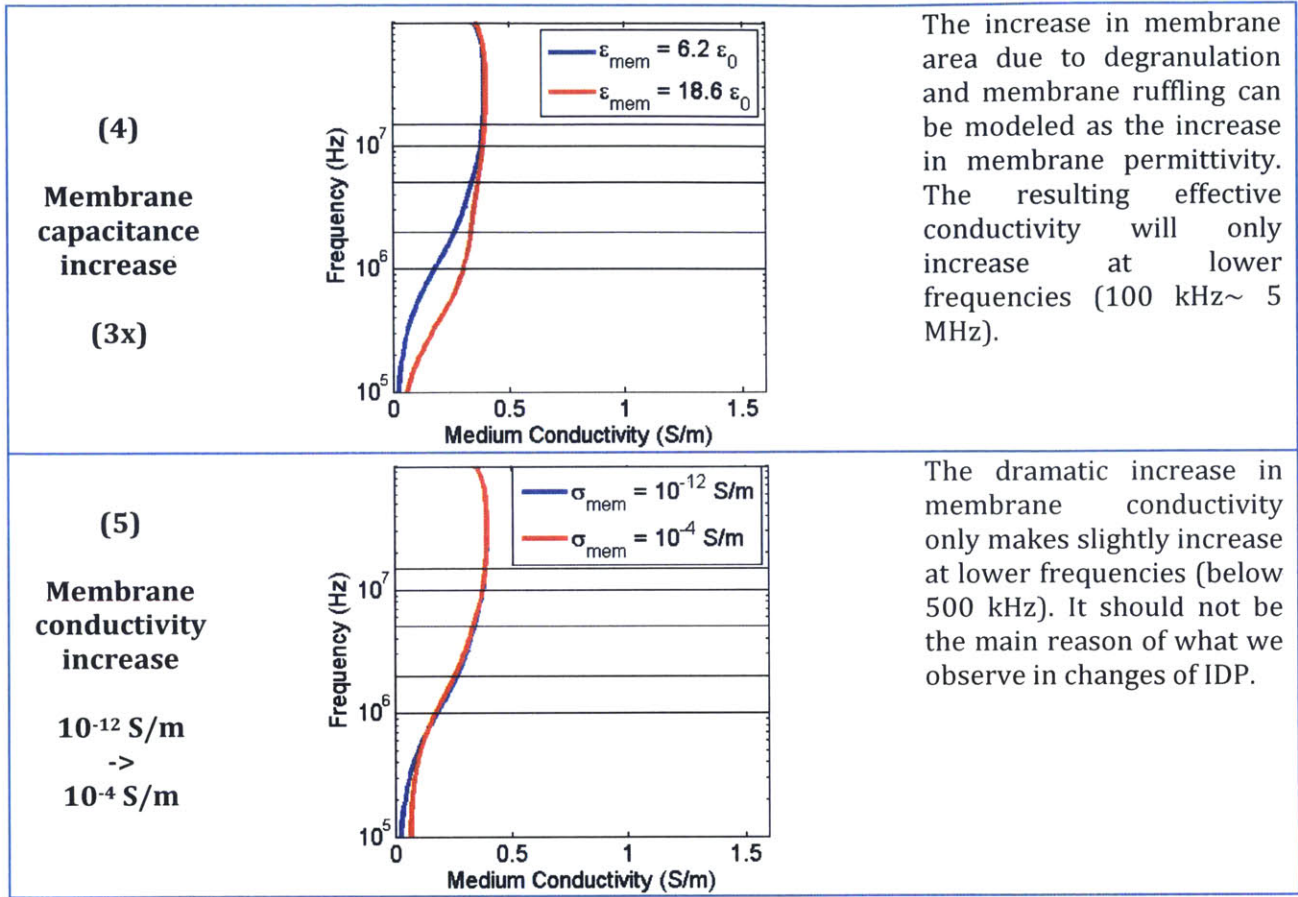
(4) membrane capacitance increase: the membrane ruffling of neutrophil and degranulation process may increase the surface area of neutrophil membrane, and thus increase membrane capacitance. The increase of membrane capacitance results in increase of effective conductivity at lower frequencies, which does not match our observation. If we consider the cell as a RC (cytoplasm as resistor as and membrane as capacitor) circuit, at lower frequencies the cell is not conductive because the capacitor has high impedance (like an open circuit). At higher frequencies, the cell becomes conductive because the impedance of the capacitor drops. At extreme high frequencies, the impedance purely depends on the resistor (cytoplasm). Increasing the capacitance of the capacitor will move the corner frequency of the transition down to even lower frequencies (RC up, f down).

(5) membrane conductivity increase: before NETosis, the incomplete plasma membrane will result in increasing membrane conductivity. The simulated model, the membrane conductivity barely affects the IDPs. However, for a broken membrane the change in cytoplasmic conductivity may be more serious.

To summarize, neutrophil activation may result in changes in different parameters in the double-shell model. While the resulting trend may due to more than multiple effects, the increase of cytoplasmic conductivity is the most probable dominant effect based on the result trend in IDS experiment.

Table 3-2 The change in IDPs at different frequencies under (1) volume increase (2) cytoplasmic conductivity increase (3) nuclear membrane disintegration (4) membrane capacitance increase (5) membrane conductivity increase (blue: non-activated, red: activated). The five black lines indicate 1 MHz, 2 MHz, 5 MHz, 10 MHz, and 15 MHz.

Electrical changes of neutrophil activation	Changes in effective conductivity at different frequencies	Comments
<p>(1)</p> <p><b>Volume increase</b></p> <p>R = 6 <math>\mu\text{m}</math> -&gt; R = 7 <math>\mu\text{m}</math></p> <p>Volume increased by 59%</p>		<p>The size change reduces the effective conductivity in higher frequencies. It is known the size will increase after the activation. However, the effect of size change in the double shell model affects pretty little. The intracellular conductivity change during the size change may be more of a dominant effect of what we observe in IDS.</p>
<p>(2)</p> <p><b>Cytoplasmic conductivity increase</b></p> <p>0.3 S/m -&gt; 0.45 S/m</p>		<p>The increase of cytoplasmic conductivity makes the effective conductivity also increase at higher frequencies but not low frequencies. The trend is similar to what we observe in IDS experiments.</p>
<p>(3)</p> <p><b>Nuclear membrane disintegration</b></p> <p>20 nm -&gt; 0 nm</p>		<p>Reducing the nuclear membrane from 20 nanometer to zero will not affect effective conductivity at high and low frequencies but only slightly increase the effective in between 1 MHz and 10 MHz.</p>



### 3.7 Conclusion

We have successfully isolated and activated neutrophils and used our platforms to screen through the electrical changes across many conditions: different frequencies, conductivities, and drug inhibitions. We observed repeatable and consistent electrical changes using both IDS and DEP spring, namely, an increase in effective conductivity at higher frequencies (above 5MHz). In search of the underlying mechanism, the result of the inhibition that the electrical changes accompanying neutrophil activation could due to actin-based activity, such as endocytosis and exocytosis. We build a double shell model of a typical neutrophil and interrogated different activation related phenomena with their effects on electrical changes. The model shows qualitatively and quantitatively the changes in effective conductivity at both high and low frequencies. By comparing the model with the trend we found that the increase in cytoplasmic conductivity is the dominant reason for this change in dielectrophoretic behavior.

After the *in vitro* study, we are confident that we can quantify actual electrical changes due to neutrophil activation, and that the changes are reflected in our DEP platform at high frequencies. This sets us up for the *in vivo* studies in the subsequent chapters. While we still do not fully understand the mechanism underlying the electrical changes, we show that with our high-throughput platform, we are capable of screening the electrical changes under different treatment allowing more sophisticated neutrophil function assays.



## Chapter 4 Monitoring sepsis progression in a murine model

In this chapter, we design an experiment to study the progression of circulating neutrophil activation in septic mice. To understand the systemic immune response, we measure multiple parameters including IL-6 and IL-10 cytokines to be correlated with neutrophil activation. We evaluate the prognostic value of neutrophil activation by comparing between survivors and non-survivors. The resulting data may be useful for modeling of immune response and patient stratification.

In section 4.4, we describe the electrical profiling of leukocytes using IDS for the same experiment. We describe the trend we observe, the interpretation of the electrical profile of leukocytes and the diagnostic and prognostic value of IDS leukocyte activation index.

### 4.1 Motivation

Sepsis is a condition that has 30~50% mortality with 18 million patients suffering worldwide yearly [1]. Traditional sepsis diagnosis is based on systemic inflammatory response syndrome (SIRS) plus clinical signs of pathogen. However, diagnosis of sepsis is not straightforward, especially in the intense care unit (ICU). Patients in ICU usually have other clinical issues that might have overlapping syndromes as sepsis. Currently, many suspected septic patients are treated with antibiotics, which tends to promote the drug resistance for bacteria and results in a long-term crisis of declining antibiotic treatment efficacy. Therefore, accurate and precise diagnosis of sepsis is important, especially to rule out patients that do not need antibiotic treatment. For example, research has shown that using CD64 marker expressed on neutrophils has high sensitivity (96%) and NPV (97%) with reasonable specificity (72%) in neonatal sepsis [71], and thus could become useful to reduce antibiotic usage in newborn children, which can hinder the development of the immune system. Note that the cut off value can be tuned to each both high sensitivity (90%) and specificity (91%). Some clinical studies have started to use biomarkers like C-reactive protein (CRP) [72] or procalcitonin (PCT) [8] as criteria for ruling out infections or changing therapy for suspected septic patients. However, neither can alone diagnose sepsis with enough specificity. In the future, combined panels or scores might provide better diagnosis and prognosis in sepsis [73]. In this study, we implemented a multi-parametric time series study to monitor sepsis progression in murine model in search of potential markers for diagnosis, prognosis and guiding therapy.

One particular interesting target of monitoring is neutrophil. Neutrophils are important mediators of the innate immune response. For defense of invading microbes, neutrophils are released from the bone marrow and migrate to the infection site. Excessive neutrophil stimulation is often considered as an important factor of systemic inflammatory response syndrome. Specifically, presence of immature granulocytes or band cell counts is correlated with sepsis [6]. In addition to immature cell counts, phenotypes expressed by receptors of neutrophils have also been found to rapidly changing during post-injury systemic inflammation [74]. Therefore, neutrophil activation can be an important sepsis diagnosis target for host response in addition to current SIRS criteria of existing white blood cell counts and band cells percentage. For therapeutic purposes, removal of activated neutrophils can also be an interesting target for mitigating an overreacting immune response.

Several murine models have been used to study sepsis because of their comprehensive immune profiling and availability of genetically modified animals. In particular, cecal-ligation and puncture (CLP) method has been used more than 3 decades and remains one of the standard ways of inducing sepsis in mice. In CLP method, a specified percentage of the cecum in the anesthetized animal is ligated and then punctured to release cecal content for inducing infection and inflammation. While genomic responses of sepsis mouse models have been argued correlates poorly with human [75], the CLP murine model is still the most popular method because it recreates human sepsis progression with similar hemodynamics [76]. Like in human sepsis, CLP murine model presents both hyper- and hypo-inflammatory responses supported by elevated proinflammatory cytokines and apoptotic lymphocytes and dendritic cells, respectively. Thus, the CLP murine model is appropriate for studying neutrophil activation as an innate response to bacterial sepsis. In the long run, removing activated neutrophils in CLP murine model could also be used as a preclinical model of intervention.

In addition to neutrophils, we include multiple parameters that relate to neutrophil activation to understand sepsis at a system level. Multi-parametric analysis enables numerous correlation studies that grow rapidly with the number of observations and therefore help us understand a bigger picture of the immune status. Being able to monitor evolution of systemic inflammatory response over time within individual animals is more valuable than sacrificing animals at each time point because we can reveal the trends of time-dependent immune status in individual animals and thus reduce the effect of heterogeneous responses to the stimulation. The information gathered by combining temporal study with multi-parametric measurement at each time point may reveal more accurate trends of immune status changes that cause deaths. Song et al. developed a multi-parametric model in rats and built a neutrophil trafficking model out of the multi-parametric data but without explicitly measuring neutrophil counts and activation level and treated them as hidden variables [77]. By quantifying circulating neutrophil counts and activation status along with other parameters, researchers may build more comprehensive models of the neutrophil trafficking in sepsis.

Repeated blood draws are not typically used in murine models due to the mouse's limited blood volume (~1 ml), even for healthy mice. Recently, Weixelbaumer et al. demonstrated daily blood draws from mice with 20 ~ 35  $\mu$ L sample each time [78]. The RBC counts and hemoglobin concentration were 20% lower than the control group but WBC counts, platelet counts and IL-6 level were similar. Here we developed methods to perform multiple (up to 6 time points) blood draws from single animals using preinstalled catheter instead of facial vein bleeding [79]. In addition, we developed a work flow for measuring more parameters that can be analyzed from each sample, in the process demonstrating comprehensive immune-profiling across time points for monitoring CLP sepsis in mice.

The goals of this study are: (1) determining if neutrophil activation is correlated with survival outcome; (2) determining the relation between circulating leukocyte counts, neutrophil activation, and cytokine levels during sepsis progression.

## 4.2 Study design and methods

This study is designed to capture important dynamics from the CLP murine model. We aim to capture the hemodynamics and cytokine dynamics for both hyper and hypo-inflammatory response, and therefore our blood collection time points will include both early and later time points after CLP procedure.

### Time and volume

To capture the overall dynamics, we sample peripheral blood before the CLP surgery, and 6hr, 24hr, 48hr, 72hr, and 144hr after the surgery (similar to Song et al. [77]). Figure 4-1 depicts the experimental workflow, showing repeated monitoring of sepsis progression in the CLP model. The total amount of blood drawn for the 7 days while alive is 100  $\mu$ L, which is about 10% of the mice total blood volume ( $\sim$  1 mL). Too much volume would result in excessive loss of blood which may affect the sepsis outcome. We keep our blood drawn volume below the reported volume ,35  $\mu$ L, that does not affect mortality [78]. The protocol is approved by the MIT Committee on Animal Care and our sponsor DARPA.

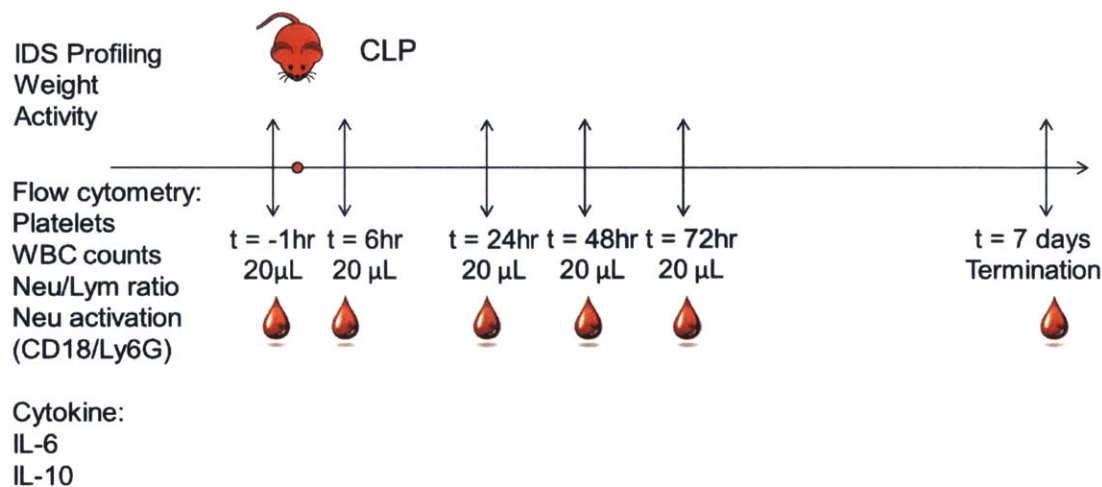


Figure 4-1 Timeline of the blood collection in CLP murine model with 8 independent parameters measured.

### Biomarker selection

We monitored sepsis progression with IDS activation, white blood cell counts, neutrophil/lymphocyte ratio, IL-6, IL-10 as well as mouse weight and activity. Cytokine (IL-6, IL-10) profiling was measured with Luminex multiplex bead-based assays (eBioscience). IL-6 is an pro-inflammatory cytokine and an important mediator for acute phase immune response, which has been shown that its 6 hour concentration correlates with mortality [80]. IL-10 is another cytokine that counters the pro-inflammatory cytokine-induced inhibition of neutrophil apoptosis [81]. IL-10 is elevated during both pro-inflammatory and anti-inflammatory state. At the time of the study, the Luminex assays offer 10 different multiplex cytokines measurement: GM-CSF, IFN-gamma, IL-1alpha, IL-2, IL-4, IL-5, IL-6, IL10, IL-17, TNF-alpha. However, after investigation of sensitivity, we only find IL-6 and IL-10 above the detection level under this dilution.

### Multiple blood collection

We collected blood from 6-8 week C57BL/6 male mice (~25 grams) bearing right carotid and left internal jugular catheters (Charles River laboratories, Wilmington, MA), which are originally placed for the study of dialysis-like therapeutics. The setup is in Figure 4-2. After removal of 20  $\mu\text{L}$  of blood, we instilled  $\sim 50 \mu\text{L}$  of PBS to prevent volume depletion. Then we injected  $\sim 30 \mu\text{L}$  of Heparin to avoid catheter clogging and to make the next blood draw easier. Most blood draws were done using the venous catheter with only a few requiring arterial catheter sampling because of clogged venous catheters.

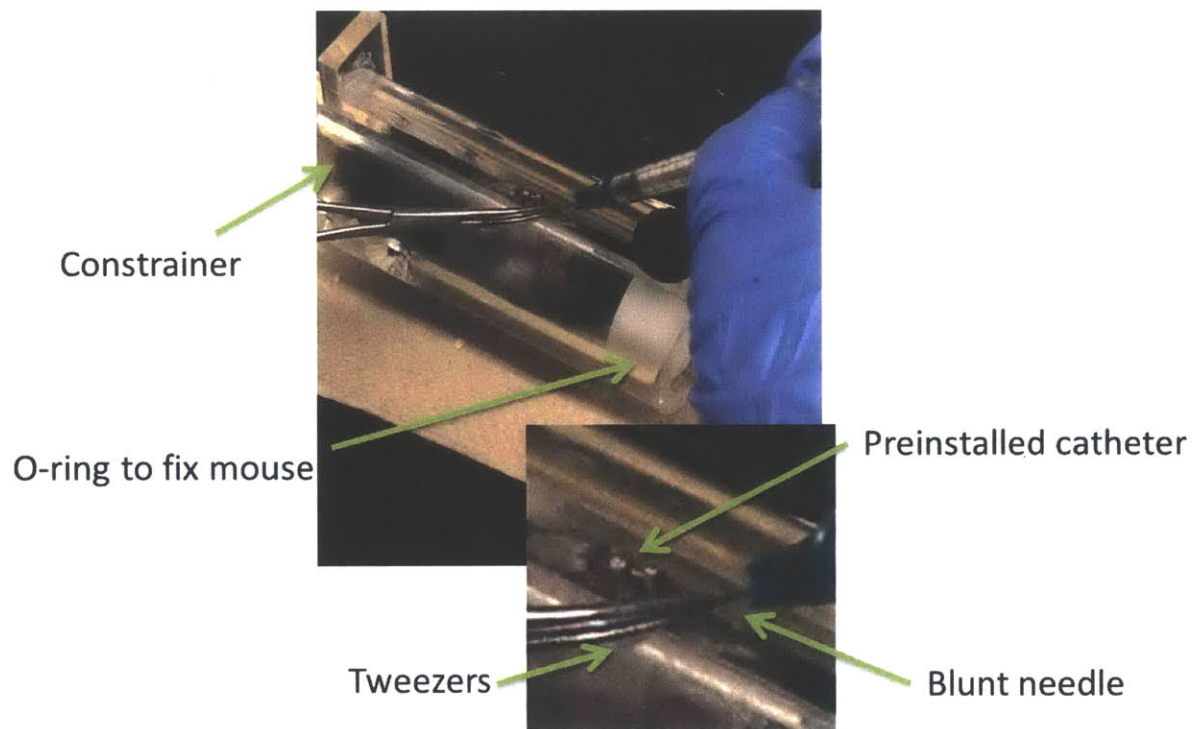


Figure 4-2 Collecting peripheral blood from pre-installed catheter. The mouse was put into plastic cylindrical restrictor to fix its movement. The preinstalled catheter was lengthened by tweezers. Stainless steel plug was removed before the needle put inside the catheter.

### Blood processing

For the blood analysis work flow, we collected the blood from the Brigham and Womens Hospital (BWH) and brought the blood to MIT for analysis. The collection time difference between the first mouse and the last mouse is less than 1 hour (3~5 min each). The transfer time is around 1 hour. The samples were analyzed within 5 hours after the blood had been drawn.

The samples were processed according to the chart in Figure 4-3. The 20  $\mu\text{L}$  blood was split into two: one half (10  $\mu\text{L}$ ) for cytokine/platelets/WBC counts which needs to be enumerated directly, and the other half for measuring neutrophil-lymphocyte-ratio and neutrophil activation level.

The sample processing of the first half only involves dilution but does not include any centrifugation steps that might introduce errors of cell concentration. We diluted the first 10  $\mu\text{L}$  of mouse blood 15x in PBS (without calcium and magnesium). The diluted sample is then split to 10  $\mu\text{L}$  for total white blood cell enumeration and another 140  $\mu\text{L}$  for plasma extraction by spinning down the WBCs, RBCs, and platelets. To quantify the total leukocyte counts and platelet counts, the 10  $\mu\text{L}$  diluted sample was stained with the platelet marker, CD41a-FITC (1:50, eBioscience, San Diego, CA), and the leukocyte marker, CD45-APC (1:100, eBioscience, San Diego, CA), for 30 min at 4°C and then diluted for flow cytometry analysis with a BD Accuri C6 flow cytometer. To quantify cytokines inside the plasma, we froze the samples in -80°C and sent the samples to eBioscience (now part of Affymetrix) for quantification. The multiple cytokines in the diluted plasma were quantified through multiplex beads assay (Luminex). Each sample was measured twice with 50  $\mu\text{L}$  of diluted plasma each time.

For the second half of the sample, the highly concentrated red blood cells prevent us from measuring the neutrophil-lymphocyte-ratio and neutrophil activation without dilution. To effectively identify neutrophil-lymphocyte ratio with sufficient cell numbers, we used RBC lysing buffer to remove the majority of red blood cells and lower the RBC concentration. Namely, the whole blood was lysed with 1 $\times$  RBC lysis buffer (1:10, eBioscience, San Diego, CA) and washed twice with 1 $\times$  PBS to enrich leukocytes. We then used the enriched leukocytes to measure neutrophil-lymphocyte ratio/ neutrophil activation level/ and electrical profile of leukocytes, respectively. To measure neutrophil-lymphocyte ratio, 25  $\mu\text{L}$  of enriched leukocytes were stained with CD45-APC (1:100, eBioscience, San Diego, CA) and enumerated through flow cytometry. The lymphocyte count and neutrophil count were determined by gating based on fluorescence signal and side scatters. For neutrophil activation assay, 25  $\mu\text{L}$  of enriched leukocytes was incubated with Ly-6G (Gr-1)-APC (1:100, eBioscience, San Diego, CA) and CD18-FITC (1:100, eBioscience, San Diego, CA) at 4 °C for 30 minutes. Activated neutrophils were gated based on up-regulation of both Ly-6G and CD18 which was pre-determined using healthy and PMA-stimulated neutrophils (data not shown). The remaining 150  $\mu\text{L}$  stained by nucleic acid stain Syto 64 (1:1000, Life Technologies, Carlsbad, CA) and measured in iso-dielectric separation device for quantifying their electrical properties.

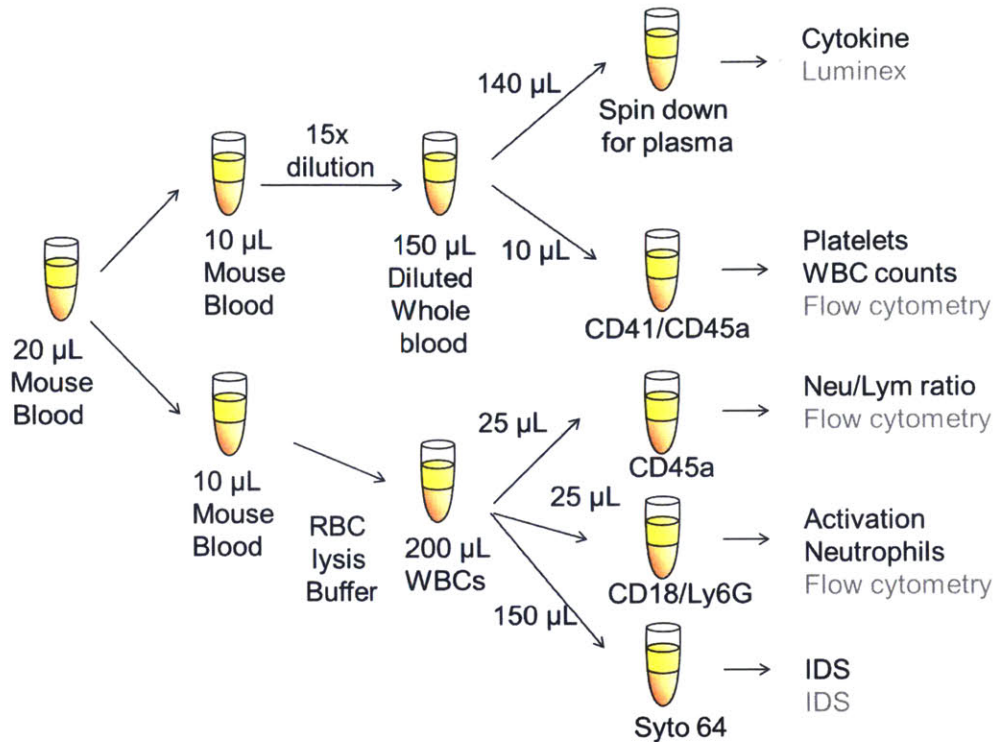


Figure 4-3 The sample sparing assay work-flow for obtaining multiple biomarkers from 20 µL of whole blood.

### CLP severity

We ran 4 sets of experiments (1 week/experiment). We studied 8 mice each week for an adequate timing of blood drawing, processing and analyzing. In week 1, we used the 50% of cecal-ligation and puncture 1 hole with 19g needle. The survival rate for the first week was too high to study the lethal conditions. Therefore for the next three weeks, we used a higher severity of CLP to reduce the survival rate, which is 75% of cecal-ligation and 2 holes with 19g needle. However, for the second week of data we did not have CD18/Ly6G neutrophil activation data and therefore will not be included in the analysis.

### Activity and weight

The mice were monitored with a camera to record their activity and exact time of death. We recorded the time of the animal reaching for food and water. We measured their weights before the blood collection to track their progression in weight.

## 4.3 Results

### 4.3.1 Severe injured CLP mice with neutrophil activation data (CD 18/Ly6G)

The result of the severe injured CLP mice is in Figure 4-4. The survival rate is 44% (7 out of 16). For the 9 non-survivors, 5 mice died between 24 hours and 48 hours after CLP, 1 died between 48 hours and 72 hours, and 3 died at 72 hours and 144 hours. We discussed trend of individual parameters as the following:

- (a) The platelet counts: On average, the platelet counts decrease a little and then increase after 48 hours. Two of the three mice died after 72 hours did not have the platelet rebound, which is similar to the finding of Drechsler et al.[82] where a 2-fold separation between survivors and non-survivors was found at 72 hours.
- (b) The white blood cell counts: The total white cell counts drop quickly in the first 48 hours and there are rebounds after 48 hours. There is no significant difference between survivors and non-survivors.
- (c) The neutrophil-to-lymphocyte ratio: The neutrophil-to-lymphocyte ratio increase for the first 48 hours, indicating the reduction of lymphocytes in acute phase infection is more than the reduction of neutrophils in circulation.
- (d) The neutrophil counts: The neutrophil counts decrease for the first 48 hours then rebound to the -1 hour base lines, even exceeding the numbers if survived. At 24 hours, the neutrophil count of the non-survivors is significantly lower than survivors. Drechsler et al.[82] also had the same finding but was not statistically significant in their study.
- (e) The activated neutrophil counts (Ly6G<sup>+</sup>CD18<sup>+</sup>): The total number of neutrophils becomes lower and the neutrophil activation percentage becomes higher. As a result, the number of activated neutrophil count does not change much for the first 48 hours.
- (f) The activated neutrophil percentage (Ly6G<sup>+</sup>CD18<sup>+</sup>): The activation percentage of neutrophil depends on the expression levels of Ly6G and CD18. After 24 hours, a few mice died with high level of activation percentage. After 48 hours, another mouse died with high level of activation percentage. At 24 hours, the neutrophil activation percentage of non-survivors is significantly higher than the survivors.
- (g) The lymphocyte counts: Similar to the neutrophil counts, the lymphocyte counts decrease for the first 48 hours then rebound to a higher level but not higher than the baseline.
- (h) The IL-6 level in plasma: IL-6 increases dramatically at 6 hours. For survivors, the level of IL-6 is significantly lower at 24 hours than non-survivors. Almost all mice died with elevated IL-6.
- (i) The IL-10 level in plasma: Similar to IL-6, IL-10 increases at 6 hours. For survivors, the level of IL-10 is significantly lower at 24 hours than non-survivors. Almost all mice died with elevated IL-10.

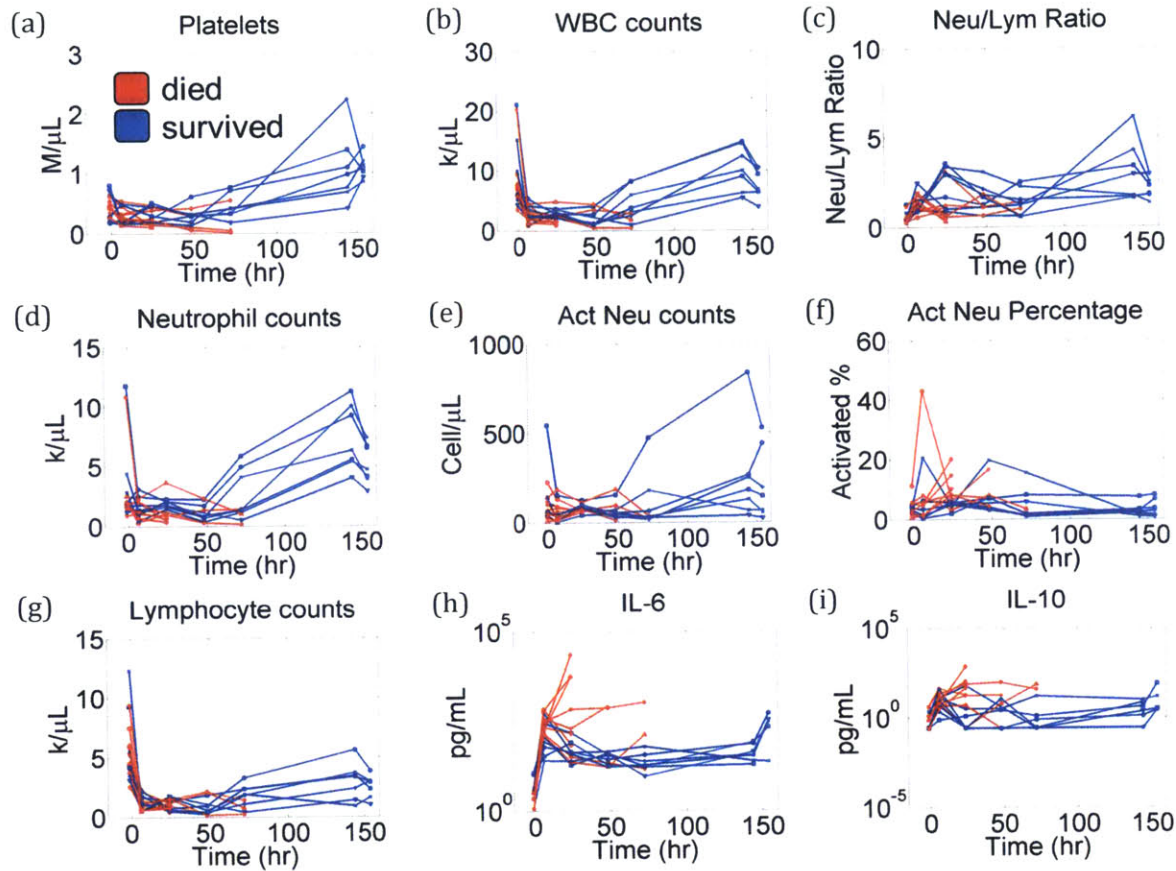


Figure 4-4 Data of 16 mice with multi-parametric time series profiling. Mice blood was drawn at -1, 6, 24, 48, 72, 144 hours after the CLP procedure. The last time point plotted at 154 hours indicate data from the heart at 144 hours. (a) The platelet counts. (b) The white blood cell counts. (c) The neutrophil-to-lymphocyte ratio. (d) The neutrophil counts deduced by b and c. (e) The activated ( $\text{Ly6G}^+\text{CD18}^+$ ) neutrophil counts deduced by d and f (f) The activated ( $\text{Ly6G}^+\text{CD18}^+$ ) neutrophil percentage (g) The lymphocyte counts deduced by b and c (h) The level of IL-6 in plasma (in logarithmic scale) (i) The level of IL-10 in plasma (in logarithmic scale)

To summarize, before the mice died, they usually have four signs at the 24 hour time points compared with surviving mice:

- (1) lower neutrophil concentration (usually  $< 600$  cells/  $\mu\text{L}$ )
- (2) higher activated neutrophil percentage defined by Ly6G/CD18 gating ( $>10\%$ )
- (3) elevated levels of IL-6 ( $>1000$  pg/mL for 15x dilution)
- (4) elevated levels of IL-10 ( $>15$  pg/mL for 15x dilution).

In the following section, we apply statistical analysis to this dataset to understand the prognostic value of these parameters.



### 4.3.2 Comparison between survivors vs non-survivors with severely injured mice

We conduct statistical tests to distinguish survivors versus non-survivors using non-parametric sign rank test (Mann-Whitney U test) and unpaired t-test (Student's t-test with Welch's correction). Both tests return the same level of statistical significance in terms of  $P \geq 0.05$  (ns, not labeled),  $P < 0.05$  (\*) or  $P < 0.01$  (\*\*). The result of 24 mice including the data from week2 with the same CLP severity is shown in Figure 4-5. Only 5 parameters among all time points show statistical difference: neutrophil counts, neutrophil-lymphocyte ratio, activated neutrophil percentage, IL-6, and IL-10. All of them happened at the 24 hours after the CLP. It matches our observations in 4.3.1.

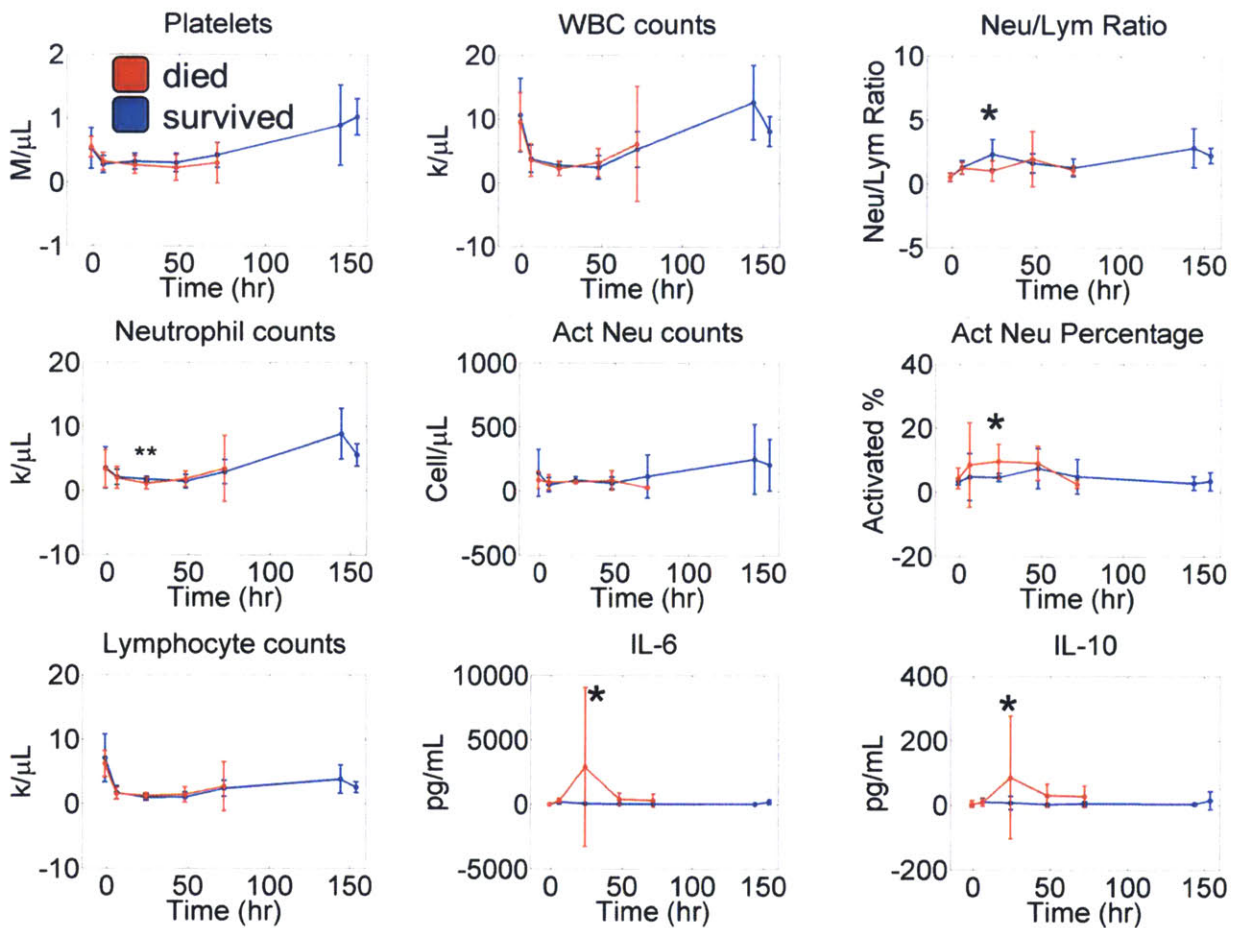


Figure 4-5 Comparison of survivors and non-survivors with multi-parametric time series profiling (N = 24, for all 75% ligation, 2 holes mice). At 24 hours, 5 parameters have significant difference ( $P < 0.05$  under both Mann-Whitney U test and Student's t-test with Welch's correction). However there is no statistical significance at other time points.

### 4.3.3 Correlation between parameters and between time points

In addition of finding the correlation with death, we would like to determine if significant correlations exist between these parameters, both at the same time points and across time points. We investigated the correlation between parameters at 24 hours (Figure 4-6). We found that the activated neutrophil percentage correlates well with IL-6/IL-10 but not with WBC counts. This suggests that measuring activated neutrophils may provide information distinct from complete blood counts. Other than this finding, we also found some expected findings, like (1) WBC correlates with lymphocyte counts and neutrophil counts. (2) IL-6 correlates with IL-10.

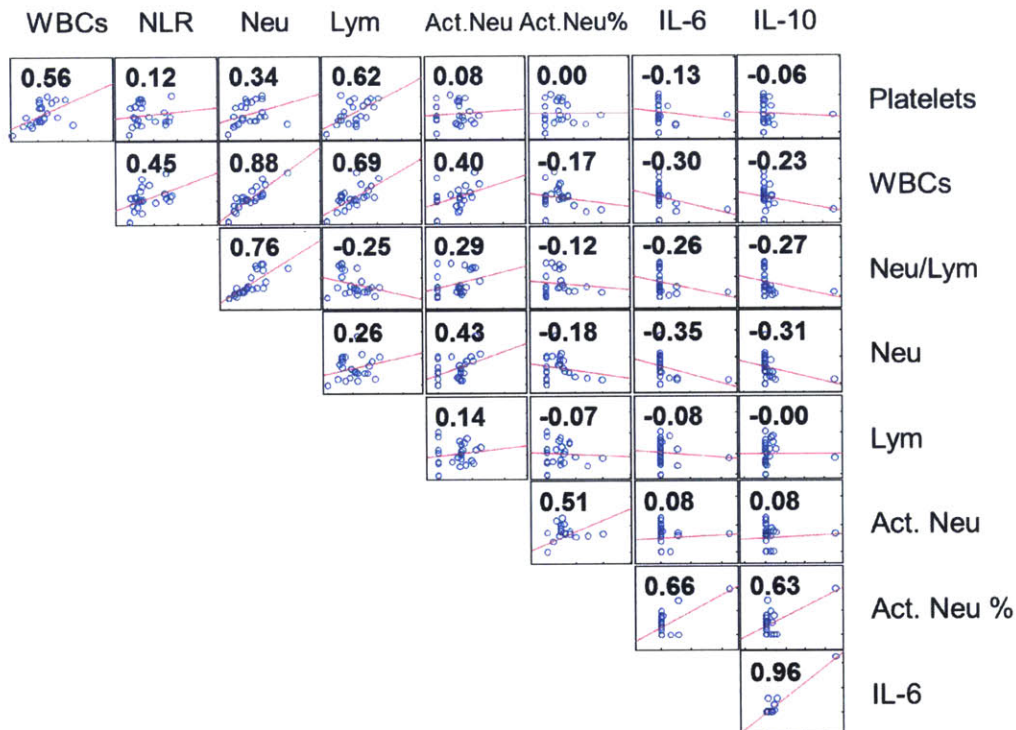


Figure 4-6 Correlation plot between parameters at 24 hours after CLP procedure. The number on each box indicates the correlation coefficient of the column parameter and the row parameter. Given the 24 mice,  $R > 0.405$  or  $R < -0.405$  will correspond to  $p$ -value  $< 0.05$  (two-tailed probability),  $R > 0.47$  or  $R < -0.47$  will correspond to  $p$ -value  $< 0.01$  (two-tailed probability).

We also investigated the correlation between parameters at the 24 hour and 6 hour time points to find earlier markers for treatment candidates (Figure 4-7). We found that the 6 hour IL-10 level correlates modestly ( $R=0.4$ ) with 24-hour activated neutrophil percentages, but it was not statistically significant ( $p=0.06$ ). We also found the 6 hour IL-6 level correlates negatively with the 24 hours neutrophil-to-lymphocytes ratio, possibly due to more neutrophil recruitment to the infection site from more intense inflammatory response.

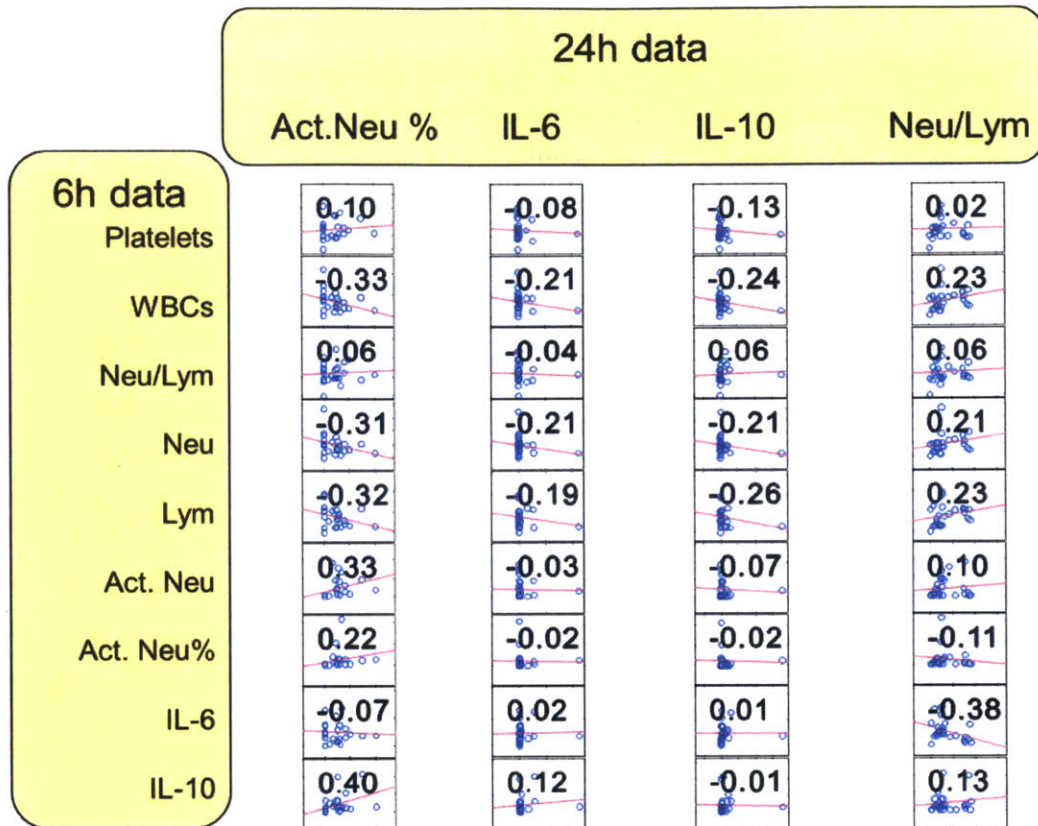


Figure 4-7 Correlation plots between 6 hour data and 24 hour data. The number on each box indicates the correlation coefficient of the column parameter and the row parameter. Given the 24 mice,  $R > 0.405$  or  $R < -0.405$  will correspond to  $p$ -value  $< 0.05$  (two-tailed probability),  $R > 0.47$  or  $R < -0.47$  will correspond to  $p$ -value  $< 0.01$  (two-tailed probability).

#### 4.3.4 Discussion and conclusion

After the injury, the lymphocytes and neutrophils are recruited to the infection site and thus reducing the number of white blood cells in circulation. At the same time, neutrophil expression level of CD18/Ly6G also increases after the injury, consistent with the activation of neutrophils to enhance adhesion. IL-6 and IL-10 elevation are the effect of acute phase inflammatory response. For prognosis, we observe non-survivors have lower neutrophil counts, higher neutrophil activation percentage, higher IL-6 level, and higher IL-10 level.

We correlated the parameters at 24 hours with each other and found neutrophil activation percentage correlates with IL-6 level and IL-10 level but does not correlates with neutrophil counts and white blood cell counts. Therefore, neutrophil activation may be an important marker in the hyper-inflammatory phase and independent of white blood cell counts and neutrophil counts.

#### 4.4 IDS electrical profiling of leukocytes and its correlation with flow cytometry

Based on the result *in vitro* characterization of neutrophil activation (3.3), we suggest that there are quantifiable electrical changes upon neutrophil activation at 10 MHz. From the *in vivo* study we discussed above, we understand there are quantifiable changes neutrophil activation (Ly6G/CD18) in circulation blood of septic mice. We want to understand if we can measure the neutrophil activation in septic mice with IDS.

However, the blood volume in mouse is much smaller than human. Isolating neutrophils from mouse blood requires at least 500  $\mu$ L using the mice negative selection kit (EasySep MACS kit). Given that we want to do multiple tests with the blood, we choose to use RBC lysis buffer and characterize the electrical profile of leukocyte instead of neutrophils. Dino Dicarolo's group utilized mechanical phenotyping of leukocytes in pleural fluid and found significant difference between healthy patients and patients with cancer/immune activation [35, 83]. Therefore, we believe that measuring leukocyte population may also give us enough signals to monitor murine sepsis progression.

##### 4.4.1 Comparing electrical profiling of leukocyte in IDS and neutrophil activation in flow cytometry

Prior to the study of time series experiment in section 4.1-4.3, we initiated a set of experiments of electrical profiling of leukocytes. We correlated the IDS leukocyte activation level with neutrophil activation level in flow cytometry at different time points after CLP. The experiment shown in this section (4.4.1) is designed by Javier Prieto and implemented by Javier Prieto and me.

Figure 4-8a illustrates the process flow of the experiments. We sacrificed the mice at 6 hours, 12 hours and 24 hours time points and measured their activation in IDS and flow cytometry. To quantify the activation level of neutrophils, we first gate the granulocyte population and evaluate the Ly6G marker and CD18 marker on the granulocyte population. Cells with over-expressed Ly6G or CD18 are estimated as activated neutrophils. The percentage of activation is calculated by the number of activated cells over the total granulocytes. For IDS, we quantify the activated leukocyte by counting the number of leukocytes that shift to higher effective conductivity at 10 MHz.

Figure 4-8b is the means and standard deviations of the activation level for IDS and flow cytometry. After the injuries, the neutrophil activation percentage of flow cytometry increases significantly. For IDS, the average of leukocyte activation percentage decreases a little at 6 hours and increase after 12 and 24 hours. For mice 24 hours after CLP, IDS leukocyte activation is significantly higher than healthy mice.

Figure 4-8c is the correlation between the IDS leukocyte activation and flow cytometry neutrophil activation percentage. The correlation is positive and has high correlation coefficients ( $R^2 = 0.71$ ,  $p < 0.001$ ). This nice correlation is leveraged by the fact that there are 3 very sick animals of 24 hours CLP with both high activation in IDS and flow cytometry. If we remove the three points, the  $R^2$  dropped to 0.616. If we further remove the CLP 12 hour data the  $R^2$  drop to 0.329.

While we have a very interesting result suggesting that IDS leukocyte profiling can also indicate sepsis progression, we further designed the time series study (section 4.1-4.3) to evaluate if we can

really use IDS leukocyte activation to monitor sepsis progression at different time points for the same animal.

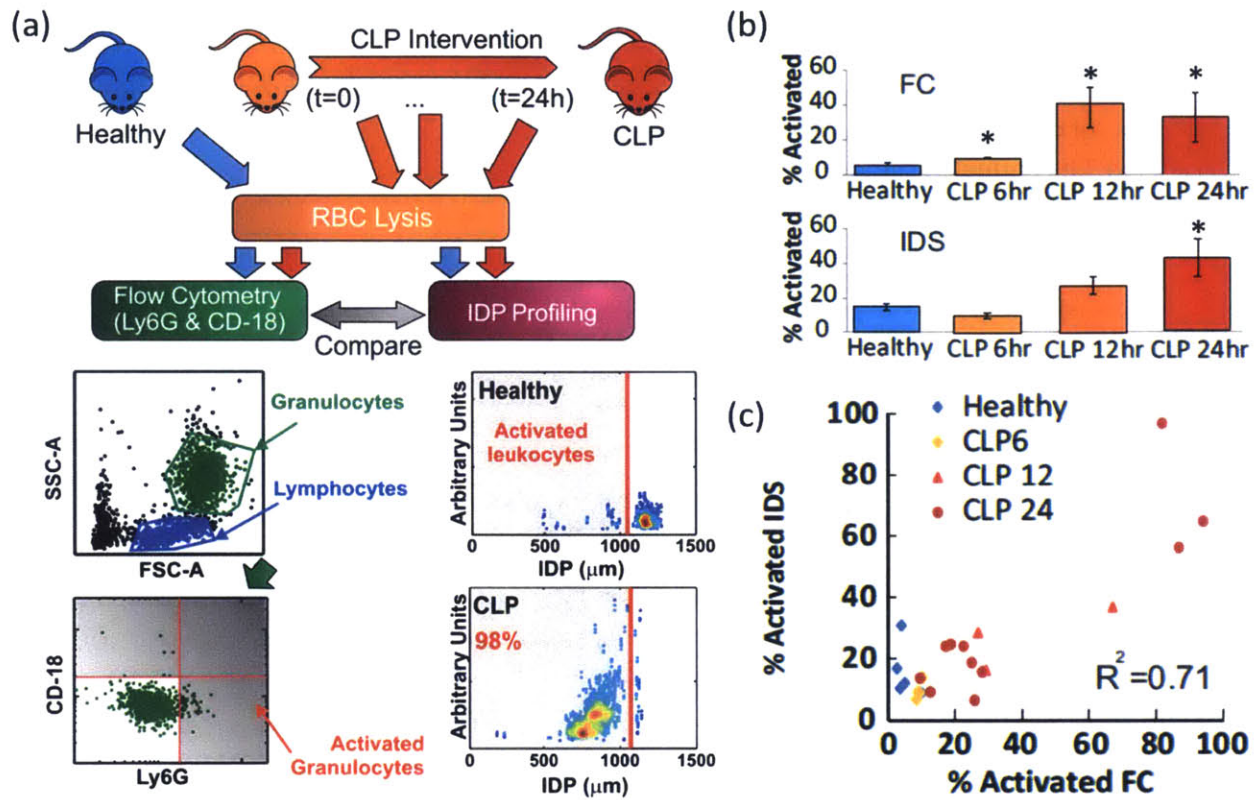


Figure 4-8 (a) Monitoring sepsis progression in a CLP mouse model with IDS leukocyte profiling and flow cytometry granulocyte profiling. (b) The percentage of activated cells increases over time in both IDS and flow cytometry (\*  $p < 0.05$  under MW U-test). (c) The correlation between IDS activation percentage and flow cytometry activation percentage ( $R = 0.84$ ,  $R^2 = 0.71$ ,  $p < 0.001$ ,  $N = 19$ ).

#### 4.4.2 Diagnostic and prognostic values of IDS leukocyte activation and neutrophil activation in flow cytometry

Using the method describe in section 4.2, we obtained the data both IDS and flow cytometry activation of 16 mice. However, there are a few differences between the two experiments.

- (1) In 4.4.1, the mice were sacrificed and the blood samples were collected from heart. In this section 4.4.2, the blood samples were collected through pre-installed catheter. The baseline of activation level might be higher than the healthy control in 4.4.1 because of potential inflammation due to the pre-installed catheter.
- (2) The CLP was done with different persons and have different variability in injury severity.

Figure 4-9a and Figure 4-9b are the mean and standard deviation of activation level in flow cytometry and IDS. The activation levels are lower than what we found in 4.4.1. While comparing the value of two activation percentage is not fair due to different sample processing and gating, there are larger differences between the 6 hours and healthy in 4.4.1, compared to differences between the 6 hours and -1 hours in 4.4.2. In other words, changes in neutrophils activation or

activation leukocytes after the CLP procedure are more dramatic in 4.4.1 than 4.4.2. There are a few possible reasons that make this difference.

- (1) The base line in 4.4.2 is not as low as 4.4.1 because the mice in 4.4.2 may not be as healthy as 4.4.1 after the installing of catheter.
- (2) The CLP surgeries were done by different persons and may result in variation. This set of experiment has lower injury levels.
- (3) The animal variations could also be the reasons.

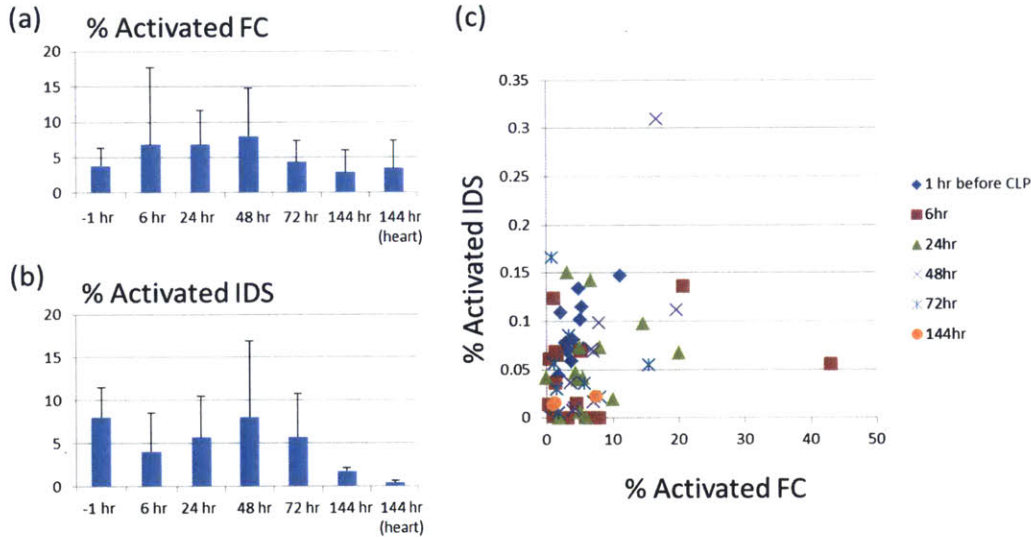


Figure 4-9 (a) The neutrophil activation percentage in flow cytometry across time after CLP. (b) The leukocyte activation percentage in IDS across time after CLP. (c) The correlation between the flow cytometry activated neutrophil percentage and IDS activated leukocyte percentage. ( $R^2 = 0.0567$ )

Overall, we did not observe a clear diagnostic value of IDS leukocyte activation percentage in the time series experiment. Figure 4-10 is the comparison between survivors and non-survivors. For flow cytometry, the non-survivors have significantly larger neutrophil activation percentage at 24 hours after CLP. In IDS, although the mean activation percentage is higher for non-survivors at 24, 48, and 72 hours, the relations do not reach statistical significance.

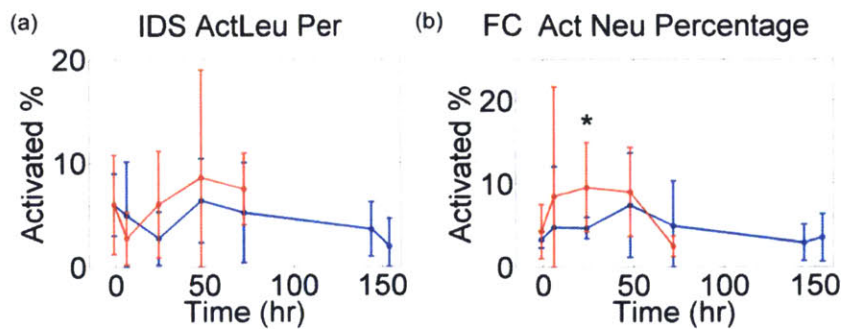


Figure 4-10 Comparison of the activation level of (a) IDS leukocytes activation percentage and (b) Flow Cytometry neutrophil activation percentage between survivors (Blue) and non-survivors (Red).

#### 4.4.3 Understanding the IDS leukocyte profile

Given the lower correlation with flow cytometry, and low diagnostic and prognostic values in the times series experiments in 4.4.2, we started to reevaluate what leukocyte activation means. There is a fundamental difference between the leukocyte population in human and mouse. In human, the majority (50%~70%) of leukocyte are neutrophils. In mouse, the majority of leukocytes (60%~90% in healthy mouse) are lymphocytes. In injured mice, the neutrophil-to-lymphocyte ratio increased average 1:1 at 6 hours after CLP.

Our explanation for 4.4.1 is that for heavily injured mice (3 at 24 hours, and 1 at 12 hours), the activation level of both increases. However, for lower activation level, the correlation of leukocyte activation level and neutrophil activation level is unclear. In 4.4.2, we observe a really low correlation between IDS leukocyte activation percentage and neutrophil activation percentage in flow cytometry. This is likely due to the fact that there are no super high activation profile animals in this set of experiment and to bring the correlation back to where it should be.

In search of the explanation of the IDS leukocyte profile, we need to understand where the lymphocytes and neutrophils are in IDS. Lymphocytes and neutrophils have different electrical properties and have been shown separable by DEP via field-flow- fractionation [47], which separates cells temporally by turning differences in cell properties into differing transverse levitation heights and in turn into axial velocity differences in a parabolic flow field [47]. However, the levitation height in DEP-FFF depends both on the dielectric properties of the cells and their density. To understand where lymphocytes and neutrophils are in IDS, we dig into the raw data of IDS profiling of mouse leukocytes stained with Syto 64 (nucleic acid stain). Figure 4-11 shows a scatter plot of the Syto 64 mean intensity versus IDP where there are two clusters of cells. In flow cytometry neutrophils have higher intensity Syto 64 than lymphocytes because of the greater abundance of nucleic acid. If we identify the brighter-staining population as putative neutrophils, then we find that that population has a generally larger IDP than the other population, which may be lymphocytes.

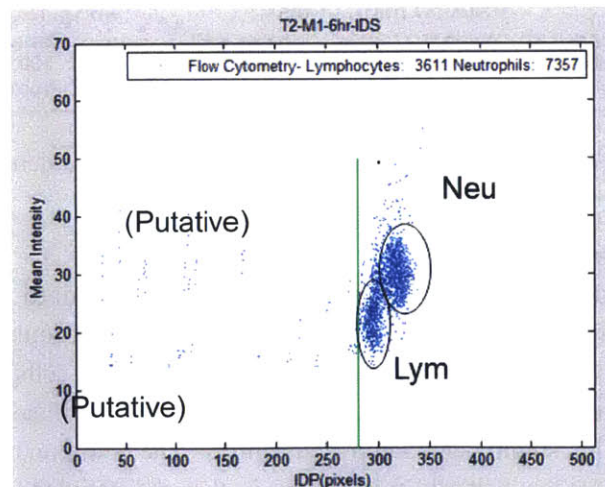


Figure 4-11 IDS scatter plot of Syto 64 mean intensity and iso-dielectric point (IDP). Putative neutrophils have higher Syto 64 mean intensity and larger IDP while putative lymphocytes have smaller Syto 64 mean intensity and lower IDP. The green gate indicates the threshold for leukocyte activation.

This finding informs us that some activated neutrophils may overlap with main lymphocyte population and cannot be detected in IDS leukocyte activation index.

#### 4.4.4 Human leukocyte subpopulation profiling compared to activated neutrophils

To confirm the finding, we repeat a neutrophil activation experiment in 3.3 but with different treatment time of PMA to simulate different degrees of activation. Figure 4-12a is the result of IDS populations under different PMA treatment time. We characterize the PBMCs (obtained from Mono-Poly resolving media upper layer) from the same sample and overlay the population with activated neutrophils in Figure 4-12b. We found that slightly activated neutrophils (10 min treatment) overlapped with the PBMCs band. If we put a leukocyte activation gate (green line), based on the total leukocyte population, we might not detect leukocyte activation until the degree of activation becomes very high (PMA 50 min). However, if we gate the neutrophil activation from a pure neutrophil population, the sensitivity of neutrophil activation may be much higher. Therefore in the next chapter for the human experiment, we will try to focus on neutrophils instead of leukocytes.

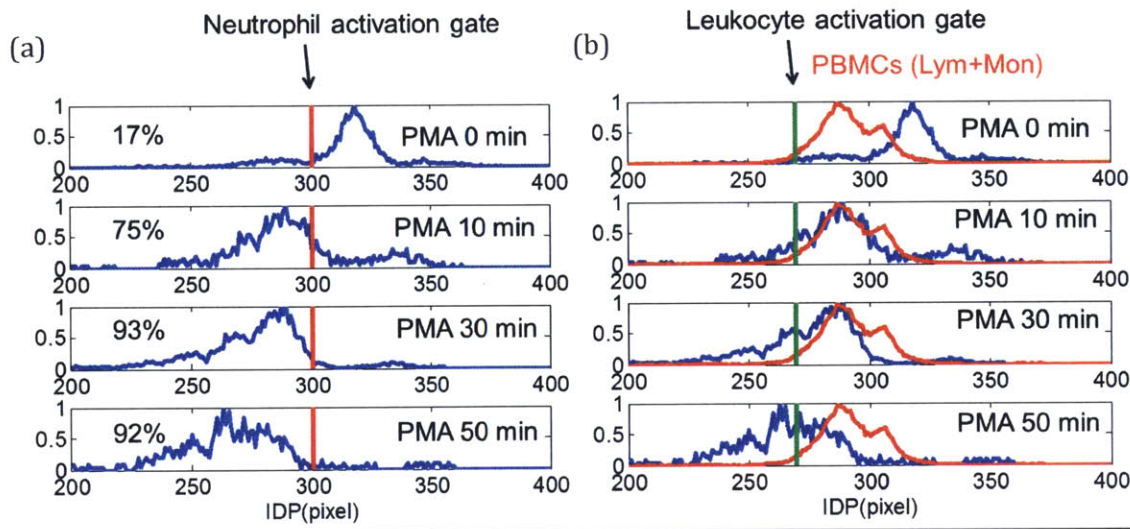


Figure 4-12 (a) IDP distribution of PMA activation of neutrophils with different durations. (b) Overlay the PBMCs population with the neutrophil profiles.

#### 4.4.5 New gating strategy for mice data

Based on the characterization in 4.4.4, we reevaluated the mice data in a new way. Instead of measuring the cells only for activated leukocyte and non-activated leukocytes, we separate the IDS result into three intervals: high conductive cells, middle conductive cells, and low conductive cells (Figure 4-13). The high conductive cells are likely activated leukocytes. The middle conductive cells are likely to be lymphocytes and slightly activated neutrophils. The low conductive cells are likely non-activated neutrophils. The reason behinds this gating is that the activated neutrophils may mix with lymphocytes in IDS while non-activated neutrophils are cleaner to quantify.



From the new three parts electrical profiling, we found qualitatively similar trends on cell counts deduced from flow cytometry (Figure 4-14). Interestingly, the low conductivity cells counts (e.g., non-activated neutrophils) are also significantly different between survival groups and non-survival groups at 24 hours. This result indicates that to find prognostic value in the IDS leukocyte profile, counting the lower conductivity cells (likely non-activated neutrophils) may best distinguish survivors and non-survivors. This finding is consistent with the fact that the non-survivors have (1) higher activation of neutrophils (2) low number of neutrophils. However, due to the low activation rate of neutrophils, we cannot conclude whether quantifying non-activated neutrophil is better than quantifying total neutrophil counts.

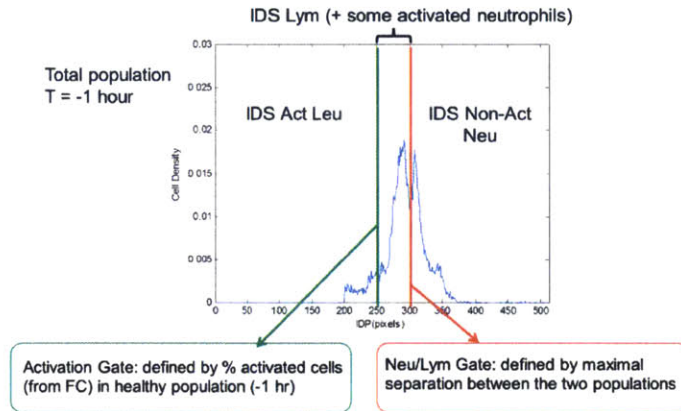


Figure 4-13 The gating for IDS includes three parts. The left most part are cells with highest conductivity (likely activated leukocytes). The middle part contains cells with medium conductivity (likely lymphocytes with slightly activated neutrophils). The rightmost part contains cells with lower conductivity (likely the non-activated neutrophils).

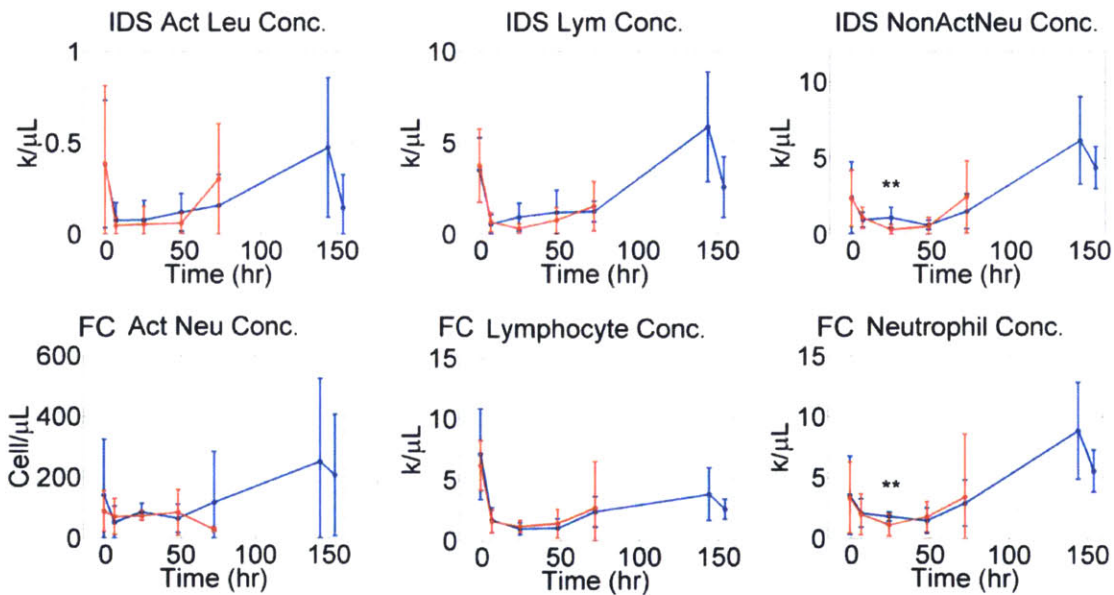


Figure 4-14 Comparison between IDS 3parts electrical profiling with the hypothetical flow cytometry parameters. (Red: Survivors, Blue: Non-survivors)

## 4.5 Conclusion

We found neutrophil activation (Ly6G/CD18) an important marker for sepsis progression, which not only increased during sepsis progression but also differed in activation level between survival group and non-survival group. The activation level of neutrophils does not correlate with white blood cell counts but it correlates with IL-10, IL-6 in the hyper-inflammatory phase. The information indicates neutrophil activation can be a potential sepsis marker for both diagnosis and prognosis.

For IDS, we characterized leukocyte activation at different time points after CLP. In 4.4.1, we found good diagnostic value at 24 hours, and the level of leukocyte activation percentage correlates well with the level of neutrophil activation percentage in flow cytometry. However, in the multi-parametric time series experiment (4.4.2), the diagnostic and prognostic value of IDS leukocyte activation level is low, and it did not correlate well with neutrophil activation percentage in flow cytometry. In 4.4.3 and 4.4.4, we estimate IDS populations of the lymphocyte population in mice and the PBMCs in human. We conclude that in order to reach higher sensitivity of activation test, the neutrophil needs to be isolated. Therefore, in Chapter 5, we quantify only the neutrophil population. To make use of the IDS electrical profiling of leukocyte, we designed a new gating strategy and found the lower conductive cell counts have prognostic value.

## **Chapter 5 Monitoring sepsis in human patients**

From Chapter 3 and 4.4.4, we understand that under PMA treatment, the IDPs of neutrophils will shift around 30-70 pixel units at 10 MHz. In this chapter, we are going to characterize the IDPs of neutrophils for human patients to see if we can observe the high activation level in septic patients. We want to compare the IDS results between septic and healthy patients. We also want to correlate IDS results with the surface markers on neutrophils, namely CD66b, CD11b, and CD18. Secondly, in search of a better condition of differentiating septic versus healthy patients, we created different treatments for neutrophils, namely stimulating the cells with the patients' own diluted plasma, diluted plasma + fMLP, diluted plasma + PMA. We obtained some interesting results suggesting that incubating neutrophils with their own diluted plasma at body temperature may enhance the difference between critically-ill and healthy patients in terms of expression level on neutrophils. In the end, we describe integration of the IDS device with a spiral trapezoid inertial sorter for leukocyte isolating. This integrated system can characterize the electrical properties of thousands of WBCs from a 20  $\mu$ L of blood in 15 minutes, enabling future point-of-care application.

### **5.1 Monitoring neutrophil activation in human patients**

#### **5.1.1 Motivation**

We have studied leukocyte activation in mice in Chapter 4. The blood volume is very small compared to human cases and therefore it is hard to isolate neutrophils for IDS characterization. In human studies, we have enough samples so that we can isolate neutrophils and compare the result with flow cytometry.

Why do we believe there is neutrophil activation in septic patients? There have been a few studies on circulating neutrophil function in septic patients, mostly on adhesion related functions, such as CD64 marker [13], CD 11b [84], HLA-DR, CD66b[85], etc.. Other than surface markers of neutrophils, upregulation of reactive oxygen species generation, phagocytosis, and increased apoptosis also have been found during severe sepsis and septic shock [86], assessed by DCFH-DA assay, fluorescent, and Annexin V and propidium iodide, respectively.

Interestingly, with traditional hematology analyzers, the mean cell volume of neutrophils has also been found as a potential parameter to discriminate sepsis and nonsystemic infection [87] and found comparable to procalcitonin in sensitivity and specificity for postsurgical bacterial infection. In addition to increased neutrophils volume, side scattering of neutrophils was also found to be reduced in septic patients [88]. The spread of neutrophil volume has also been found increased in patients with bacteremia [89] and has been studied in neonatal sepsis [90].

Based on these studies, we believe that there are quantifiable changes of neutrophils on both surface markers and intrinsic properties in septic patients. We want to know if we can use our technology as an intrinsic characterization tool to monitor neutrophil activation in septic patients. Our technology provides rapid result with little sample volume. Therefore, we initiated this pilot study to investigate suspected septic patients to test the feasibility of our approach.

### 5.1.2 Experimental design

This study of human patients is in collaboration with Brigham and Women’s Hospital (BWH) and under BWH’s Institutional Review Board (IRB) and MIT COUHES. Patient information was withheld until the blood characterization had been done. In the protocol, our collaborators first acquired consent from critically-ill ICU patients. The patients were sick but may or may not have sepsis. The patients’ samples were collected the next morning at 6:00~8:00 am. Two tubes of blood were drawn, one for our collaborators and one for the neutrophil activation assays. The results were compared and analyzed in the end after the clinical outcome of the patients had been determined.

Our portion of blood was around 3.5 mL, stored within a purple-top EDTA-coated tube. The blood samples were stored on ice and transferred to the laboratory within 20 minutes. Once the blood sample arrived, we isolated the neutrophils using a negative magnetic cell sorting (MACS) kit, EasySep™ Direct Human Neutrophil Isolation Kit (Stellcell Technologies). More specifically, we took 0.5 mL of whole blood, followed the standard protocol of MACS and obtained the final isolated neutrophils in 3.5 mL of buffer (PBS with 1% HSA). The process took around 30 minutes. We took 200 µL of this sample to run through IDS (with proper dilution with the same buffer if the concentration was too high) and used the rest for flow cytometry.

To characterize the rest of the isolated neutrophils in flow cytometry, we created five different tubes for different conditions as shown in Table 5-1. The five conditions expressed five different measures of neutrophil numbers and activation levels.

Table 5-1 Different treatments for neutrophils before the measurement in flow cytometry.

<b>Tube #</b>	<b>Treatment</b>	<b>Usage</b>
<b>1</b>	No staining	Quantifying cell concentration. This sample requires no staining and washing step to avoid sample loss.
<b>2</b>	Stained with markers	Measuring the raw neutrophil expression from sample.
<b>3</b>	Incubated in 37°C for 30 minutes before staining	Measuring the neutrophil expression after incubation with diluted plasma (7x). It may enhance the activation level for septic blood.
<b>4</b>	Incubated with 5 µM fMLP in 37°C for 30 minutes before staining	Measuring the neutrophil expression in response to fMLP as well as diluted plasma.
<b>5</b>	Incubated with 1 µM PMA in 37°C for 30 minutes before staining	Measuring the neutrophil expression in response to PMA as well as diluted plasma.

The treatment time of tube 3,4,5 (pure incubation, fMLP, PMA) was 30 minutes incubation at 37 °C. After the incubation, we spun down the cells and washed the sample with buffer once. Then we spun down the cells again, reduced the liquid to 100 µL and stained the tube 3,4,5 as well as tube 2 with antibodies. Table 5-2 is the list of the three different surface markers for quantifying neutrophil activation: CD66b-FITC (1:100, eBioscience, San Diego, CA), CD11b-PE (1:100, eBioscience, San Diego, CA), and CD18-APC (2:100, eBioscience, San Diego, CA).

Table 5-2 The three surface markers for quantifying neutrophil activation with flow cytometry.

Fluorophore	Marker	Function
FITC	CD66b (1:100)	CD66b is a marker for granulocytes and has been found at higher expression level after activation.
PE	CD11b (1:100)	One of the leukocyte adhesion markers. In circulating blood stream, activated neutrophils bind to the endothelial cells via selectins followed by more firm binding including CD18/CD11b to an unknown ligand.
APC	CD18 (2:100)	Another leukocyte adhesion marker that works with CD11b or CD11a.

### 5.1.3 Results

The summary of the patients' outcomes is in Figure 5-1. We successfully collected the data from 6 critically-ill patients in ICU with consents. None of them had sepsis with proven bacteria culture. Four of them were diagnosed with clinical sepsis: two were discharged home and the other two died. For the two not septic patients, one of them had acute respiratory distress syndrome (ARDS) and died after 50 days after the blood had drawn, and the other one was discharged to rehabilitation facility.

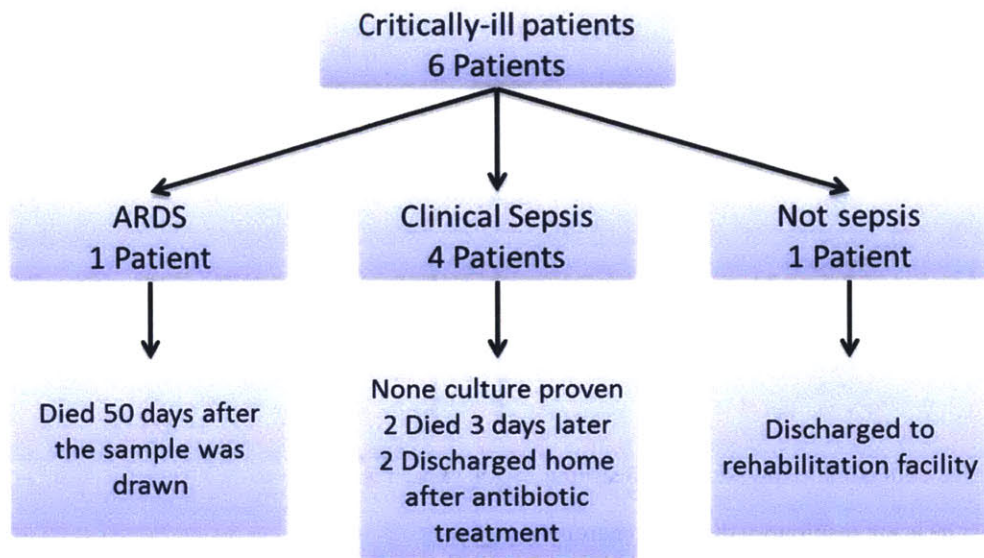


Figure 5-1 The summary of critically-ill patients' outcomes.

We have Day 0, Day 3, and Day 7 blood samples from two patients. Both of them were diagnosed as clinical sepsis. In addition, we purchased one blood sample from Research Blood Components as putative healthy control on June 30. The summary of the information is in Table 5-3, which contains the information of

- (1) the neutrophil activation assay:
  - a. mean IDP (Pixel, higher is more conductive)
  - b. mean fluorescence intensity of raw CD66b expression on neutrophils (tube 2)

- c. mean fluorescence intensity of raw CD11b expression on neutrophils (tube 2)
  - d. mean fluorescence intensity of raw CD18 expression on neutrophils (tube 2)
- (2) the result from our collaborators:
- a. the white blood cell counts
  - b. the white blood cells differential percentages of neutrophils/lymphocytes/monocytes/eosinophils/basophils/band neutrophils
  - c. the clinical diagnosis of sepsis and the survival outcome of sepsis

Table 5-3 Summary of blood test of 10 suspected septic samples (with 1 healthy control).

date	Patient ID	Outcome	IDS (Pixel*)	CD66b (MFI)	CD11b (MFI)	CD18 (MFI)	WBCs (k/ $\mu$ L)	Neu (%)	Lym (%)	Mono (%)	Eosin (%)	Baso (%)	Band (%)
11-Jun	555-D0	ARDS** Died 07-31	23	7257	4596	351	16.85	94	0	6	0	0	0
30-Jun	Healthy	Healthy	1	5088	4798	522	N/A	N/A	N/A	N/A	N/A	N/A	N/A
30-Jun	557-D0	Clinical Sepsis	27	9975	5550	588	3.47	77	2	6	0	0	15
2-Jul	557-D3	Discharged home 08-27	35	4957	4480	480	5.07	88	4.1	7.1	0.4	0	0
7-Jul	557-D7	Whole course antibiotics treatment	5	3902	6799	379	6.99	88	3.6	8.7	0	0	0
8-Jul	559-D0	Clinical Sepsis Died 07-11	3	4688	4888	479	22.64	89	4.9	4.7	1.2	0.1	0
8-Jul	560-D0	Clinical Sepsis	0	4717	3814	381	14.63	87	3.3	10	0	0.1	0
10-Jul	560-D3	Discharged home 07-21	4	3742	3185	339	12.11	82	5.9	11	0.8	0.2	0
14-Jul	560-D7	Antibiotics treatment until 07-21	28	4251	4408	445	59.85	93	1	2	2	0	2
23-Jul	561-D0	Not sepsis Discharged to rehabilitation facility	25	6875	9208	1720	7.79	67	18.2	11	3	0.3	0
23-Jul	562-D0	Clinical Sepsis Died 07-26	38	10316	9419	690	8.56	82	8.1	9.2	0.5	0.4	0

\* Pixel shifted compared to lowest value measured in this experiment.

\*\*ARDS is the acute respiratory distress syndrome.

In Table 5-3, for healthy blood, the mean IDP pixel value is only 1 pixel more than the lower number of 11 blood samples (2/11). However, this sample ranks the 7<sup>th</sup> lowest for CD66b (7/11), 6<sup>th</sup> lowest for CD11b (6/11), and 8<sup>th</sup> lowest for CD18 (8/11). If we use the level of the four markers to classify healthy versus critically-ill patients, IDS can classify the patients with the best ROC curve. However, more number of samples is needed in order to increase the power of statistical test.

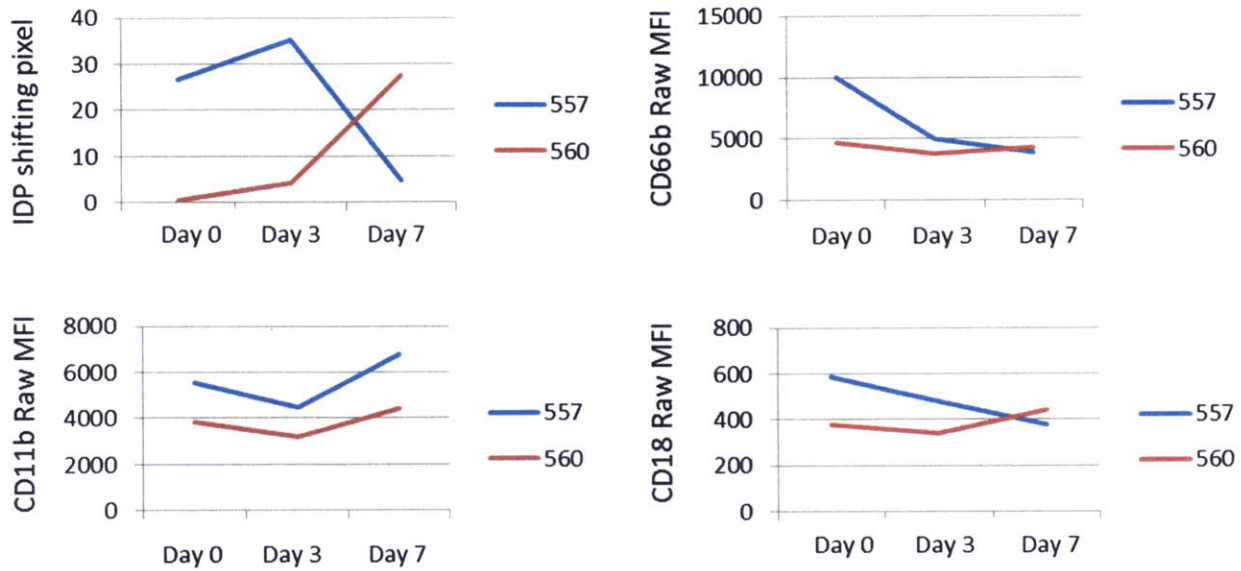


Figure 5-2 The neutrophil activation levels of IDS, CD66b, CD11b, and CD18 for two patients with sepsis who were treated with antibiotics from Day 0.

We have collected the progression of two patients with sepsis: 557 and 560. At day 0, the two patients have different abnormality of WBC counts: patient 557 has leukopenia with left-shift while patient 560 has leukocytosis. Interestingly, their IDS indexes also have the opposite trend. Patient 557 started with high IDS shifting pixel: 27 at Day 0 and 35 at Day 3. It decreased to 5 at Day 7. However, patient 560 has the opposite trend, the IDS index started with 0 at Day 0 and 4 at Day 3 and raised to 28 at Day 7. Both patients were treated with antibiotic at Day 0 and discharged home in the end. The fact that they have different white blood cells count and neutrophil activation might indicate they are in different stage of infection. The numbers in 557-D0 was pretty similar to what we saw in mice for 24 hours after CLP, low number of white blood cells with higher level of neutrophil adhesion markers and IDS indexes.

The raw data of the IDS distributions is in Table 5-4. Each figure in the IDS represents the distribution of IDPs, the horizontal axis is the IDP (decreasing from left to right) and the vertical axis is the frame number. Each dot in the figure is one cell. The density of the dots does not represent the concentration of neutrophil counts. The samples were diluted with different ratios based on concentration from flow cytometry (tube 1) to avoid the clogging in the IDS device.

We have a few observations from the raw data:

- (1) 557-D0 has 15 % of band cells from the white blood cell differential. However, in IDS distribution, we do not see any clear band that has occupied 15% of the distribution.
- (2) A lot of cells leak through the electrodes for 560-D0 and 562-D0 where the small clots form around the electrode and weaken the DEP barriers in higher conductivity regions (left side). These cells are excluded for analysis for obtaining the IDP shifting pixel value.
- (3) 557-D3 has broader distribution of IDPs but we do not have proper explanation for this data.

Table 5-4 Suspected human septic patients with IDS raw data.

date	Patient ID	IDS	CD66b	CD11b	CD18	WBC	IDS raw data	Outcome
11-Jun	555-D0	23	7257	4596	351	16.85	[REDACTED]	ARDS** Died 07-31
30-Jun	Healthy	1	5088	4798	522	N/A	[REDACTED]	Healthy
30-Jun	557-D0	27	9975	5550	588	3.47	[REDACTED]	Clinical Sepsis Discharged home 08-27
2-Jul	557-D3	35	4957	4480	480	5.07	[REDACTED]	Whole course antibiotics treatment
7-Jul	557-D7	5	3902	6799	379	6.99	[REDACTED]	
8-Jul	559-D0	3	4688	4888	479	22.64	[REDACTED]	Clinical Sepsis Died 07-11
8-Jul	560-D0	0	4717	3814	381	14.63	[REDACTED]	Clinical Sepsis
10-Jul	560-D3	4	3742	3185	339	12.11	[REDACTED]	Discharged home 07-21 Antibiotics treatment until 07-21
14-Jul	560-D7	28	4251	4408	445	59.85	[REDACTED]	
23-Jul	561-D0	25	6875	9208	1720	7.79	[REDACTED]	Not sepsis Discharged to rehabilitation facility
23-Jul	562-D0	38	10316	9419	690	8.56	[REDACTED]	Clinical Sepsis Died 07-26



### Correlation between IDS and the surface markers

In the end, we correlate the IDS level to the raw neutrophil expression of CD66b, CD11b, and CD18. The strongest correlations are CD11b with CD18 ( $R = 0.72$ ,  $p\text{-value} = 0.013$ ) and IDS with CD66b ( $R = 0.63$ ,  $p\text{-value} = 0.0367$ ). The surface marker of CD11b and CD18 are known as a pair of subunits for complement receptor 3, a receptor for macrophage-1 antigen (MAC-1). Finding the statistical significant positive correlation between CD11b and CD18 is expected. Interestingly, the IDS level is also positively correlated to CD66b with statistical significance. However, if we exclude the data points with leakage: 560-D0 & 562-D0, the correlation of IDS with CD66b drops to 0.48 and no longer is statistical significance. IDS is also positive correlated with CD11b ( $R = 0.46$ ,  $p\text{-value} = 0.15$ ) and CD18 ( $R = 0.32$ ,  $p\text{-value} = 0.35$ ) but not statistically significant.

Overall, it is hard to draw any solid conclusion with the limited number of data points we have. The goal for this pilot study is to investigate the feasibility of IDS as a tool of monitoring neutrophil activation in suspected sepsis patients. In this study, all the samples are bacteria culture negative and thus we might not have enough spread of data to see the correlation when activation levels go even higher. The dynamic range of PMA activated cells can go up 70 IDS units but the range is only 35 in this data (250->285). The PMA activated cells in CD66b, CD11b, and CD18 can go up to 30000, 50000, and 2500, while the range of raw expression of circulating neutrophils is only 10000, 10000, and 1500, respectively. With more data points and with higher activated samples, we may see the correlations better.

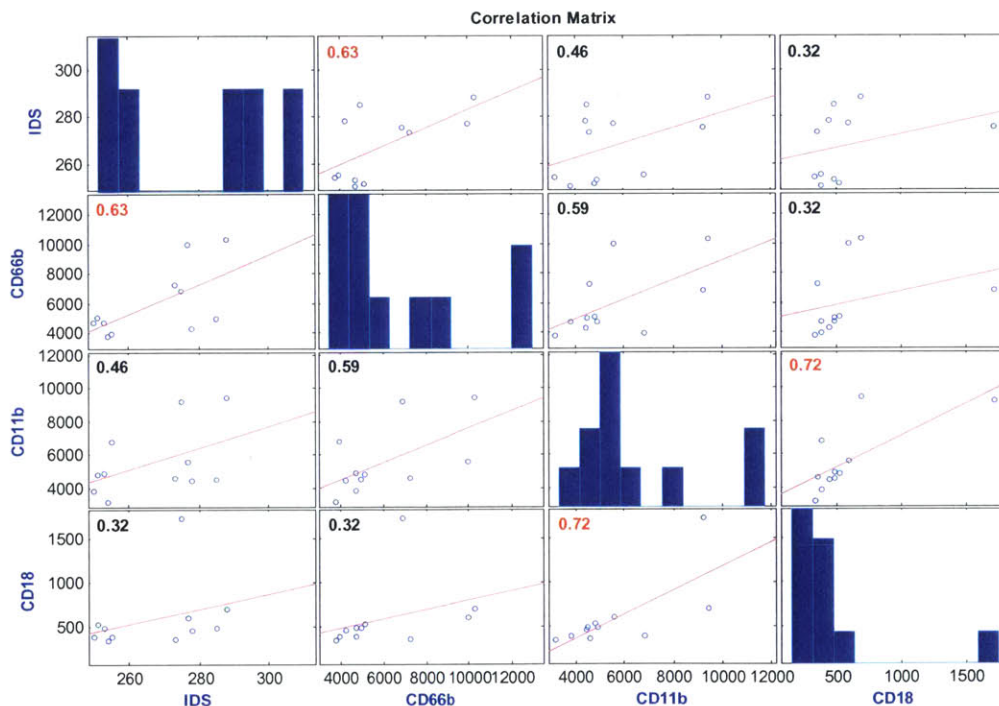


Figure 5-3 The correlation matrix between average IDPs, CD66b, CD11b, and CD18 on neutrophils. Numbers in the corners are correlation coefficients (Red indicates  $p\text{-value} < 0.05$ ).

### Surface markers expression comparison between different treatments

In Figure 5-4a, we plot the comparison for the surface expression levels of tube 2,3,4,5 from samples of healthy and critically-ill patients. For the raw expression, all the mean of CD66b, CD11b and CD18 from critically-ill patients are slightly higher than healthy control but the p-value is very high (0.48, 0.61, 0.61 for Wilcoxon rank sum test). After incubation with diluted plasma, the difference is still there and the differences between the averages become larger (p-value = 0.27, 0.12, 0.12 for Wilcoxon rank sum test). After the fMLP stimulation and PMA stimulation, the averages are more of a mix. It is possible that the fMLP and PMA activations are too strong, such that all the cells are activated to a similar level. A more precise concentration for doing the test may be found through titration.

In Figure 5-4b, we plot the expression ratio of surface markers, which is obtained by expression after treatment over raw expression. Similar to Figure 5-4a, we can observe that the cells expression go higher after incubation with diluted plasma for critically-ill patients. The p-values are (0.36, 0.18, 0.12 for Wilcoxon rank sum test) which is similar to (0.27, 0.12, 0.12) distinguishing by level of expression of incubation with diluted plasma in Figure 5-4a.

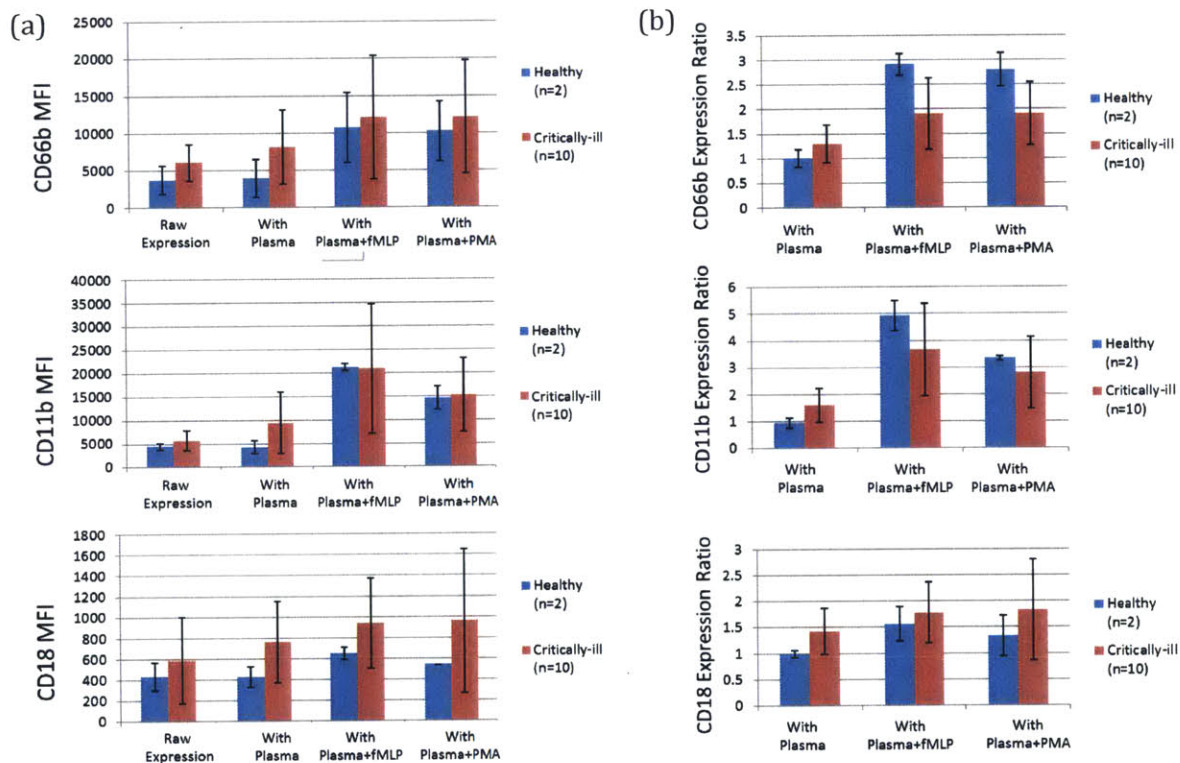


Figure 5-4 (a) Comparison of surface expression of neutrophils from the healthy donors versus critically-ill patients (the value is the average and the error bar is the standard deviation) (b) Comparison of expression ratio of surface expression under treatment with plasma, plasma +fMLP, and plasma + PMA.

Figure 5-5, Figure 5-6, and Figure 5-7 show the raw data for all the expressions for the 2 healthy control and 10 suspected septic patients. For the 5 different treatments of isolated neutrophils, tube

1 was for quantifying cell concentration and therefore was not stained. We only want to compare the values of tube 2,3,4,5.

From the raw data, 560 D7 has 10 times as many neutrophils than normal. Interestingly, the innate expression is similar to others but in tube 3, 4, 5 the levels of CD66b, CD11b are not as high as the others. They do not seem to respond to the simulants as much which may be linked to reduced or immature neutrophil function.

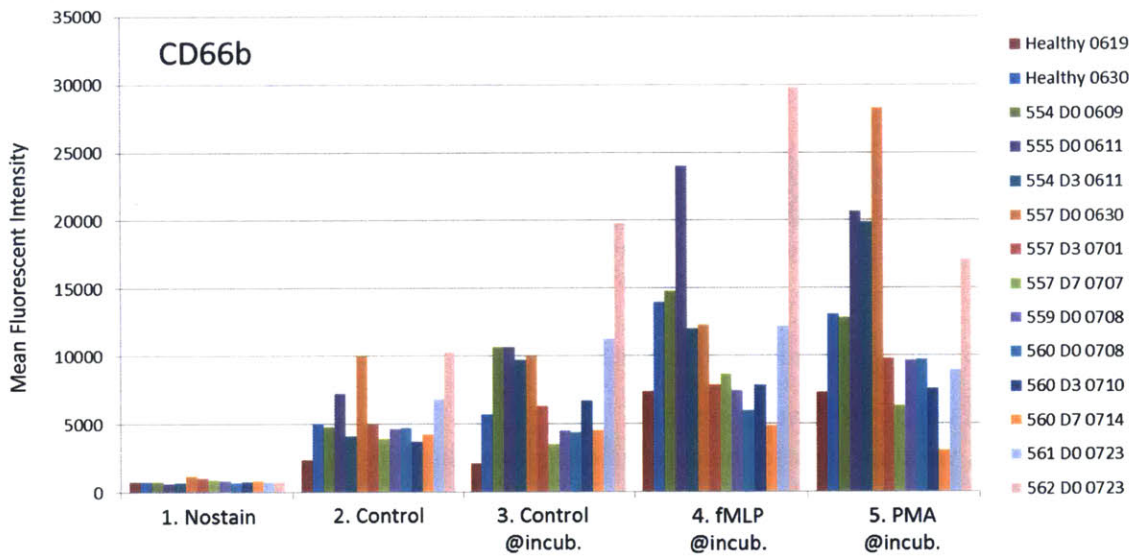


Figure 5-5 CD66b expression on neutrophils from patients.

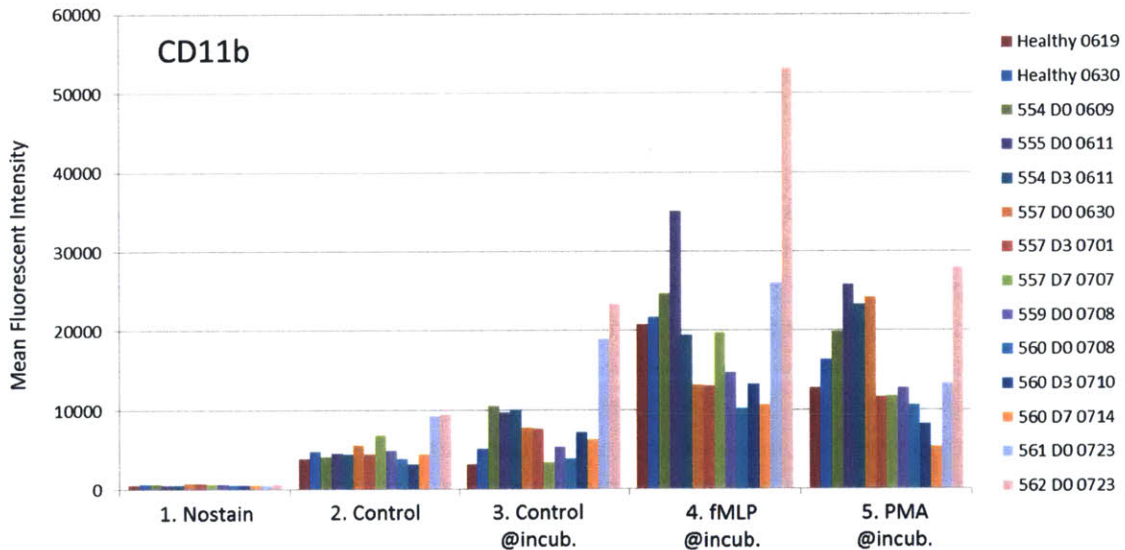


Figure 5-6 CD11b expression on neutrophils from patients.

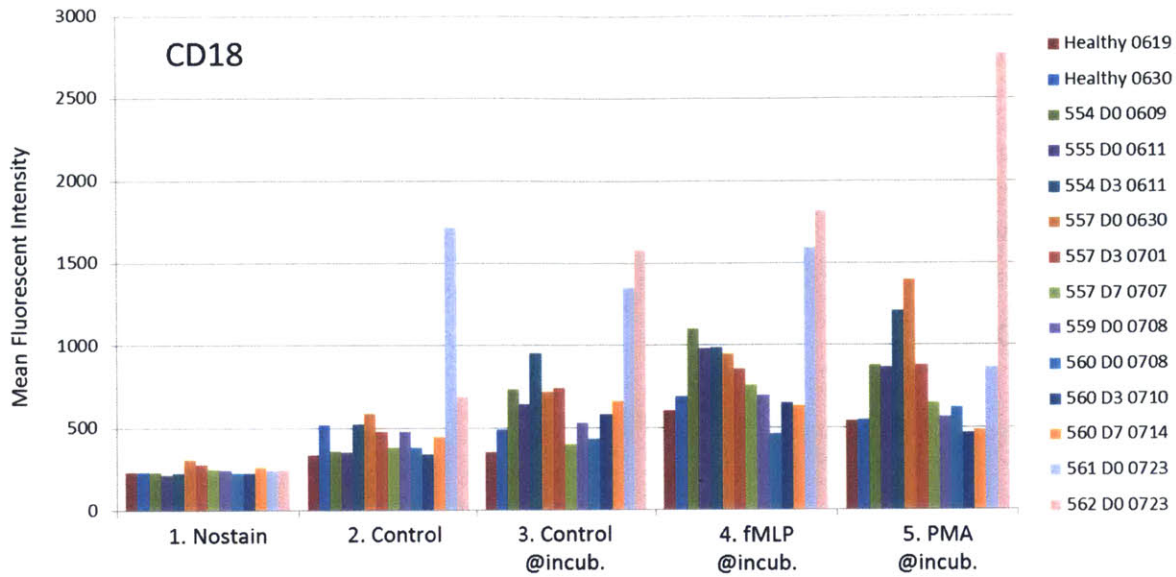


Figure 5-7 CD18 expression on neutrophils from patients.

#### 5.1.4 Conclusion and future improvement

In this pilot study, we summarized the conclusion as the following:

- (1) We collected data from 10 suspected septic patients and 1 healthy control. The IDS seems better classify the healthy versus septic patients data with limited number of data.
- (2) The correlations between mean IDS effective conductivity level and the mean fluorescent intensity of the three surface markers are all positive and they are at a similar level with correlations between the three surface adhesion markers.
- (3) After incubating with plasma, the difference between suspected septic and healthy patients increased.

#### Future improvement

- (1) The IDS distribution only occupies a very little portion of the channel. Given our knowledge of the IDPs of normal neutrophil, we can reduce the dynamic range so that we can get a larger displacement for activated neutrophils. The IDS gradient can be made shallower to increase the sensitivity of IDP movement to electrical changes can be better.
- (2) For the activation assay, the blood is better when it is not put on ice because there is a freeze shock to the cells. For measuring the native state of the neutrophils, keeping it on ice may help to prevent from non-deterministic activation. It can be better to put the cells on both room temperature and ice for measuring activation to stimuli and native activation state.
- (3) We found the signal increase after incubation with diluted plasma. It could be interesting to replace plasma with the serum which contains higher stimulation content secreted by cells during clot formation.
- (4) Instead of CD66b, CD11b, and CD18, we may try to use CD64 as one of the marker for comparison because CD64 has much literature support.

## 5.2 Integrated system with spiral device for leukocyte isolation

### 5.2.1 Motivation

Running IDS to characterize leukocytes requires red blood cell removal because the large numbers of RBCs will affect the fluidic flow of leukocytes. Running whole blood in IDS is possible but requires 1000x dilution, which heavily reduces the throughput of characterizing leukocytes. To efficiently characterize leukocytes properties, there are a few ways to remove RBCs, including density-based methods, RBCs lysing, or using MACS negative selection.

Traditional density-based methods are suitable for processing large volumes of blood but are difficult to implement in small volumes. RBC lysing is compatible with small volume but requires centrifugal steps that are time consuming and may activate cells. Using MACS negative selection is a promising method to provide pure and specific samples but pulling the majority of cells with antibodies is expensive and there are no commercial tools for small sample sizes. Therefore, to build a label-free characterization system, we choose to integrate with a spiral inertial sorter that can sort cells by size. The spiral inertial sorter is suitable for leukocyte enrichment, and has a smaller effect on activating cells than RBCs lysis buffer [91]. However, the IDS device and the spiral inertial sorter have very different flow rates. To combine the two devices with large throughput difference, we used an injection loop to store the isolating leukocyte as a reservoir.

### 5.2.2 Results

Figure 5-8 shows the integrated system for continuous monitoring of leukocytes. We diluted 10~20  $\mu\text{L}$  of whole blood into 2 mL buffer and isolated the leukocytes using the inertial sorter (which takes 3 minutes). It took less than one minute to stabilize and one minute for the concentrated leukocyte solution to fill the injection loop. The injection loop changed from load mode to inject mode in order to let leukocytes be pushed into the IDS for electrical characterization. To flush out the dead volume in the tubing, the flow rate was raised to 10  $\mu\text{L}$  per minute for 30 seconds and then turned back to 2  $\mu\text{L}$  per minute for measurement. It took around 90 seconds for the flow to go back to the correct flow rate. Then we measure the electrical profile of leukocytes for 10 minutes.

The inertial device ran at 800  $\mu\text{L}$  per minute while the IDS device ran at only 2  $\mu\text{L}$  per minute. Theoretically, any storage device can be used to mitigate the flow rate mismatch between the two. However, the injection loop stores the cells without stopping the flow and thus reduces the risk of leukocytes sedimentation and cell loss due to wall sticking. Therefore, the injection loop system has an advantage over a static reservoir.

To demonstrate we are able to monitor the leukocytes activation continuously, we used the inertial sorter and IDS device to measure the electrical profile of discarded human whole blood every 30 minutes. Mimicking the condition of monitoring septic mice, 20  $\mu\text{L}$  of sample was used every time. We successfully obtained 7 consecutive measurements of IDPs of human leukocytes. We observed that part of the distribution shifted left after 2 hours (measurement 4) which we believe could be due to activation of leukocytes (Figure 5-9).

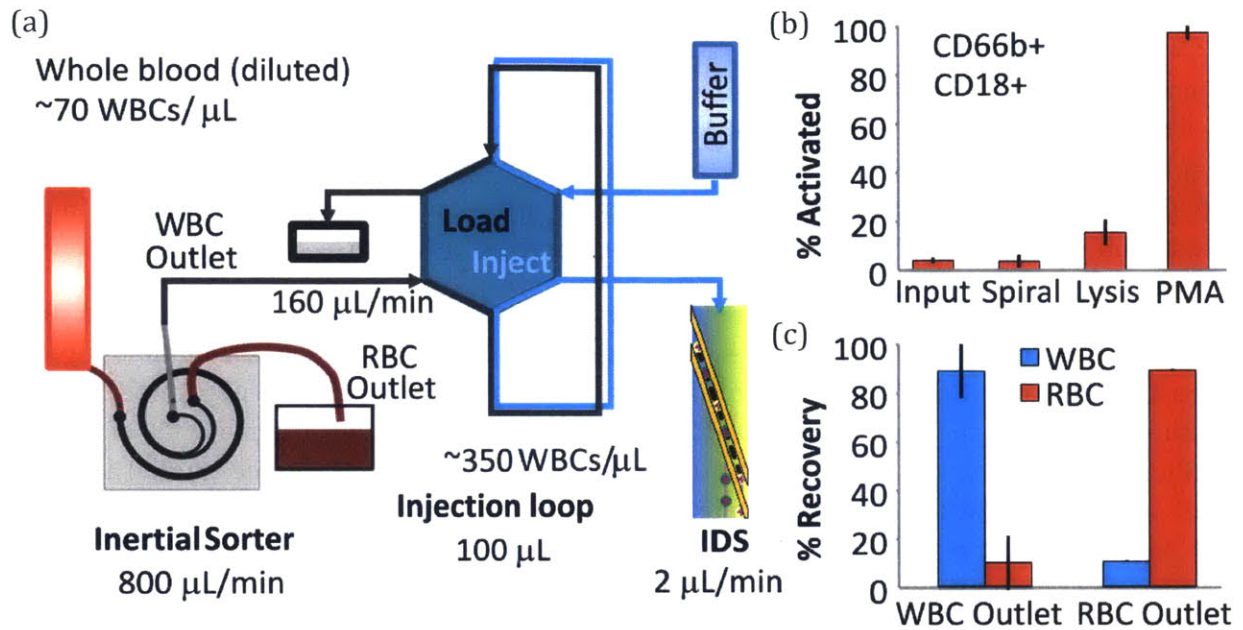


Figure 5-8 Integrated IDS system with inertial sorter. (a) A spiral inertial microfluidic sorter isolates leukocytes, and stores them in an injection loop (Load mode). The injection loop then pushes cells into the IDS device for enumeration and electrical characterization (Inject mode). (b) Comparison of leukocyte activation level between input, after spiral sorter, after RBC lysis buffer, and after PMA treatment (positive control). Spiral sorter has smaller effect on activation than RBC lysis buffer. (c) The spiral sorter removes 90 % RBCs while recovering 90 % of WBCs.

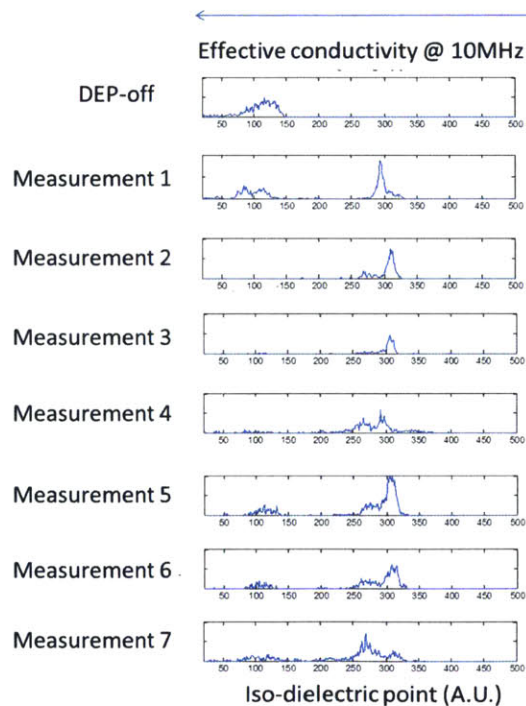


Figure 5-9 Continuous monitoring of electrical profile of human leukocytes by IDS. The human leukocytes were separated from spiral sorter and measured IDS every 30 minutes.

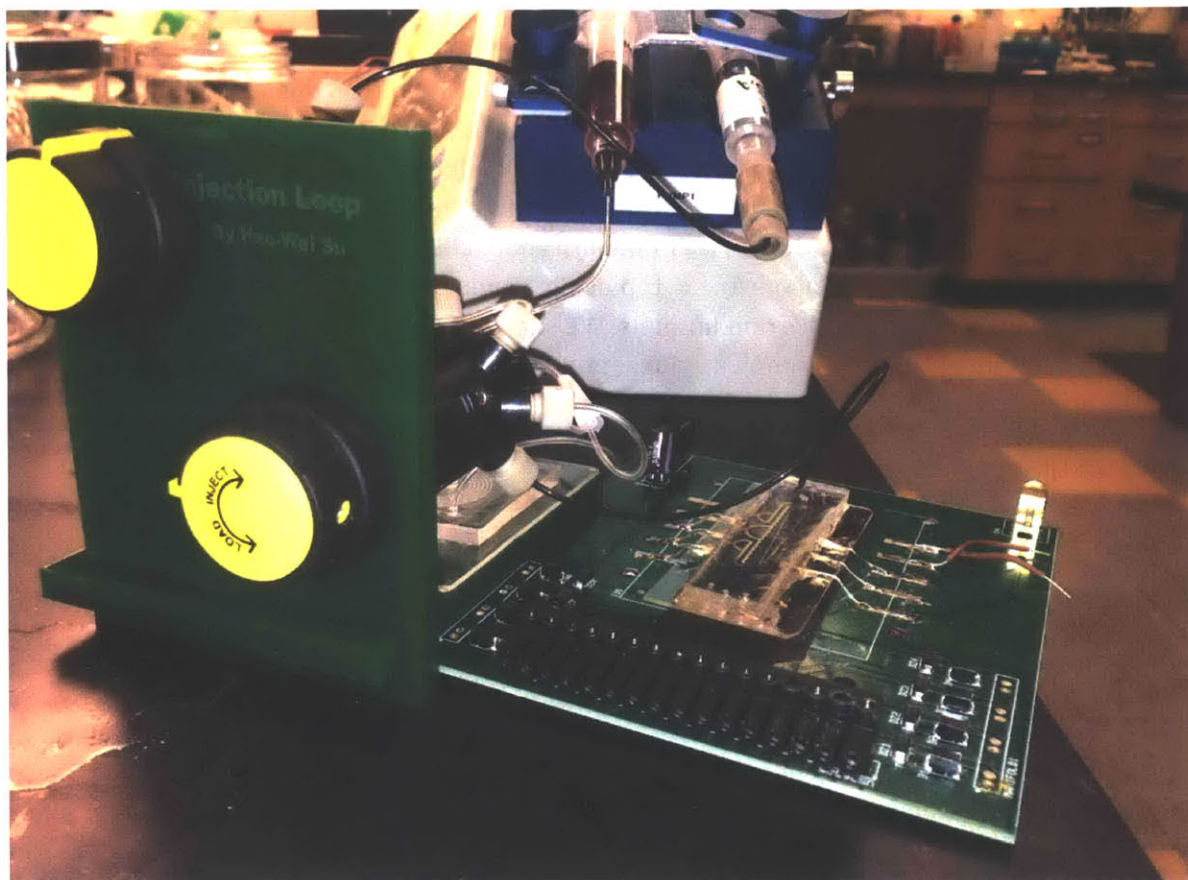


Figure 5-10 Image of an integrated system. The injection loop connects spiral device and IDS.

The image of the prototype of integrated system with injection loop is in Figure 5-10. We used a laser-cut acrylic stand to support the injection loop and fluidic switch. The injection loop and fluidic can be replaced by automated switch such as MX Series II™ (IDEX) for point-of-care devices.

### 5.2.3 Conclusion

We developed an integrated microfluidic system to measure the activation state of leukocytes from a drop of whole blood (20  $\mu\text{L}$ ) within 15 minutes, providing a simple assay to monitor sepsis progression with fine temporal resolution. In the future, it is possible to optimize the spiral inertial sorter so that we can isolate pure neutrophils population from whole blood. On the other hand, it is also possible to develop scatter or size measuring system with IDS, enabling differentiation of 3-part leukocyte differential counts. Such integrated system may provide rapid results for point of care application.

## **Chapter 6 Conclusion and Future Outlook**

### **6.1 Conclusion and contribution**

We developed an electrical characterization system to characterize the electrical properties of thousands of cells. We used this system to characterize the electrical properties of leukocytes, in particular neutrophils. We investigated the electrical changes upon neutrophil activation at different frequencies, conductivity and under different drug inhibition and found that the activated neutrophil has high effective conductivity at higher frequencies. Through modeling, we suggest that the change may mostly due to increasing cytoplasmic conductivity. We then applied the system to monitor sepsis progression in mice and humans. We successfully characterized >200 blood samples from septic mice and >10 blood samples from septic humans and paved the way to future diagnosis and monitoring of sepsis.

Here we list the main contributions in this thesis.

#### **Establishes high throughput electrical characterization tools**

We overcome the challenge of low throughput DEP characterization tools by and enable single cell measurement from sticky activation septic blood.

#### **Enables study of mechanism behinds the neutrophil activation with inhibitors**

Neutrophils have very short life time (6~10 hours) which makes the experimental design hard and time-limited. The technique we established allows enough speed to screen through different treatment of neutrophils. We showed that we can screen through different inhibitor treatment under stimulation from the same blood sample. The same experiment would be very hard to do with electro-rotation or patch clamping.

#### **Demonstrates the first dielectrophoretic tool for monitoring sepsis progression in murine model**

We show that IDS can be used to monitor sepsis blood from CLP mice. In the first set of experiments where we sacrifice mice at each time point, we can measure the level of activation correlates with flow cytometry. In the second set of experiments, we draw blood from catheter at different time points to monitor disease progression in the same animals, even though the correlation did not hold, we found the number of lower conductivity cells have prognostics value that similar to flow cytometry result.

#### **Set up work flow to study use neutrophil activation in suspected septic patients using dielectrophoresis**

We show that we are able to handle clinical samples from critically ill human subjects, enabling the use of our system to monitor sepsis progression in nearly real time.



## **6.2 Future direction**

This thesis initiates several threads that can be continued to be worked on.

### **6.2.1 Technological directions**

#### **Single cells DEP spectroscopy: Multiple frequencies measurement for the same cell**

Unlike electro-rotation and patch clamping, the current IDS method only examines the cells once. To gain more information from a single cell, DEP spring is a better method than IDS. The dielectric response of multiple frequencies can be extracted from the cells' trajectories under frequency sweeping. The original drawback of DEP spring is that it only measures cells with nDEP. We have designed a new frequency sequence methods that switch between low frequency of nDEP and the desired frequencies to achieve single cell dielectric spectroscopy.

#### **High throughput DEP**

IDS is a good approach to measure the analog distribution of DEP response. However, we have already optimized the throughput of IDS in parallel electrode structure under high conductive media. Currently, we are still limited by the life time of neutrophils thus making multiple measurements of IDS more difficult than the flow cytometry (10 minutes versus 10 seconds for characterizing a few thousands of cells). In addition, the current device is expensive to make because it must be made in a clean room. To further increase the throughput and make DEP more applicable for biological application, we need to develop a new way of making electrodes with new materials and a new fabrication method. New innovation may solve the throughput, cost, and complexity problems of current DEP devices and can potentially make the DEP devices to be cheap enough and disposable.

### **6.2.2 Biological directions**

#### **Studying neutrophil activation dynamics with DEP platform**

The label free nature of the DEP methods allows instead readout of electrical changes. Studying neutrophil activation dynamics with different stimulus and different inhibitors may unravel the true mechanism of electrical changes. Understanding the mechanism behinds electrical changes allow us to be more focused on functional study. The DEP platform allows probing at different frequencies and thus may decouple different aspects of activation individual, making our technology a platform of novel neutrophil activation assay.

#### **Studying monocyte activation and lymphocyte activation with DEP platform**

Monocytes and lymphocytes also play important roles not only in sepsis but also in other infectious illnesses. We have not thoroughly studied the electrical changes of monocytes, and lymphocytes. In the experiment activation from healthy mice leukocytes, we did not observe a clear IDS shift of mice leukocytes under PMA activation. Given that lymphocytes are the majority of leukocytes in mice, we think that electrical changes of lymphocytes under PMA activation are too subtle to be detected at 10 MHz. However, it is possible at other frequencies or with other agonists, we are able to measure quantifiable electrical changes in our platform. Monocytes are also phagocytes that may have endocytosis and reactive oxygen species production. It is very likely we can use our platform to

measure the changes in electrical properties in high frequencies. Studying monocyte activation may be a low hanging fruit given the isolation kit and experienced collaborators.

### **6.2.3 Clinical directions**

#### **Localization of infection site**

Sepsis may arise from infections from different organs or tissues. Measuring activation state of immune cells from different body liquid may help locate the infection site. For example, measuring sputum or bronchoalveolar lavage fluid may be useful for diagnosing pneumonia, getting liquid from cerebrospinal fluid may be useful to confirm meningitis.

#### **Development of a comprehensive immunological monitoring tool for sepsis**

Leukocyte and their activation state is only part of the immune system. To study the systemic uncontrolled immune response during sepsis, more biomarkers need to be monitored together. Such immunological tool may benefit accurate patient stratification and evaluate sepsis treatment.

#### **Monitoring other inflammatory diseases**

We have just started to explore the clinical value of measuring electrical properties of leukocytes. Other than sepsis, leukocyte activation also happens in many inflammatory diseases such as inflammatory bowel disease and other illnesses with chronic inflammation. It is possible that our methods are not specific to sepsis but useful in other inflammatory diseases In which a point-of-care device for measuring inflammation may be useful.

## Appendix: Detailed Protocols and MATLAB scripts

### DEP Spring Force calculation

#### Analytical expression for $q_R(x)$ , which represents the positional dependency of the DEP force

An analytical expression for the electric field on a pair of coplanar electrodes in a micro channel has been derived as the following equation via a three-step transformation using conformal mapping. [61]

$$E(x, y) = \frac{1}{2} \frac{V_{eff}}{2K(k^2)} \frac{1}{(1-v^2(u(x+iy)))(1-k^2v^2(u(x+iy)))^{-1/2} (D-BC)/(D+Cu(x+iy))^2} \frac{\pi}{h} \cosh\left(\frac{\pi}{h}\left(x+iy-\frac{ih}{2}\right)\right) \quad (\text{Eq. A1})$$

where the variable of  $B, C, D, k$  depends on the electrode gap( $g$ ), electrode width ( $W$ ), and the channel height( $h$ ). The detailed expression for these variables and the functions  $u, v, K$  can be found in reference 1, which also provides MATLAB scripts for computing the analytical solution of the electric fields.

From Eq. S1, and according to Eq. 3 of the main text, the expression of  $q_R(x)$  is then as follows:

$$q_R(x) = \frac{\partial}{\partial x} \left[ \left( \frac{E(x, y)}{V_{eff}} \right)^2 \right] \Bigg|_{y=h-R} \quad (\text{Eq. A2})$$

## Multi-Modal electrical and optical cytometry and multi-class image classification

The DEP Spring method acquires thousands of cell images within a short time. The cell image can give us cell size, cell shape (eccentricity), cell intensity while the DEP spring can give us the electrical property of the same cell by measuring the balance position of the cells. We want to build a strong automated classifier that can classify different particle types based on cell images and DEP spring. We want to compare between different classification methods. Also we want to compare the classification performance with all information and without the DEP spring.

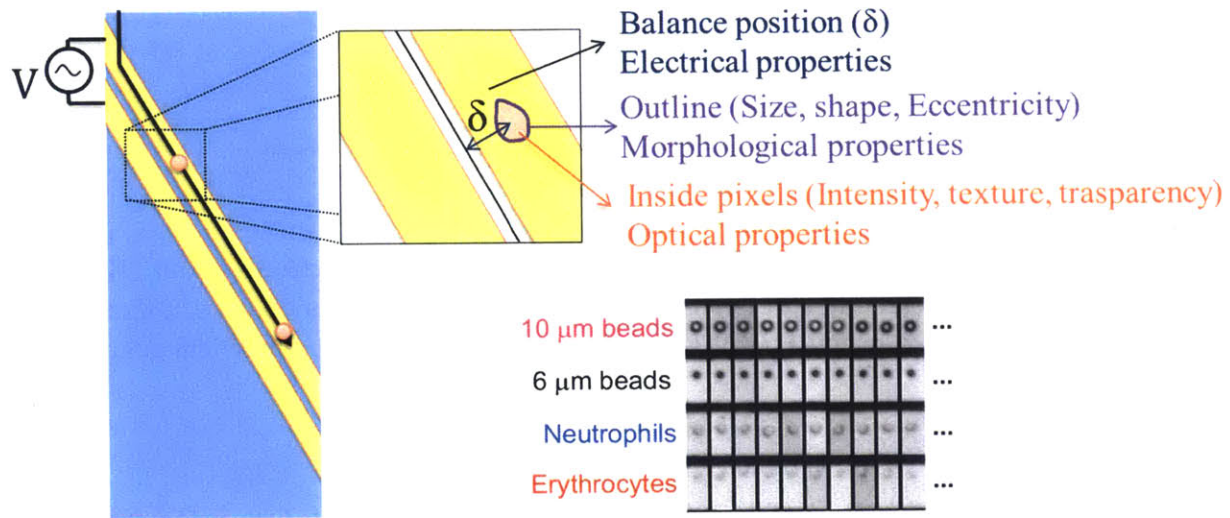


**Figure 1** The DEP-imaging cytometry extracting multiple parameters from cell images.

Datasets:

1. Images that contains 10um beads/6um beads/neutrophils/ erythrocytes
2. Images that contains activated and non-activated neutrophils

Tasks:

1. Feature extraction to obtain cell size, shape, intensity (from cell images) and their balance positions (from DEP spring) from thousands of cell samples.
2. Perform CART(classification and regression tree), multinomial logistic regression and multi-class SVM (support vector machine)to classify 10um beads/6um beads/neutrophils/erythrocytes automatically. Optimize the classifier by evaluating the testing error rate. Remove the DEP spring information (balance position) from the dataset and compare the performance identify if DEP spring can assist the classification particles.
3. Comparing the separability are activated/non-activated neutrophils using non-parametric methods.

### Task1: Data extraction:

The camera is pre-rotated so that the cells move along electrodes in the horizontal direction. The movies of cells flowing through were recorded. After getting the raw movie from the DEP imaging

flow cytometry, the image pre-processing is very important because the cell size and cell shape will change with different image threshold or different filter. To identify the cell objects, I did the following image processing (**Figure 2**) to identify the cell object: (1) Use temporal median filter to find the background (2) Subtract the background and take absolute value (3) Threshold to the binary image using Ostu's method with threshold 0.05. (4) Connect the nearby pixels and identify the object (filtered out the object smaller than 4 pixels.).(5) Filter out small object less than 4 pixels

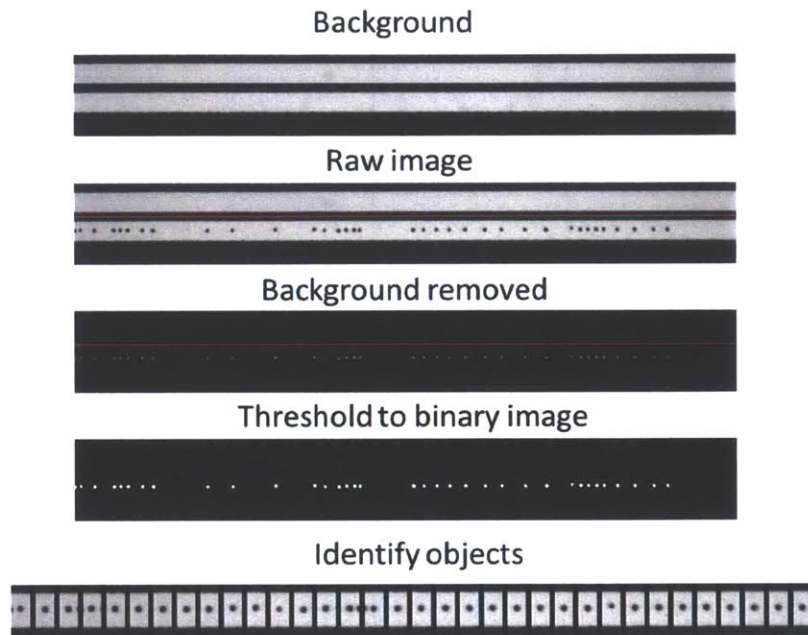


**Figure 2 Image pre-processing routine for object identification**

After the image pre-processing, I acquired the multi-parameter data matrix from each particles. For each particle the following parameters were recorded.

**Balance position ( $\delta$ ) ( $\mu\text{m}$ ):** the vertical distance between the cell centroid to the middle line of the electrodes (red line in Figure 2), which indicates the DEP forces and the electrical properties of the particles.

**Mean intensity (Arbitrary Unit):** the average intensity of the particles, this parameter is pretty different for beads and cells.

**Area ( $\mu\text{m}^2$ ):** the size of the particles, which plays an important role on cell classification. this parameter could affect by particles size or their optical properties

**Eccentricity:** roughly describe the shape of the particles. The erythrocytes usually have the larger eccentricity.

**Position:** the horizontal position, which should be irrelevant to the particle types.

**Time:** the timing where the particles got recorded, which should also be irrelevant to the particle types.

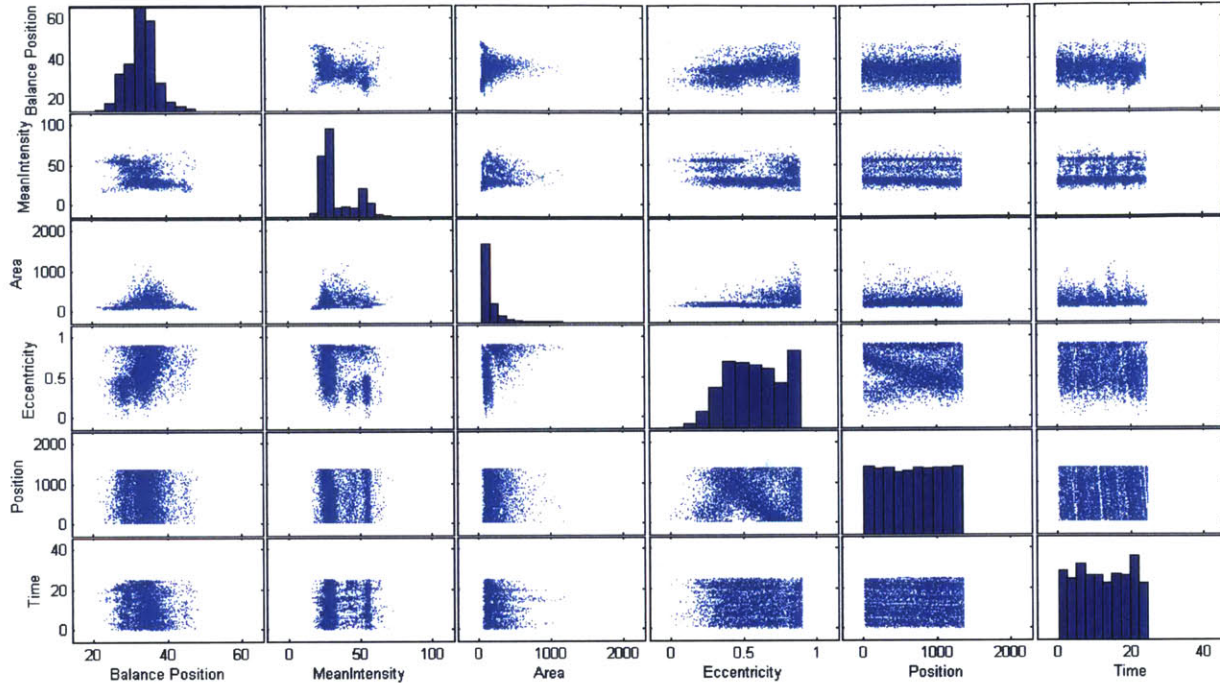


**Figure 3 Multi-parameter scatter plots for the particles.**

From the scatter plots, the time of the cell occurring in the channel and the horizontal position generally contain little information of particle types. Interestingly, we found that the eccentricity and position are slightly dependent, which comes from different lighting of different positions which makes the particle plus its shadow become somewhat eccentric as well. There is no strong co-linearity between variables as well. In theory the balance position of pure particles would have positive correlation with the cell area but in this mixture, this relationship is not very significant.

**Task 2: Multi-class classification:**

In the first dataset, we have ~8000 cell images of four different types of particles (10um beads/6um beads/neutrophils/ erythrocytes). We use 60% for the training set for the training data and 40% for validation. The goal is trying to make the computer learn to classify different particle types. We use CART/logistic regression/multi-class SVM and try to find the best classifier from them.

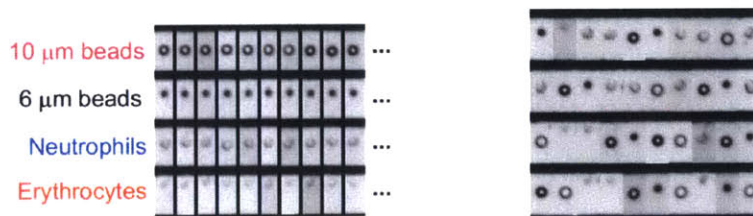


**Figure 4** The images of the training data (left) and the testing data (right)

## Method 1: Classification using CART:

CART is a local method for classification. It forms a binary decision tree to classification the input from the root to the leaves.

Model selection: After trying the minimum leaf nodes with 10, 50, 100, 200 samples. We found the pruned tree of minimum leaf nodes 100 (Original tree in appendix) to have minimum cost and being most meaningful.

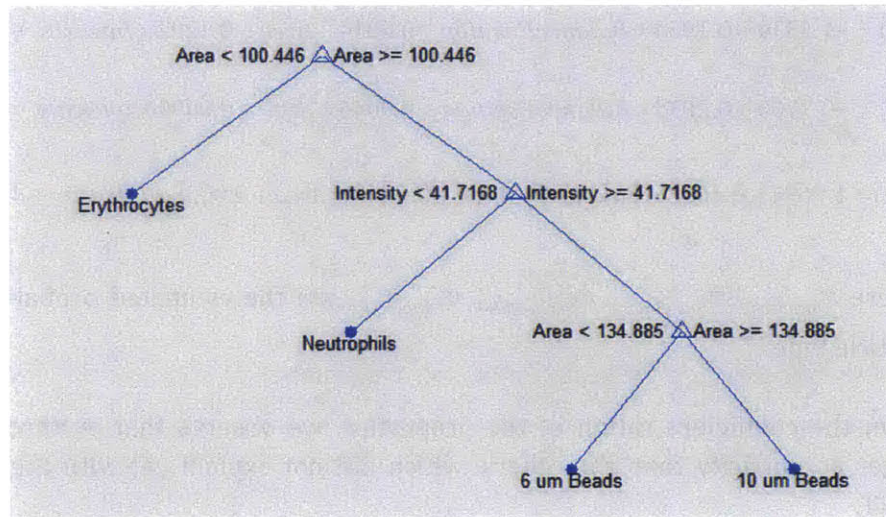


**Figure 5 Classification of particle types using CART**

The pruned tree makes perfect sense. Since the erythrocytes have smaller sizes than others (first branch). The intensity of beads is larger than the intensity of cells (second branch). Then 10  $\mu\text{m}$  beads have larger area than 6  $\mu\text{m}$  beads (third branch). The first and the second branches switch sometime in different tree configuration.

Method 2: Classification using multinomial logistic regression:

The multinomial logistic regression built the logit model that gives the probability estimate of the four particle types

Model selection: data with all explanatory variables did not converge in MATLAB due to the singularity problems. Therefore, we removed the data of position and time which we know that these are not important for cell classification. The best model is listed as below.

$$\ln\left(\frac{\pi_{6\mu\text{Beads}}}{\pi_{\text{Neutrophils}}}\right) = -1.5339 - 0.1954 \times \text{BalancePosition} - 0.0014 \times \text{Area} + 0.1292 \times \text{Intensity} + 0.8880 \times \text{Eccentricity}$$

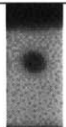
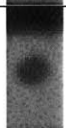
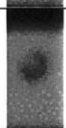

$$\ln\left(\frac{\pi_{10\mu\text{Beads}}}{\pi_{\text{Neutrophils}}}\right) = -0.7700 - 0.2035 \times \text{BalancePosition} + 0.0046 \times \text{Area} + 0.0999 \times \text{Intensity} - 0.2255 \times \text{Eccentricity}$$

$$\ln\left(\frac{\pi_{\text{Erythrocytes}}}{\pi_{\text{Neutrophils}}}\right) = 1.9694 - 0.1658 \times \text{BalancePosition} - 0.0048 \times \text{Area} + 0.0038 \times \text{Intensity} + 4.2839 \times \text{Eccentricity}$$

where  $\pi_{6\mu\text{Beads}}$ ,  $\pi_{10\mu\text{Beads}}$ ,  $\pi_{\text{Neutrophils}}$ ,  $\pi_{\text{Erythrocytes}}$  are the estimated probability of being each particle type.

From the coefficient ration of the properties, we observe that erythrocytes clearly have larger eccentricity than the others, which did not explain yet with the pruned tree from CART.

Example classification with probability estimate:

Cell images	6 um Beads $\pi_{6\mu\text{Beads}}$	10 um Beads $\pi_{10\mu\text{Beads}}$	Erythrocytes $\pi_{\text{Erythrocytes}}$	Neutrophils $\pi_{\text{Neutrophils}}$
	59.86%	27.37%	2.39%	10.38%
	24.49%	20.61%	11.09%	43.82%
	8.59%	7.01%	26.01%	58.4%
	2.9%	1.58%	83.87%	11.66%

**Figure 6 Classification of particle types using multinomial logistic regression**

The probability measure is very useful if we want to build a computer-aided human classification system. We can list up higher probability candidates and let human make the



final decision. However, to compare with CART and multi-class SVM, only the highest probability candidate is chosen to calculate the error rate.

### Method 3: Multi-class SVM:

The SVM is known as its strength of classifying two categories with high dimensional data. The variety of kernel function (ex: radial-basis function) allows SVM to classify convoluted two categories mixture. However, in multi-class separation problem, SVM might not be as powerful.

Model selection: we choose the one-against-all(OAA) multi-class SVM for the implementation.

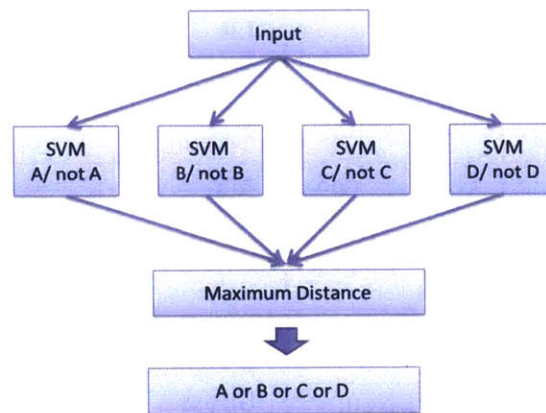


**Figure 7 Classification of particle types using one-against all multi-class SVM**

The MATLAB function does not support multiclass SVM so I built my own multiclass SVM using the one-against-all classifier and decide the class with maximum distance. However, the distance output has preference on the classifiers that usually have larger distance. It makes all the predictions into 6  $\mu\text{m}$  beads or 10  $\mu\text{m}$  beads. Therefore, I normalized the distance to have zero mean and standard deviation one. The results have better performance. Another improved method is described in Vladimir Vapnik [Vapnik, V. (1998). Statistical Learning Theory. Wiley-Interscience, NY.] is to transform the distance into a probability measure. After trying several combination of kernel(RBF, linear, quadratic ) and cost(1, 10, 100). I find the best one is RBF with cost 1. However, I found the classification result is still biased to the beads. If a particle belongs to two of the classifiers (e.g. 6  $\mu\text{m}$  beads and neutrophils). The particle tends to be classified as 6  $\mu\text{m}$  beads because it has larger positive distance than neutrophils.

**Performance comparison between three different methods:**

The three methods were compared by their best testing error rates. The expected error rates for random guess should be 75%. The CART has the best average cross-validation error rate 22%, while logistic regression ranks the second 33%. Multi-class SVM did not perform well even after the distance normalization 59%. As we can see in the confusion matrix, in SVM all the particles are intended to be classified as 6  $\mu\text{m}$  or 10  $\mu\text{m}$  beads. For the random guess, as expected, the error rate is around 75%.

With all information (balance position + optical): Confusion matrix and testing error rates

<table border="1"> <thead> <tr> <th><b>CART</b></th> <th colspan="4">True</th> </tr> <tr> <th>Predicted</th> <th>6<math>\mu\text{m}</math> B.</th> <th>10<math>\mu\text{m}</math>B.</th> <th>Ery.</th> <th>Neu.</th> </tr> </thead> <tbody> <tr> <td>6 <math>\mu\text{m}</math> B.</td> <td>324</td> <td>76</td> <td>51</td> <td>55</td> </tr> <tr> <td>10 <math>\mu\text{m}</math>B.</td> <td>27</td> <td>244</td> <td>56</td> <td>45</td> </tr> <tr> <td>Ery.</td> <td>35</td> <td>75</td> <td>1128</td> <td>88</td> </tr> <tr> <td>Neu.</td> <td>35</td> <td>62</td> <td>82</td> <td>738</td> </tr> </tbody> </table> <p>Testing error rate:0.2201</p>					<b>CART</b>	True				Predicted	6 $\mu\text{m}$ B.	10 $\mu\text{m}$ B.	Ery.	Neu.	6 $\mu\text{m}$ B.	324	76	51	55	10 $\mu\text{m}$ B.	27	244	56	45	Ery.	35	75	1128	88	Neu.	35	62	82	738	<table border="1"> <thead> <tr> <th><b>LR</b></th> <th colspan="4">True</th> </tr> <tr> <th>Predicted</th> <th>6<math>\mu\text{m}</math> B.</th> <th>10<math>\mu\text{m}</math>B.</th> <th>Ery.</th> <th>Neu.</th> </tr> </thead> <tbody> <tr> <td>6 <math>\mu\text{m}</math> B.</td> <td>315</td> <td>25</td> <td>81</td> <td>85</td> </tr> <tr> <td>10 <math>\mu\text{m}</math>B.</td> <td>128</td> <td>26</td> <td>69</td> <td>149</td> </tr> <tr> <td>Ery.</td> <td>44</td> <td>36</td> <td>1125</td> <td>121</td> </tr> <tr> <td>Neu.</td> <td>26</td> <td>30</td> <td>260</td> <td>601</td> </tr> </tbody> </table> <p>Testing error rate: 0.3377</p>					<b>LR</b>	True				Predicted	6 $\mu\text{m}$ B.	10 $\mu\text{m}$ B.	Ery.	Neu.	6 $\mu\text{m}$ B.	315	25	81	85	10 $\mu\text{m}$ B.	128	26	69	149	Ery.	44	36	1125	121	Neu.	26	30	260	601
<b>CART</b>	True																																																																				
Predicted	6 $\mu\text{m}$ B.	10 $\mu\text{m}$ B.	Ery.	Neu.																																																																	
6 $\mu\text{m}$ B.	324	76	51	55																																																																	
10 $\mu\text{m}$ B.	27	244	56	45																																																																	
Ery.	35	75	1128	88																																																																	
Neu.	35	62	82	738																																																																	
<b>LR</b>	True																																																																				
Predicted	6 $\mu\text{m}$ B.	10 $\mu\text{m}$ B.	Ery.	Neu.																																																																	
6 $\mu\text{m}$ B.	315	25	81	85																																																																	
10 $\mu\text{m}$ B.	128	26	69	149																																																																	
Ery.	44	36	1125	121																																																																	
Neu.	26	30	260	601																																																																	
<table border="1"> <thead> <tr> <th><b>SVM</b></th> <th colspan="4">True</th> </tr> <tr> <th>Predicted</th> <th>6<math>\mu\text{m}</math> B.</th> <th>10<math>\mu\text{m}</math>B.</th> <th>Ery.</th> <th>Neu.</th> </tr> </thead> <tbody> <tr> <td>6 <math>\mu\text{m}</math> B.</td> <td>415</td> <td>73</td> <td>16</td> <td>2</td> </tr> <tr> <td>10 <math>\mu\text{m}</math>B.</td> <td>129</td> <td>69</td> <td>171</td> <td>3</td> </tr> <tr> <td>Ery.</td> <td>160</td> <td>373</td> <td>772</td> <td>21</td> </tr> <tr> <td>Neu.</td> <td>145</td> <td>117</td> <td>648</td> <td>7</td> </tr> </tbody> </table> <p>Testing Error rate: 0.5953</p>					<b>SVM</b>	True				Predicted	6 $\mu\text{m}$ B.	10 $\mu\text{m}$ B.	Ery.	Neu.	6 $\mu\text{m}$ B.	415	73	16	2	10 $\mu\text{m}$ B.	129	69	171	3	Ery.	160	373	772	21	Neu.	145	117	648	7	<table border="1"> <thead> <tr> <th><b>Random Guess</b></th> <th colspan="4">True</th> </tr> <tr> <th>Predicted</th> <th>6<math>\mu\text{m}</math> B.</th> <th>10<math>\mu\text{m}</math>B.</th> <th>Ery.</th> <th>Neu.</th> </tr> </thead> <tbody> <tr> <td>6 <math>\mu\text{m}</math> B.</td> <td>139</td> <td>95</td> <td>124</td> <td>137</td> </tr> <tr> <td>10 <math>\mu\text{m}</math>B.</td> <td>85</td> <td>82</td> <td>106</td> <td>95</td> </tr> <tr> <td>Ery.</td> <td>320</td> <td>323</td> <td>341</td> <td>335</td> </tr> <tr> <td>Neu.</td> <td>255</td> <td>238</td> <td>214</td> <td>232</td> </tr> </tbody> </table> <p>Testing Error rate: 0.7546</p>					<b>Random Guess</b>	True				Predicted	6 $\mu\text{m}$ B.	10 $\mu\text{m}$ B.	Ery.	Neu.	6 $\mu\text{m}$ B.	139	95	124	137	10 $\mu\text{m}$ B.	85	82	106	95	Ery.	320	323	341	335	Neu.	255	238	214	232
<b>SVM</b>	True																																																																				
Predicted	6 $\mu\text{m}$ B.	10 $\mu\text{m}$ B.	Ery.	Neu.																																																																	
6 $\mu\text{m}$ B.	415	73	16	2																																																																	
10 $\mu\text{m}$ B.	129	69	171	3																																																																	
Ery.	160	373	772	21																																																																	
Neu.	145	117	648	7																																																																	
<b>Random Guess</b>	True																																																																				
Predicted	6 $\mu\text{m}$ B.	10 $\mu\text{m}$ B.	Ery.	Neu.																																																																	
6 $\mu\text{m}$ B.	139	95	124	137																																																																	
10 $\mu\text{m}$ B.	85	82	106	95																																																																	
Ery.	320	323	341	335																																																																	
Neu.	255	238	214	232																																																																	

With only optical information (no balance position): Confusion matrix and testing error rates

<b>CART</b>					<b>LR</b>				
Predicted	True				Predicted	True			
	6 $\mu$ m B.	10 $\mu$ mB.	Ery.	Neu.		6 $\mu$ m B.	10 $\mu$ mB.	Ery.	Neu.
6 $\mu$ m B.	351	59	35	50	6 $\mu$ m B.	307	15	70	103
10 $\mu$ mB.	55	233	41	39	10 $\mu$ mB.	124	28	74	142
Ery.	60	73	1093	93	Ery.	26	25	1092	176
Neu.	66	73	60	740	Neu.	27	33	363	516
Testing error rate: 0.2256					Testing error rate: 0.3774				

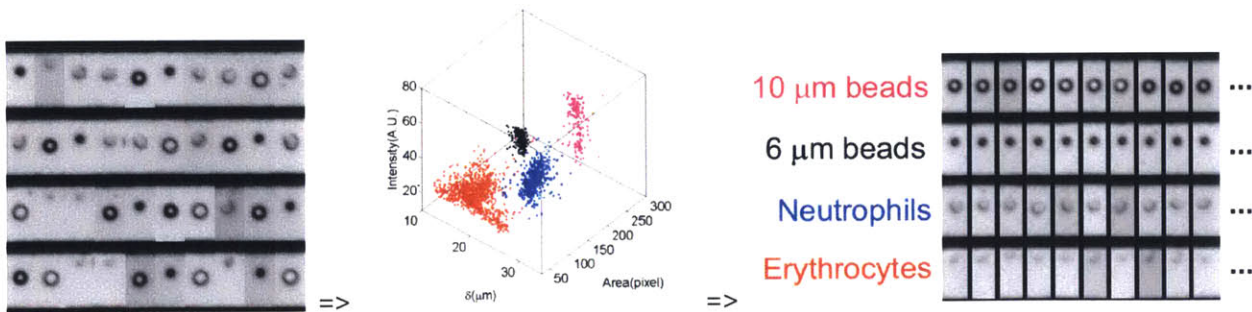
  

<b>SVM</b>					<b>Random Guess</b>				
Predicted	True				Predicted	True			
	6 $\mu$ m B.	10 $\mu$ mB.	Ery.	Neu.		6 $\mu$ m B.	10 $\mu$ mB.	Ery.	Neu.
6 $\mu$ m B.	415	73	16	2	6 $\mu$ m B.	115	128	122	130
10 $\mu$ mB.	129	69	171	3	10 $\mu$ mB.	84	94	89	101
Ery.	160	373	772	21	Ery.	335	340	341	303
Neu.	145	117	648	7	Neu.	223	238	203	275
Testing Error rate: 0.6062					Testing Error rate: 0.7357				

All the error rates increase when the balance position information is removed. It seems like adding the balance position (electrical properties) can better distinguish the particle types.

**Task 2 discussion and conclusion:**

1. SVM is not as good as CART and LR for multi-class classification problem. LR has lowest error rates.
2. CART for cell and particle classification have more common sense. The erythrocytes have smaller sizes than others. The intensity of beads is larger than neutrophils. Then 10  $\mu$ m beads have larger area than 6  $\mu$ m beads, which all literally meaningful.
3. The linear regression gave a good probability model of the classification. Unlike CART, it preserves the chances of being the difference class, which could be useful for computer-aided human classification.
4. The DEP spring (balance position) can improve the classification result.



**Figure 8** Automated classification by the winner (CART)

### Task 3 Classification of non-activated and activated neutrophils

Neutrophils play an important role in human immune system. Monitoring neutrophils activation could assist in real-time medical application such as sepsis diagnosis. When neutrophils are activated, their electrical and optical properties might change and reflect the disease progression. In this dataset, we measure the properties of normal neutrophils (blue) and the PMA treated activated neutrophils cells (red) are compared in the following graph. We found that both their balance position ( $\delta$ ) and size change after the PMA activation (artificial activation).

However, after comparing the area under the receiver operation curve, we found that the electrical properties have slightly better separability than the cell size.

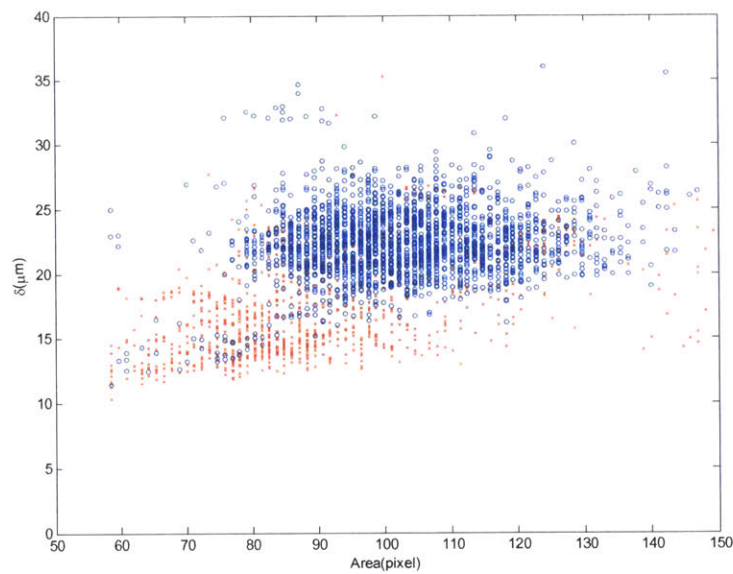


**Figure 9** The electrical properties ( $\delta$ ) and the cell size differences for the normal neutrophils (blue) and PMA activated neutrophils (red)

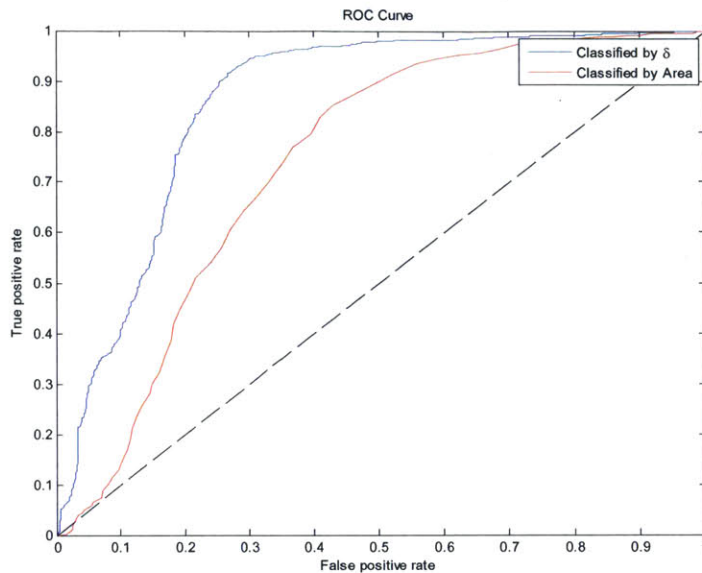


**Figure 10** The receiver operation curve

**Conclusion:**

DEP imaging flow cytometry gather high-throughput multi-dimensional data from the cell images. Automated classification of cells allows us to quantify number of cells in individual cell types. For examples, the five part differential blood cell count can be done automatically. The main goal of this project is testing methods of multi-class classification for cell properties separation. In the end, CART with simple classifiers (stump) has better performance to the multi-class problem than the logistic regression or RBF SVM which have more complicated separation hyperplanes. This might due to the fact that the properties of these particles are pretty distinct and clear thus simple classifiers would be enough.

Traditional methods for cell classification only use the optical properties to distinguish the cells. In this project, we specifically introduce the additional dimension - the electrical properties - to simultaneously determine the particle type. The result shows that the balance position (which embeds the dielectric properties of the cells) indeed improves the accuracy of the classification.

DEP imaging flow cytometry could distinguish the neutrophils with different activation levels. In the future, if we have more time resolution of the neutrophil activation, we might able to apply a more sophisticated regression on the neutrophil activation level, even a graphical inference model of individual parameter and their interaction, which can significantly impact the field of cellular biology and decease diagnosis.

## Protocol: White blood cells separation using IDS

### Materials:

1. Assembled IDS device (check with multimeter for short-circuits beforehand)
2. Three glass syringes (Hamilton, 81320)
3. Tubing (Upchurch, 1474; 0.062"×0.004")
4. Adapters for tubing and syringes
5. Whole blood with anti-coagulant (1uL whole blood diluted in to 500uL 1X PBS/ 0.2%EDTA)

### Sample Preparation:

1. Prepare high and low conductivity solutions:  
High: 1X PBS/0.2%EDTA/0.5%BSA  
Low: 0.25mM Sucrose solution/0.2%EDTA  
Medium: mix 1:1 from High and Low for the intermediate conductivity.
2. Add fluorescent stain at an appropriate concentration (0.5µl of SYTO-63 dyes in 0.5ml of cell suspension) and mix gently
3. Incubate at room temperature (shielding from light) for ~15 minutes.
4. (Optional) Centrifuge and wash out the residual stain for 3 times
5. While cells are staining, fill the device manually with 7.5% BSA: load from one of the inlets, with the other inlets and outlets left open.
6. Fill until droplets appear at the other inlets and outlets, removing any bubbles that enter the device; *keep droplets in place until you have inserted tubing (see Device set-up)*.
7. Fill the low conductivity and intermediate conductivity syringes, being careful to eliminate any bubbles trapped inside the syringe. Adjust to an appropriate volume.
8. Fill the high conductivity syringe and remove bubbles, leaving only ~50-100 µl of solution in the syringe; this facilitates preventing bubbles from entering when the cells are loaded, since it's easier to fill a wet syringe than a dry one.
9. Load cells into the pre-wetted high conductivity syringe; fill to the same volume as the other two syringes.
10. Connect tubing to the three syringes

### Device set-up:

1. Put syringes on the syringe pump and clamp into place.
2. Let the pump run at 5~10 µl/min until you see droplets forming at the ends of the tubing
3. Turn down the flow rate to 1 µl/min.
4. Plug tubing directly into inlets of the device, merging the droplet from the tube with the droplet over the inlet. Insert tubing to ~3/4 the depth of the PDMS, proceeding from lowest to highest conductivity
5. Position under the microscope and secure device base with tape to the stage when it is in position.
6. Connect alligator clips from function generator to the PCB.
7. Turn on camera and function generator to begin the experiment.
8. You should see a separation in the frequency of 2MHz- 5MHz with 10 Vpp sinewave.
9. **Do not try to lower the frequency below 200kHz.** It would result in electrolysis and ruin the electrode.

**Clean-up:**

1. When the experiment is finished, disconnect the syringe containing the cells from the device, leaving the other two connected. Keep the pump running, allowing the device to flush out for several minutes
2. Remove other syringes and rinse the device thoroughly with deionized water (manually, as in the initial filling step)
3. Insert nitrogen stream into one inlet and slowly turn nitrogen valve until it begins to dry out the device
4. Rinse the three syringes thoroughly with deionized water and store for the next experiment.
5. Disconnect device and check to see that the channel is completely dry and it is ready to use for the next experiment.

## PBMCs separation protocol (Ficoll)

Adapted from Chistopher Love lab

### 1.1 Materials

- 50mL Conical Tubes
- 15mL Conical Tubes
- Pipette Tips
- Sterile 250mL bottles

### 1.2 Reagents/Buffers

- Ficoll-Paque Plus GE Healthcare Cat#17-1440-02 or similar@ Room temperature
- HBSS
- Trypan Blue Counting Solution

### 1.3 Equipment

- Centrifuge
- Microscope
- Hemacytometer

## 2.0 Procedure

Day before blood arrives

1. Make Sure there is a centrifuge at room temperature for blood processing. To ensure this open the centrifuge door and turn it off.

Day of blood arrival

1. Before blood arrives:
  - a. Set centrifuge to room temperature(18-20°C).
  - b. Allow Ficoll to reach room temperature (store Ficoll at 4°C after using).
2. Transfer whole blood from collection tube to 250mL container.
  - a. Alternatively if blood comes in the form of a leukopack/buffy coat: Transfer buffy coat from blood bag to sterile plastic media bottle, carefully clamp off tube, and cut with scissors. These bags may be flimsy and difficult to handle, get an assistant to help stabilize the bag.
3. Estimate blood volume and dilute 1:1 with room temp HBSS. Mix well by inverting several times.
  - a. Altertively if buffy coat: Dilute 1:4 with HBSS

Buffy coat(higher density of WBCs)

4. Aliquot blood into 30mL portions oin 50mL tubes.
5. Slowly underlay 11mL Ficoll in each tube(can also do it overlay).
6. Centrifuge for 30 min at 400g, 18-20°C with no brake
7. Remove 5mL of the upper plasma layer containing plasma and most of the platelets. Transfer to fresh tube. Save sample for freezing. Aliquot into cryovials, label with patient ID #, date and plasma dilution. Freeze at -80°C.



8. After taking the plasma aliquot, aspirate the plasma from all 10 tubes – be careful not to disturb the PBMC layer.
9. Transfer the mononuclear cell layer to another centrifuge tube via a transfer pipette removing the band and some of the layer above and below. Split layer into 4 50mL conical tubes equally and wash cells by adding an excess of HBSS to fill tubes.
10. Centrifuge at 400g for 10 min at 4°C.
11. Remove supernatant; resuspend cells in each 50mL conical tube and combine into 1 50mL conical tube and wash by adding an excess of HBSS.
12. Centrifuge at 400g for 10 min. at 4°C.
13. Remove supernatant; resuspend cells in 20mL and count cells by taking 10uL on Hemacytometer.
  - a. Equation =  $\text{Count}(\text{average per 1 square}) * \text{DF} * 10^4$
14. Take aliquot of cells for HLA typing.
15. Centrifuge at 400g for 10 min. at 4°C.
16. Cells are now ready for freezing or sorting. Refer to specific protocol.

## Neutrophil density isolation and activation protocol

### Materials:

- 1) PBS ++ 20mLs (need to be kept in the refrigerator)+ 1% BSA
- 2) PBS - - 8W0mLs + 1% BSA
- 3) Sucrose 270mM with 1%BSA
- 4) Heparin
- 5) Monopoly density based separation media. Keep in room temperature.
- 6) 1.6mM PMA (in the big fridge)

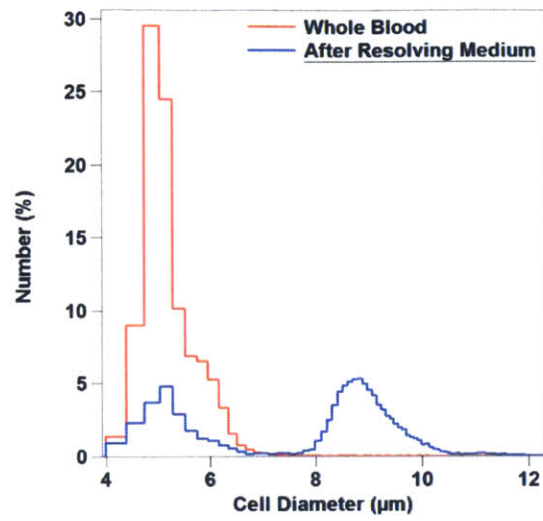
### Steps:

- 1) Add in 3mLs of Monopoly density media into 15 mL falcon tubes and then 4mL of blood.
- 2) Use 400g to centrifuge for 40mins, use slow ramp down.
- 3) Prepare PMA solution: 1.5  $\mu$ L PMA(1.6 mM) into 2.5 mL PBS ++ to make a 1 $\mu$ M PMA in PBS++/1% BSA
- 4) Take out the tubes from centrifuge, suck out the plasma, suck out the upper layer(FR1), the mononuclear layer, and the second later(FR2), PMNs,
- 5) FR2 in to 15 mL falcon tube and fill to 12 mL with PBS -
- 6) Centrifuge the tubes in 250g for 10 mins.
- 7) Suck out supernatant, resuspend the FR2 in PBS - -
- 8) Mix 0.5 mL of resuspended FR2 with 0.5 mL PMA to activate. Mix another 0.5 mL FR2 with 0.5mL PBS++ as control.
- 9) 20 min incubation under 37°C water bath.
- 10) Count the cells with remaining FR2.
- 11) 5 min / 2500 rpm in small centrifuge to spin down the two vials and then resuspend in PBS - -

### Optional

Add in Syto dye 1  $\mu$ L to 7e6 cells Incubate for 15 mins

Use 5 mins 2500rpm to spin down the cells.



Coulter Counter size characterization of diluted whole blood and granulocytes fraction (FR2) enriched from Mono-Poly resolving medium.

## FACS protocol for mice platelets and WBCs enumeration/ Neu-Lym ratio/IDS

(Updated 04082014)

### Reagents

1x PBS buffer (with 0.5% BSA), lysis buffer (eBioscience)  
CD41a-FITC (eBioscience), CD45-APC (eBioscience)  
**20 uL** of mouse whole blood (10 +10 uL)

### Platelets and WBCs enumeration

1. Add **10 uL** of whole blood to 140  $\mu$ L of PBS buffer. (**15x dilution**), take 10  $\mu$ L and dilute to 50  $\mu$ L precede (75x). Spin down the rest and collect the plasma (~120  $\mu$ L) for future use.
2. Add 0.5  $\mu$ L of CD41, 0.5  $\mu$ L of CD45 to the 50  $\mu$ L diluted blood samples
3. Stain 30 mins, 4°C
4. Take all from the stained sample, add in 200  $\mu$ L of PBS (**375x dilution**)
5. FACS analysis, **slow speed**, constant time measurement of 1min
6. Typical volume analyzed ~13.4  $\mu$ L
7. Cell concentration/uL = cell number/13.4 x 375

### WBCs and neutrophil activation

1. Add **10  $\mu$ L** of whole blood to 90  $\mu$ L (1:10 v/v) of lysis buffer (room temp) (eBioscience)
2. Incubate 3 mins, room temp
3. Quench with 1mL of 1x PBS (with 0.5% BSA)
4. Spin down. (300g or 1800rpm, 4 min, 4 deg, Voldman rotor) remove supernatant and resuspend to 200 uL sample (20x)
5. Spilt the sample into 2 tubes with 150  $\mu$ L (for IDS) and 50  $\mu$ L each.
6. Add 0.5 uL CD45 to the 50 uLWBCs samples
7. Stain 30mins, 4 deg
8. Add 150  $\mu$ l PBS buffer to WBCs. (**4x dilution**)
9. FACS analysis, **slow speed**, constant time measurement of 2 min
10. Typical volume analyzed ~26  $\mu$ L
11. Cell concentration/ $\mu$ L = cell number/26 x 80

## Human neutrophil activation assay protocol

### Reagents

1x PBS buffer (with 1% HSA)  
CD66b-FITC (eBioscience), CD11b-PE (eBioscience), CD18-APC (eBioscience)  
EasySep™ Direct Human Neutrophil Isolation Kit (Stellcell Technologies)

### 5 tubes:

1. No stain
2. Stain, no incubation
3. Stain, with incubation
4. Stain, with incubation + 5 $\mu$ M fMLP
5. Stain, with incubation + 1 $\mu$ M PMA

### Neutropil Isolation Procedures:

1. Put 0.5 mL of whole blood in 15mmx75mm BD FACS tube.
2. Add in 50  $\mu$ L magnetic beads and 50 mL cocktail of EasySep Direct Human Neutrophil Isolation Kit.
3. Incubate 5 minutes
4. Add in 3 mL buffer and put the tube in magnets.
5. Incubate 5 minutes
6. Poor the liquid out in a new 15mmx75 FACS tube. Add in 50 mL magnetic beads.
7. Incubate 5 minutes
8. Put the tube in magnets.
9. Incubate another 5 minutes
10. Poor the liquid out in a new 15mmx75 FACS tube. Put the new tube in magenets.
11. Incubate another 5 minutes
12. Poor the liquid out in a new 15mmx75 FACS tube.
13. The cell are now ready to use (3~3.5 mL to use).

### Neutropil Activation Procedures:

1. Take 3 tubes for sample 3,4,5, and add 0.5 mL of isolated cells in each.
2. Put another 0.5 mL of buffer/10 $\mu$ M fMLP/2 $\mu$ M PMA in sample 3,4,5.
3. Incubate sample 3,4,5 in 37 degree incubator for 30 minutes.
4. Add in another 0.5 mL to each to dilute the stimulants.
5. Spin down the cells with 2800 rpm for 4 minutes on 4°C.
6. Remove the supernatant until 0.1 mL
7. Add 100  $\mu$ L to tube 2
8. Add 50 uL of premixed stain to tube 2,3,4,5 (1 $\mu$ L CD66b, 1 $\mu$ L CD11b , 2 $\mu$ L CD18 per sample)
9. Place tubes on ice and invubate for 30 minutes.
10. Add another 1.35 mL to each tube for washing the stain.
11. Spin down the cells with 2800 rpm for 4 minutes on 4°C.
12. Remove the excess liquid until 0.1 mL

13. Add 200  $\mu\text{L}$  buffer to each tube and gently pipette.
14. Add 100  $\mu\text{L}$  isolated cells to tube 1. Add 200  $\mu\text{L}$  buffer to tube 1.
15. Now 5 tubes are ready to be measured in flow cytometry.

**Flow cytometry setting:**

1. Medium speed
2. Each sample runs for 2 minutes.

## Fabrication Process Flow

### Starting Materials:

150-mm-diameter, 762- $\mu\text{m}$ -thick Pyrex wafers (Bullen Ultrasonics, Eaton, OH)

150-mm-diameter, 650- $\mu\text{m}$ -thick Silicon wafers (WaferNet, Inc., Son Jose, CA)

Step	Description	TRL Machine	Parameters
Electrode patterning, 6" Pyrex wafer			
1	Piranha clean	Acid hood	
2	Dehydration bake	HMDS oven	155°C, 3 mins, wait for air cool
3	Photoresist coat	Coater	NR-7 photoresist: - Spread 6s, 750 rpm - Spin 30s, 2500 rpm
5	Prebake	Hotplate station	155°C(plate setting), 90s, air cool to ambient
6	UV expose	EV1	20 s continuous, soft contact
7	Post-expose bake	Hotplate station	120°C(plate setting), 2 min
8	Develop, rinse and spin dry	Photo-wet bench	RD6 in a shallow beaker: - Gently agitate for 10s - Rinse with dH <sub>2</sub> O - Use fresh RD6 with each wafer
9	Metal evaporation	E-beam	100Å Ti, 2000Å Au
10	Liftoff metal	Solvent-Au	
11	Protective resist coat	Coater	AZ 5214E, 500 rpm final speed
12	Bake	Hotplate station	120°C, 2 min
13	Dice wafer	Die saw	

Step	Description	Machine	Parameters
Microfluidic Channel Patterning, 6" Silicon wafer			
1	Dehydration bake	Hotplate station	200°C, 30 min
2	SU-8 Spin	SU-8 spinner	SU-8 2015(20 µm thickness):  Dispense~6ml SU-8 (1ml per inch diameter)  Ramp to 500 rpm at 100 rpm/sec accel and hold for 5-10 seconds  Ramp to 2250 rpm at 300 rpm/second and hold for total of 30 seconds
3	Prebake	Hotplate station	Slow ramp from 60°C to 95°C, hold at 95°C for 2 min; cool to ambient
4	UV expose	EV1	Flow chamber mask, 12 seconds. 30 µm separation
5	Post-expose bake	Hotplate station	Slow ramp from 60°C to 95°C, hold at 95°C for 2 min; cool to ambient
6	Develop	Solvent-Au	~ 3-5 min soak in PM Acetate  30s spin while spraying with PMA  30s spin while spraying with IPA  30s spin dry
7	Silanize wafer	EML acid hood	Put 3-4 drops of HMDS into cup in vacuum jar.  Lean wafer against wall of jar, exposing both front and back  Close jar, turn on vacuum for 5-10 min  Turn vacuum off, let it sit ~ 30 min



## Reference

- [1] "Focus on sepsis," *Nat Med*, vol. 18, pp. 997-997, 2012.
- [2] R. C. Bone, R. A. Balk, F. B. Cerra, R. P. Dellinger, A. M. Fein, W. A. Knaus, R. Schein, and W. J. Sibbald, "Definitions for sepsis and organ failure and guidelines for the use of innovative therapies in sepsis. The ACCP/SCCM Consensus Conference Committee. American College of Chest Physicians/Society of Critical Care Medicine," *Chest Journal*, vol. 101, pp. 1644-1655, 1992.
- [3] I. Jawad, I. Lukšić, and S. B. Rafnsson, "Assessing available information on the burden of sepsis: global estimates of incidence, prevalence and mortality," *Journal of global health*, vol. 2, 2012.
- [4] D. Pittet, S. Rangel-Frausto, N. Li, D. Tarara, M. Costigan, L. Rempe, P. Jebson, and R. Wenzel, "Systemic inflammatory response syndrome, sepsis, severe sepsis and septic shock: incidence, morbidities and outcomes in surgical ICU patients," *Intensive care medicine*, vol. 21, pp. 302-309, 1995.
- [5] A. Kumar, D. Roberts, K. E. Wood, B. Light, J. E. Parrillo, S. Sharma, R. Suppes, D. Feinstein, S. Zanotti, and L. Taiberg, "Duration of hypotension before initiation of effective antimicrobial therapy is the critical determinant of survival in human septic shock\*," *Critical care medicine*, vol. 34, pp. 1589-1596, 2006.
- [6] M. A. Ansari-Lari, T. S. Kickler, and M. J. Borowitz, "Immature granulocyte measurement using the Sysmex XE-2100 relationship to infection and sepsis," *American journal of clinical pathology*, vol. 120, pp. 795-799, 2003.
- [7] B. S. Dahler-Eriksen, J. F. Lassen, E. D. Lund, T. Lauritzen, and I. Brandslund, "C-reactive protein in general practice-how commonly is it used and why?," *Scandinavian journal of primary health care*, vol. 15, pp. 35-38, 1997.
- [8] V. Nobre, S. Harbarth, J. Graf, P. Rohner, and J. Pugin, "Use of procalcitonin to shorten antibiotic treatment duration in septic patients: a randomized trial," *American journal of respiratory and critical care medicine*, vol. 177, p. 498, 2008.
- [9] J. Watson, A. Round, and W. Hamilton, "Raised inflammatory markers," *BMJ*, vol. 344, 2012.
- [10] M. R. Pinsky, J.-L. Vincent, J. Devière, M. Alegre, R. J. Kahn, and E. Dupont, "Serum cytokine levels in human septic shock. Relation to multiple-system organ failure and mortality," *Chest Journal*, vol. 103, pp. 565-575, 1993.
- [11] R. Uusitalo-Seppälä, P. Koskinen, A. Leino, H. Peuravuori, T. Vahlberg, and E. M. Rintala, "Early detection of severe sepsis in the emergency room: diagnostic value of plasma C-reactive protein, procalcitonin, and interleukin-6," *Scandinavian journal of infectious diseases*, vol. 43, pp. 883-890, 2011.
- [12] S. HARBARTH, K. HOLECKOVA, C. L. FROIDEVAUX, D. Pittet, B. RICOU, G. E. GRAU, L. VADAS, and J. Pugin, "Diagnostic value of procalcitonin, interleukin-6, and interleukin-8 in critically ill patients admitted with suspected sepsis," *American journal of respiratory and critical care medicine*, vol. 164, pp. 396-402, 2001.
- [13] J. J. Hoffmann, "Neutrophil CD64 as a sepsis biomarker," *Biochemia medica*, vol. 21, pp. 282-290, 2011.
- [14] H. Haag, F. Locher, and O. Nolte, "Molecular diagnosis of microbial aetiologies using Sepsitest™ in the daily routine of a diagnostic laboratory," *Diagnostic microbiology and infectious disease*, vol. 76, pp. 413-418, 2013.
- [15] S. Mera, D. Tatulescu, C. Cismaru, C. Bondor, A. Slavcovici, V. Zanc, D. Carstina, and M. Oltean, "Multiplex cytokine profiling in patients with sepsis," *Apmis*, vol. 119, pp. 155-163, 2011.
- [16] C. Pierrakos and J.-L. Vincent, "Sepsis biomarkers: a review," *Crit Care*, vol. 14, p. R15, 2010.

- [17] R. W. Peeling, K. K. Holmes, D. Mabey, and A. Ronald, "Rapid tests for sexually transmitted infections (STIs): the way forward," *Sexually transmitted infections*, vol. 82, pp. v1-v6, 2006.
- [18] F. Chaves, B. Tierno, and D. Xu, "Quantitative Determination of Neutrophil VCS Parameters by the Coulter Automated Hematology Analyzer New and Reliable Indicators for Acute Bacterial Infection," *American journal of clinical pathology*, vol. 124, pp. 440-444, 2005.
- [19] S. F. van Eeden, M. E. Klut, B. A. Walker, and J. C. Hogg, "The use of flow cytometry to measure neutrophil function," *Journal of immunological methods*, vol. 232, pp. 23-43, 1999.
- [20] V. Brinkmann, U. Reichard, C. Goosmann, B. Fauler, Y. Uhlemann, D. S. Weiss, Y. Weinrauch, and A. Zychlinsky, "Neutrophil extracellular traps kill bacteria," *Science*, vol. 303, pp. 1532-1535, 2004.
- [21] M. T. Quinn, F. Deleo, and G. M. Bokoch, *Neutrophil methods and protocols* vol. 412: Springer, 2007.
- [22] G. F. Weber, B. G. Chousterman, S. He, A. M. Fenn, M. Nairz, A. Anzai, T. Brenner, F. Uhle, Y. Iwamoto, and C. S. Robbins, "Interleukin-3 amplifies acute inflammation and is a potential therapeutic target in sepsis," *Science*, vol. 347, pp. 1260-1265, 2015.
- [23] L. d. S. Borges, J. R. Bortolon, V. C. Santos, N. R. de Moura, A. Dermargos, M. F. Cury-Boaventura, R. Gorjão, T. C. Pithon-Curi, and E. Hatanaka, "Chronic inflammation and neutrophil activation as possible causes of joint diseases in ballet dancers," *Mediators of inflammation*, vol. 2014, 2014.
- [24] J. E. De Larco, B. R. Wuertz, and L. T. Furcht, "The potential role of neutrophils in promoting the metastatic phenotype of tumors releasing interleukin-8," *Clinical Cancer Research*, vol. 10, pp. 4895-4900, 2004.
- [25] R. S. Hotchkiss and I. E. Karl, "The pathophysiology and treatment of sepsis," *New England Journal of Medicine*, vol. 348, pp. 138-150, 2003.
- [26] J. Cohen, S. Opal, and T. Calandra, "Sepsis studies need new direction," *The Lancet infectious diseases*, vol. 12, pp. 503-505, 2012.
- [27] S. C. Williams, "After Xigris, researchers look to new targets to combat sepsis," *Nature medicine*, vol. 18, pp. 1001-1001, 2012.
- [28] D. G. Remick, "Cytokine therapeutics for the treatment of sepsis: why has nothing worked?," *Current pharmaceutical design*, vol. 9, pp. 75-82, 2003.
- [29] J. H. Kang, M. Super, C. W. Yung, R. M. Cooper, K. Domansky, A. R. Graveline, T. Mammoto, J. B. Berthet, H. Tobin, and M. J. Cartwright, "An extracorporeal blood-cleansing device for sepsis therapy," *Nature medicine*, 2014.
- [30] K. Linden, V. Scaravilli, S. F. Kreyer, S. M. Belenkiy, I. J. Stewart, K. K. Chung, L. C. Cancio, and A. I. Batchinsky, "EVALUATION OF THE Cytosorb (R) HEMOADSORPTIVE COLUMN IN A PIG MODEL OF SEVERE SMOKE AND BURN INJURY," *Shock*, 2015.
- [31] H. W. Hou, H. Y. Gan, A. A. S. Bhagat, L. D. Li, C. T. Lim, and J. Han, "A microfluidics approach towards high-throughput pathogen removal from blood using margination," *Biomicrofluidics*, vol. 6, p. 024115, 2012.
- [32] R. P. Dellinger, M. M. Levy, A. Rhodes, D. Annane, H. Gerlach, S. M. Opal, J. E. Sevransky, C. L. Sprung, I. S. Douglas, and R. Jaeschke, "Surviving Sepsis Campaign: international guidelines for management of severe sepsis and septic shock, 2012," *Intensive care medicine*, vol. 39, pp. 165-228, 2013.
- [33] A. Rhodes, G. Phillips, R. Beale, M. Cecconi, J. D. Chiche, D. De Backer, J. Divatia, B. Du, L. Evans, and R. Ferrer, "The Surviving Sepsis Campaign bundles and outcome: results from the International Multicentre Prevalence Study on Sepsis (the IMPReSS study)," *Intensive care medicine*, vol. 41, pp. 1620-1628, 2015.
- [34] C. N. Jones, M. Moore, L. Dimisko, A. Alexander, A. Ibrahim, B. A. Hassell, H. S. Warren, R. G. Tompkins, S. P. Fagan, and D. Irimia, "Spontaneous Neutrophil Migration Patterns during Sepsis after Major Burns," *PLoS one*, vol. 9, p. e114509, 2014.

- [35] D. R. Gossett, T. Henry, S. A. Lee, Y. Ying, A. G. Lindgren, O. O. Yang, J. Rao, A. T. Clark, and D. Di Carlo, "Hydrodynamic stretching of single cells for large population mechanical phenotyping," *Proceedings of the National Academy of Sciences*, vol. 109, pp. 7630-7635, 2012.
- [36] K. Lollike and M. Lindau, "Membrane capacitance techniques to monitor granule exocytosis in neutrophils," *Journal of immunological methods*, vol. 232, pp. 111-120, 1999.
- [37] A. W. Griffith and J. M. Cooper, "Single-cell measurements of human neutrophil activation using electrorotation," *Analytical chemistry*, vol. 70, pp. 2607-2612, 1998.
- [38] R. Pethig and D. B. Kell, "The passive electrical properties of biological systems: their significance in physiology, biophysics and biotechnology," *Physics in medicine and biology*, vol. 32, pp. 933-970, 1987.
- [39] D. Holmes, D. Pettigrew, C. H. Reccius, J. D. Gwyer, C. van Berkel, J. Holloway, D. E. Davies, and H. Morgan, "Leukocyte analysis and differentiation using high speed microfluidic single cell impedance cytometry," *Lab on a Chip*, vol. 9, pp. 2881-2889, 2009.
- [40] F. Lacy, M. Kadima-Nzujii, F. J. Malveaux, and E. L. Carter Jr, "Distinguishing between activated and nonactivated eosinophils by AC impedance measurements," *Biomedical Engineering, IEEE Transactions on*, vol. 43, pp. 218-221, 1996.
- [41] S. Ha, "A malaria diagnostic system based on electric impedance spectroscopy," Massachusetts Institute of Technology, 2011.
- [42] X. Hu, W. M. Arnold, and U. Zimmermann, "Alterations in the electrical properties of T and B lymphocyte membranes induced by mitogenic stimulation. Activation monitored by electro-rotation of single cells," *Biochimica et Biophysica Acta (BBA)-Biomembranes*, vol. 1021, pp. 191-200, 1990.
- [43] O. P. Hamill, A. Marty, E. Neher, B. Sakmann, and F. Sigworth, "Improved patch-clamp techniques for high-resolution current recording from cells and cell-free membrane patches," *Pflügers Archiv*, vol. 391, pp. 85-100, 1981.
- [44] J. Voldman, "Electrical forces for microscale cell manipulation," *Annu. Rev. Biomed. Eng.*, vol. 8, pp. 425-454, 2006.
- [45] R. Pethig, "Review article-dielectrophoresis: status of the theory, technology, and applications," *Biomicrofluidics*, vol. 4, 2010.
- [46] Z. R. Gagnon, "Cellular dielectrophoresis: applications to the characterization, manipulation, separation and patterning of cells," *Electrophoresis*, vol. 32, pp. 2466-2487, 2011.
- [47] J. Yang, Y. Huang, X.-B. Wang, F. F. Becker, and P. R. Gascoyne, "Differential analysis of human leukocytes by dielectrophoretic field-flow-fractionation," *Biophysical journal*, vol. 78, pp. 2680-2689, 2000.
- [48] P. R. Gascoyne, X.-B. Wang, Y. Huang, and F. F. Becker, "Dielectrophoretic separation of cancer cells from blood," *Industry Applications, IEEE Transactions on*, vol. 33, pp. 670-678, 1997.
- [49] M. Stephens, M. Talary, R. Pethig, A. K. Burnett, and K. I. Mills, "The dielectrophoresis enrichment of CD34+ cells from peripheral blood stem cell harvests," *Bone marrow transplantation*, vol. 18, pp. 777-782, 1996.
- [50] S. Shim, K. Stemke-Hale, J. Noshari, F. F. Becker, and P. R. Gascoyne, "Dielectrophoresis has broad applicability to marker-free isolation of tumor cells from blood by microfluidic systems," *Biomicrofluidics*, vol. 7, p. 011808, 2013.
- [51] V. Gupta, I. Jafferji, M. Garza, V. O. Melnikova, D. K. Hasegawa, R. Pethig, and D. W. Davis, "ApoStream™, a new dielectrophoretic device for antibody independent isolation and recovery of viable cancer cells from blood," *Biomicrofluidics*, vol. 6, p. 024133, 2012.
- [52] S. Velugotla, S. Pells, H. K. Mjoseng, C. R. Duffy, S. Smith, P. De Sousa, and R. Pethig, "Dielectrophoresis based discrimination of human embryonic stem cells from differentiating derivatives," *Biomicrofluidics*, vol. 6, p. 044113, 2012.

- [53] S.-I. Han, S.-M. Lee, Y.-D. Joo, and K.-H. Han, "Lateral dielectrophoretic microseparators to measure the size distribution of blood cells," *Lab on a Chip*, vol. 11, pp. 3864-3872, 2011.
- [54] M. D. Vahey and J. Voldman, "An equilibrium method for continuous-flow cell sorting using dielectrophoresis," *Analytical chemistry*, vol. 80, pp. 3135-3143, 2008.
- [55] H.-W. Su, J. L. Prieto, and J. Voldman, "Rapid dielectrophoretic characterization of single cells using the dielectrophoretic spring," *Lab on a Chip*, vol. 13, pp. 4109-4117, 2013.
- [56] H. A. Pohl and J. S. Crane, "Dielectrophoresis of cells," *Biophysical Journal*, vol. 11, pp. 711-727, 1971.
- [57] M. Vahey, "A Microfluidic Platform for the Genome-Wide Analysis of Electrical Phenotype: Physical Theories and Biological Applications," *MIT EECS PhD Thesis*, 2010.
- [58] A. Irimajiri, T. Hanai, and A. Inouye, "A dielectric theory of "multi-stratified shell" model with its application to a lymphoma cell," *Journal of Theoretical Biology*, vol. 78, pp. 251-269, 1979.
- [59] K. Asami, Y. Takahashi, and S. Takashima, "Dielectric properties of mouse lymphocytes and erythrocytes," *Biochimica et Biophysica Acta (BBA)-Molecular Cell Research*, vol. 1010, pp. 49-55, 1989.
- [60] Y. Huang, X.-B. Wang, F. F. Becker, and P. Gascoyne, "Introducing dielectrophoresis as a new force field for field-flow fractionation," *Biophysical journal*, vol. 73, pp. 1118-1129, 1997.
- [61] N. Demierre, T. Braschler, P. Linderholm, U. Seger, H. Van Lintel, and P. Renaud, "Characterization and optimization of liquid electrodes for lateral dielectrophoresis," *Lab on a Chip*, vol. 7, pp. 355-365, 2007.
- [62] M. Evander, A. J. Ricco, J. Morser, G. T. Kovacs, L. L. Leung, and L. Giovangrandi, "Microfluidic impedance cytometer for platelet analysis," *Lab on a Chip*, vol. 13, pp. 722-729, 2013.
- [63] S. P. Desai, M. D. Vahey, and J. Voldman, "Electrically addressable vesicles: tools for dielectrophoresis metrology," *Langmuir*, vol. 25, pp. 3867-3875, 2009.
- [64] J. Dunlop, M. Bowlby, R. Peri, D. Vasilyev, and R. Arias, "High-throughput electrophysiology: an emerging paradigm for ion-channel screening and physiology," *Nature reviews Drug discovery*, vol. 7, pp. 358-368, 2008.
- [65] J. Cheng, J. Xu, X. Zhu, L. Liu, X.-B. Wang, and L. Wu, "Apparatus and method for high throughput electrorotation analysis," ed: Google Patents, 2002.
- [66] I. Torsteinsdottir, N. Arvidson, R. Hallgren, and L. Hakansson, "Enhanced expression of integrins and CD66b on peripheral blood neutrophils and eosinophils in patients with rheumatoid arthritis, and the effect of glucocorticoids," *Scandinavian journal of immunology*, vol. 50, pp. 433-439, 1999.
- [67] T. Schmidt, J. Zündorf, T. Gröger, K. Brandenburg, A.-L. Reiners, J. Zinserling, and N. Schnitzler, "CD66b overexpression and homotypic aggregation of human peripheral blood neutrophils after activation by a gram-positive stimulus," *Journal of leukocyte biology*, vol. 91, pp. 791-802, 2012.
- [68] B. Davis, R. Walter, C. Pearson, E. Becker, and J. Oliver, "Membrane activity and topography of F-Met-Leu-Phe-Treated polymorphonuclear leukocytes. Acute and sustained responses to chemotactic peptide," *The American journal of pathology*, vol. 108, p. 206, 1982.
- [69] H. Ziervogel, R. Glaser, D. Schadow, and S. Heymann, "Electrorotation of lymphocytes-the influence of membrane events and nucleus," *Bioscience reports*, vol. 6, pp. 973-982, 1986.
- [70] W. M. Arnold, R. K. Schmutzler, S. Al-Hasani, D. Krebs, and U. Zimmermann, "Differences in membrane properties between unfertilised and fertilised single rabbit oocytes demonstrated by electro-rotation. Comparison with cells from early embryos," *Biochimica et Biophysica Acta (BBA)-Biomembranes*, vol. 979, pp. 142-146, 1989.
- [71] P. C. Ng, G. Li, K. M. Chui, W. C. Chu, K. Li, R. P. Wong, K. W. Chik, E. Wong, and T. F. Fok, "Neutrophil CD64 is a sensitive diagnostic marker for early-onset neonatal infection," *Pediatric research*, vol. 56, pp. 796-803, 2004.

- [72] H. N. Bomela, D. E. Ballot, B. J. Cory, and P. A. Cooper, "Use of C-reactive protein to guide duration of empiric antibiotic therapy in suspected early neonatal sepsis," *The Pediatric infectious disease journal*, vol. 19, pp. 531-535, 2000.
- [73] J.-L. Vincent and M. Beumier, "Diagnostic and prognostic markers in sepsis," 2013.
- [74] J. Pillay, F. Hietbrink, L. Koenderman, and L. Leenen, "The systemic inflammatory response induced by trauma is reflected by multiple phenotypes of blood neutrophils," *Injury*, vol. 38, pp. 1365-1372, 2007.
- [75] J. Seok, H. S. Warren, A. G. Cuenca, M. N. Mindrinos, H. V. Baker, W. Xu, D. R. Richards, G. P. McDonald-Smith, H. Gao, L. Hennessy, C. C. Finnerty, C. M. López, S. Honari, E. E. Moore, J. P. Minei, J. Cuschieri, P. E. Bankey, J. L. Johnson, J. Sperry, A. B. Nathens, T. R. Billiar, M. A. West, M. G. Jeschke, M. B. Klein, R. L. Gamelli, N. S. Gibran, B. H. Brownstein, C. Miller-Graziano, S. E. Calvano, P. H. Mason, J. P. Cobb, L. G. Rahme, S. F. Lowry, R. V. Maier, L. L. Moldawer, D. N. Herndon, R. W. Davis, W. Xiao, R. G. Tompkins, t. Inflammation, and L. S. C. R. P. Host Response to Injury, "Genomic responses in mouse models poorly mimic human inflammatory diseases," *Proceedings of the National Academy of Sciences*, vol. 110, pp. 3507-3512, February 26, 2013 2013.
- [76] L. DeJager, I. Pinheiro, E. Dejonckheere, and C. Libert, "Cecal ligation and puncture: the gold standard model for polymicrobial sepsis?," *Trends in microbiology*, vol. 19, pp. 198-208, 2011.
- [77] S. Song, J. Hogg, Z.-Y. Peng, R. Parker, J. A. Kellum, and G. Clermont, "Ensemble models of neutrophil trafficking in severe sepsis," *PLoS Comput Biol*, vol. 8, pp. 1-16, 2012.
- [78] K. M. Weixelbaumer, P. Raeven, H. Redl, M. van Griensven, S. Bahrami, and M. F. Osuchowski, "Repetitive low-volume blood sampling method as a feasible monitoring tool in a mouse model of sepsis," *Shock*, vol. 34, pp. 420-426, 2010.
- [79] J. Hoff, "Methods of blood collection in the mouse," 2000.
- [80] D. G. Remick, G. R. Bolgos, J. Siddiqui, J. Shin, and J. A. Nemzek, "Six at six: interleukin-6 measured 6 h after the initiation of sepsis predicts mortality over 3 days," *Shock*, vol. 17, pp. 463-467, 2002.
- [81] M. Keel, U. Ungethüm, U. Steckholzer, E. Niederer, T. Hartung, O. Trentz, and W. Ertel, "Interleukin-10 counterregulates proinflammatory cytokine-induced inhibition of neutrophil apoptosis during severe sepsis," *Blood*, vol. 90, pp. 3356-3363, 1997.
- [82] S. Drechsler, K. M. Weixelbaumer, H. Redl, M. van Griensven, S. Bahrami, and M. F. Osuchowski, "Experimentally approaching the ICU: monitoring outcome-based responses in the two-hit mouse model of posttraumatic sepsis," *J Biomed Biotechnol*, vol. 2011, p. 357926, 2011.
- [83] T. Henry, D. R. Gossett, Y. S. Moon, M. Masaeli, M. Sohsman, Y. Ying, K. Mislick, R. P. Adams, J. Rao, and D. Di Carlo, "Quantitative diagnosis of malignant pleural effusions by single-cell mechanophenotyping," *Science translational medicine*, vol. 5, pp. 212ra163-212ra163, 2013.
- [84] I. Nupponen, S. Andersson, A.-L. Järvenpää, H. Kautiainen, and H. Repo, "Neutrophil CD11b expression and circulating interleukin-8 as diagnostic markers for early-onset neonatal sepsis," *Pediatrics*, vol. 108, pp. e12-e12, 2001.
- [85] A. M. Kobold, J. Tulleken, J. Zijlstra, W. Sluiter, J. Hermans, C. Kallenberg, and J. C. Tervaert, "Leukocyte activation in sepsis; correlations with disease state and mortality," *Intensive care medicine*, vol. 26, pp. 883-892, 2000.
- [86] P. S. Martins, E. G. Kallas, M. C. Neto, M. A. Dalboni, S. Blecher, and R. Salomao, "Upregulation of reactive oxygen species generation and phagocytosis, and increased apoptosis in human neutrophils during severe sepsis and septic shock," *Shock*, vol. 20, pp. 208-212, 2003.
- [87] D. Mardi, B. Fwity, R. Lobmann, and A. Ambrosch, "Mean cell volume of neutrophils and monocytes compared with C-reactive protein, interleukin-6 and white blood cell count for

- prediction of sepsis and nonsystemic bacterial infections," *International journal of laboratory hematology*, vol. 32, pp. 410-418, 2010.
- [88] D. H. PARK, K. Park, J. Park, H. H. PARK, H. Chae, J. Lim, E. J. OH, Y. Kim, Y. J. PARK, and K. Han, "Screening of sepsis using leukocyte cell population data from the Coulter automatic blood cell analyzer DxH800," *International journal of laboratory hematology*, vol. 33, pp. 391-399, 2011.
- [89] F. Chaves, B. Tierno, and D. Xu, "Neutrophil volume distribution width: a new automated hematologic parameter for acute infection," *Archives of pathology & laboratory medicine*, vol. 130, p. 378, 2006.
- [90] I. H. Celik, G. Demirel, H. T. Aksoy, O. Erdeve, E. Tuncer, Z. Biyikli, and U. Dilmen, "Automated determination of neutrophil VCS parameters in diagnosis and treatment efficacy of neonatal sepsis," *Pediatric research*, vol. 71, pp. 121-125, 2012.
- [91] L. Wu, G. Guan, H. W. Hou, A. A. S. Bhagat, and J. Han, "Separation of leukocytes from blood using spiral channel with trapezoid cross-section," *Analytical chemistry*, vol. 84, pp. 9324-9331, 2012.